SYNCHRONIZATION AND CRITICAL BEHAVIOR IN β-CELL NETWORKS: TOWARDS THE ENGINEERING OF THE ISLETS OF LANGERHANS

by

THOMAS H. HRAHA

B.S., Colorado State University, 2008

A thesis submitted to the
Faculty of the Graduate School of the
University of Colorado in partial fulfillment
of the requirements for the degree of
Master of Science
Bioengineering
2013

This thesis for the Master of Science degree by

Thomas H. Hraha

has been approved for the

Department of Bioengineering

By

Kendall Hunter, Chair

Richard Benninger

Robin Shandas

6/19/2013

Hraha, Thomas H. (M.S., Bioengineering)

Synchronization and Critical Behavior in β-Cell Networks:
Towards the Engineering of the Islets of Langerhans

Thesis directed by Assistant Professor Richard KP Benninger

ABSTRACT

The pancreatic islets of Langerhans' are multicellular micro-organs which are integral to maintaining glucose homeostasis through secretion of insulin. Beta cells within islets synchronize their insulin release through cell-cell communication to create large bursts to meet physiological needs. However, in patients with diabetes there is a reduction in this cell-cell coupling which leads to a hindered insulin response.

To better characterize the effect of cell-cell coupling in β-cell synchronization, we studied the differences in real-time coupling dynamics between 2D and 3D cell structures. Using a novel system for aggregating β-cells back into 3D structures of defined size, we were able to show that the uncoordinated behavior seen in 2D cell networks is ameliorated by the 3D cell structure. Using this system to aggregate primary islet cells, we found that the resulting 'pseudo-islets' had higher viability and functionality compared to normal islets at two week, indicating they may yield higher post-transplant viability and increase transplant effectiveness.

Applying these findings to a network model of cell synchronization, we were then able to theoretically show how reductions in the fractal dimension of cell coupling (number of nearest neighbors a cell can coupling with) can lead to a diabetic phenotype. Furthermore, we were able to apply this model in a predictive manner to forecast the existence of a critical point of cell coupling, below which a diabetic phenotype is established. This was then verified through islet with genetic mutations.

The form and content of this abstract are approved. I recommend its publication

Approved: Richard KP Benninger

TABLE OF CONTENTS

Chapter

I. INTRODUCTION AND BACKGROUND **1**

Introduction 1

Overview of Glucose-Stimulated Insulin Secretion (GSIS) 2

Diabetes 3

Islet Architecture 3

Beta Cell Electrophysiology and the Triggering Pathway 6

Amplification Pathway and Exocytosis 9

The Insulin Response 12

The Oscillatory Nature of GSIS 13

Cell-Cell Coupling in GSIS 11

Beta Cell Heterogeneity 14

Overview of Relevant Mathematical Models 18

Applications of Transgenic Mouse Model 20

Islet Transplantation 14

Engineering Islets 27

Lattice-Resistor Network Model of Islet Connectivity 28

II. MATERIALS AND METHODS 33

Cell Culture and Aggregate Formation 33

Insulin Secretion Assay 35

Microscopy 36

Matlab Analysis 36

Development of Transgenic Models 40

Bond Percolation Simulations for Size-Scaling and Dimensionality Comparisons 40

High Glucose (Synchronization) Simulations 41

Low glucose (Suppression) Simulations 53

Bond Percolation Simulations for Discrete Modeling of Islet Dynamics 54

III. RESULTS PART 1: DIMENSIONALITY AND SIZE-SCALING OF COORDINATED Ca^{2+} DYNAMICS IN PANCREATIC β-CELL NETWORKS 45

$[Ca^{2+}]_i$ Dynamics and Insulin Secretion Under Two- and Three-Dimensional Coupling 45

Dimension and Size-Dependence of $[Ca^{2+}]_i$ Synchronization 47

Sub-Regions of Synchronization in Two-Dimensional Cell Clusters 50

Wave Velocity Under Two- and Three-Dimensional Coupling 51

Dimension and Size-Dependence of Basal $[Ca^{2+}]_i$ Suppression 52

Network Lattice Model of $[Ca^{2+}]_i$ Dynamics 54

IV. RESULTS PART 2: REAGGREGATION OF PRIMARY ISLET CELLS INTO 'PSEUDO-ISLETS' OF DEFINED SIZE BY MICROWELL CELL 58

Primary Islet Cells Uniformly Aggregate to Defined Sizes in 3D PEG Microwell Arrays 60

Pseudo-Islets Show Comparable Viability and Functionality to Fresh Islets 60

Day 7 and 14 Pseudo-Islets are Better than Age-Matched Normal Islets 62

Summary of Results 63

V. RESULTS PART 3: PERCOLATION MODELING PREDICTS LOW-GLUCOSE BEHAVIOR IN K_{ATP} CHANNEL GENETIC MUTANTS 65

Model Predictions 66

Cell Activity as a Function of Coupling Conductance in KIR6.2[AAA] Mice 69

Cell Activity as a Function of Excitability in KIR6.2[ΔN2-30,K185Q] Mice 70

Summary of Findings 71

VI. DISCUSSION 72

Dimensionality and Size-Scaling of Coordinated $[Ca^{2+}]_i$ Dynamics in β-cells 72

Insufficient β-cell Coupling in Two-Dimensions 73

Network Model Describes Dimension and Size-Scaling of $[Ca^{2+}]_i$ Dynamics 75

Physiological Importance of Dimensionality and Size-Scaling in Network Architecture 77

Re-Aggregation of Primary Islet Cells into Functional Pseudo-Islet 79

Primary Islet Cells Readily Aggregate to Form 3D Pseudo-Islets of Defined Size 80
Pseudo-Islets Show Superior Viability and Functionality 82
Applications to Human Work 84
Percolation Modeling Predicts Low-Glucose Behavior in K_{ATP} Channel Genetic Mutants 86
Percolation Modeling Accurately Predicts the Increase in Low Glucose Activity of KIR6.2[AAA] Islets as a Function of Gap Junction Coupling 88
Percolation Modeling Predicts Critical Behavior in Fasting Insulin Secretion in KIR6.2[ΔN2-30,K185Q] Expressing Mice 89
Implications of the Model for Overactive K_{ATP} Channels 92
Future Directions 98

REFERENCES 99

CHAPTER 1

INTRODUCTION & BACKGROUND

"The greatest challenge today, not just in cell biology and ecology but in all of science, is the accurate and complete description of complex systems. Scientists have broken down many kinds of systems. They think they know most of the elements and forces. The next task is to reassemble them, at least in mathematical models that capture the key properties of the entire ensembles"

- *Edward Wilson*

Introduction

The pancreatic islets of Langerhans' are multicellular micro-organs which are integral to maintaining glucose homeostasis through secretion of the hormones insulin and glucagon. Normally, the cells of this organ are electrically coupled to produce insulin in coordinated bursts in response to elevated blood glucose. These insulin bursts are the result of complex triggering and amplification pathways which are subject to a complex array of inputs. Impairment of the islets ability to accomplish this leads to hyperglycemia, and is implicated in the development of type 1 and type 2 diabetes. Many studies indicate that the pulsatile dynamics of insulin secretion are important for insulin action and maintaining insulin sensitivity, and insulin pulsatility. Therefore, factors that regulate in-vivo insulin dynamics are important for regulating glucose homeostasis.

Currently, the best treatment option for type 1 diabetics is islet transplantation. However, a lack of donor tissue and low post-transplant islet viability are major hurdles towards making this a widely available option. The engineering of islets from donor tissue,

or de novo from stem cells, has the ability to ameliorate this problem. However, these engineered islets must be shown to display similar physiology and have sufficiently developed electrical coupling. Therefore, a working model of both the electrophysiogical coupling of the triggering pathway with integration of components of the amplification pathway would provide a benchmark to which engineered islets can be compared. In addition, the tools developed to build these models would be helpful in studying the development and pathophysiology of diabetes mellitus.

Much work has been done in the last 50 years to understand the electrophysiology and molecular biology of the β-cell. However, relatively little is known regarding how these cells interact with each other to produce such exquisite coordination to maintain glucose homeostasis. This paradigm also reflects the changes taking place in scientific research in general; while the last 50 years have been focused on reductionism, or dissecting the intricacies of biological systems, high level computing and instrumentation will allow the next 50 years to be focused on how these intricate systems interact to produce life and disease.

Overview of Glucose-Stimulated Insulin Secretion

Pancreatic β-cells synthesize and secrete insulin at appropriate rates to maintain blood glucose levels within a relatively small range. Any alteration in their function has a profound effect on glucose homeostasis and often leads to disease. This apparently simple role of the β-cell in glucose physiology contrasts sharply with the complexity of its regulation, which is controlled by an intricate array of metabolic, electrophysiological, hormonal and sometimes pharmacological factors.

When blood glucose rises above its normal level of ~5mM, the pancreatic β-cell responds by releasing insulin into the blood. Because the Km[1] of the β-cell glucose receptor GLUT2 is ~20mM, a rise in extracellular glucose in this range causes a proportionate increase in glucose entry. Glucose-stimulated insulin secretion (GSIS) from β-cells is regulated by a series of molecular events including an elevated ATP/ADP ratio following glucose metabolism, subsequent ATP-sensitive K^+ (K_{ATP}) channel closure, membrane depolarization, Ca^{2+} influx to increase intracellular free-calcium activity ($[Ca^{2+}]_i$), and the triggering of insulin granule exocytosis. Other important steps independent of this 'K_{ATP}-dependent' or 'triggering pathway' include cAMP elevations which elevate insulin granule trafficking to the plasma membrane and augment exocytosis, therefore referred to the 'amplifying pathway' (Henquin, 2000).

Glucose concentrations over ~7 mM generate synchronous oscillations in β-cell intracellular Ca^{2+} concentration ($[Ca^{2+}]_i$), which lead to pulsatile insulin secretion. Although insulin can be secreted through steps independent of Ca^{2+}, primarily through hormonal control, the fraction of insulin released by this mechanism is only minor fraction of insulin released in the presence of Ca^{2+} (Komatsu, et al., 1997). Therefore, the sequence of events leading to insulin secretion may have Ca^{2+}-independent steps, however the physiological regulation by glucose is achieved through Ca^{2+}-dependent pathways.

Diabetes

When insulin secretion is absent or impaired, peripheral tissues fail to respond to insulin, resulting in hyperglycemia leading ultimately to diabetes (MacDonald & Rorsman,

[1] Where K_m is defined by Michaelis-Menten kinetics to be the substrate concentration at which the reaction rate (in this case entry rate which is defined by receptor affinity) is half of the maximal.

2006). Diabetes affects more than 285 million people worldwide, with type 2 diabetics making up about 90% of the cases. It has an annual cost of $132 billion to the American medical system and is associated with several long-term complications including nerve damage, kidney failure, microcirculatory impairment, and a greater risk for heart disease and stroke (MacDonald & Rorsman, 2006).

The vast majority of cases of diabetes fall into two broad categories: type 1 and type 2. Type 1, or juvenile-onset, diabetes results from a cellular-mediated autoimmune destruction of the β-cells. Though the rate of β-cell destruction varies between patients, the resulting impairment is usually large enough to require peripheral insulin injection (Mellitus, 2006).

In contrast, type II diabetes accounts for greater than 85% of cases. In this variant, β-cells persist, but for reasons that remain to be elucidated they fail to secrete insulin in sufficient quantities to maintain proper blood glucose levels (MacDonald & Rorsman, 2006) This disruption in secretion seen prior to the onset of type II diabetes (LeRoith, 2002), and when combined with the development of insulin resistance in peripheral tissues, the results in chronic hyperglycemia. Thus, understanding the electrophysiological mechanisms regulating β cell function and interactions is crucial towards understanding the pathogenesis of type II diabetes.

Islet Architecture

The pancreatic islets of Langerhans play a central role in the regulation of blood glucose homeostasis through the regulated secretion of the hormones insulin and glucagon. The endocrine tissue of the pancreas is organized as cell clusters approximately 100-400μm

in diameter called the islets of Langerhans, which are dispersed throughout the pancreatic exocrine tissue and receive a rich vascular (blood vessel) supply. Islets are composed of three main cells types: pancreatic α cell occupy constitute ~15% of the mouse islet mass and secrete the hormone glucagon in response to low blood glucose. Glucagon increases blood glucose, thereby opposing the actions of insulin. Pancreatic δ cells, which constitute ~5% of the mouse islet mass, secrete somatostatin, which acts in a paracrine fashion to inhibit the secretion of both insulin and glucagon (Reichlin, 1983). Finally, the insulin-secreting β cells are by far the most abundant cell type, comprising ~80% of the islet mass.

Detailed quantitative studies assessing the cell composition (Stefan et al. 1982; Rahier et al. 1983; Clark et al. 1988) have found that human islets are composed ~70% β-cells, 20% α-cells < 15% δ- and other cells. However, more recent studies suggest the there is a lower number of β-cells (50-60%) and a higher number of α-cells (30-40%) (Sakuraba et al. 2002; Street et al. 2004; Brissova et al. 2005).

Although much work has been done with regards to quantifying the cell types in islets, few have examined the cytoarchitecture across species. In rodent islets, the predominating β-cells are clustered mainly in the core of the islet, whereas cells expressing glucagon (α-cells) and somatostatin (δ-cells) are mainly localized to the periphery. In contrast, human islets have shown to have glucagon- and somatostatin-positive cells homogeneously scattered throughout the islet, however recent evidence has shown that this effect may be due to the age of human islets studying, typically being from older individuals compared to weeks-old mice. This is explained in more detail in the discussion. To estimate the degree of clustering or segregation of similar cell types in the islet, Cabrera, et al. quantified the proportion of α- and β-cells exclusively adjacent to cells of the same type (homotypic association) or adjacent to cells of other types (heterotypic associations).

In mouse islets, they found that 71% of β-cells showed homotypic associations, whereas in human islets only 29% showed these associations (Cabrera, et al., 2006). This suggests that the paracrine effects of other cell types may play a more important role in human islets, which was further supported by evidence showing that ~86% of δ-cells were found to be closely opposed to blood vessels.

However, recent evidence suggests that the cytoarchitecture seen in human islets by Cabrera et al. may be the result of a changing cell composition over time (Bosco et al. 2010; Kilimnkik et al. 2011). In a better statistically powered study, Bosco, et al. demonstrated that while larger human islets have a heterogeneous core composed of α- and β-cells, smaller human islets maintain the core-mantle structure seen in mice islets. Furthermore, they found that the α-cells within the core the islet were focused around the edges of the vasculature and therefore postulate that this architecture in larger islets still facilitates a 'folded' mantle-core structure around the vasculature (Bosco et al. 2010).

Nevertheless, these aspects of the cellular architecture must be taken into consideration when applying findings regarding intercellular electrical synchronization and when attempting to engineer islets *de novo*. It appears that differences in islet cytoarchitecture may lead to functional differences in islet behavior, with human islets having more of a reliance on neuro-endocrine secretions. It is therefore important to consider the relative proportions and locations of cell types when attempting to engineer islets using hydrogel scaffolds or when aggregating cells de-novo. Also, the lower percentage of β-cells within the human islet may lead to less cell-cell electrical coupling, although this has never been shown.

Beta Cell Electrophysiology and the Triggering Pathway

Pancreatic β cells have multiple ion channels which allow for the flow of ions (mostly Ca^{2+} and K^{+}) into and out of the cell. Due to the charged nature of these ions, their flux across the membrane can give rise to sharp changes in voltage (action potentials). In β-cells, these action potentials are stimulated through intracellular glucose metabolism.

The cell membrane gives rise to small voltage changes by manipulating the concentration gradient of ions using selective permeability. If the concentrations of positive and negative ions on either side of the cell membrane are equal, there will be no difference in the electrical potential gradient. However, if the membrane was permeable to an ion (K+ in the case of the beta cell) then the inward flux of this ion down its concentration gradient would create a charge imbalance and therefore a potential gradient. As more K+ ion move through the channel, the magnitude of the charge difference (or voltage) increases until a repulsive force caused by excess positive K+ ions leads to an equilibrium. If a membrane is only permeable to K+ ions (which is the approximate case for the beta cell), then the electrical potential E_{k+} (in volts) is given by the Nernst equation

$$E_k = \frac{RT}{ZF} ln \frac{[K_e]}{[K_i]}$$

where K_e and K_i are the extracellular and intracellular concentrations of K+ ions, respectively; R is the gas constant 1.987 calories / (degree*mol); T is the absolute temperature in Kelvins (293°K for 20°C); Z is the +1; and F is the Faraday constant equal to 23,062 cal / (mol*V) or 96,000 coulombs / (mol*V). At 20°C, this reduces to:

$$E_k = 0.059 log_{10} \frac{[K_e]}{[K_i]}$$

Therefore, at a 10-fold concentration the magnitude of the difference is 0.059V (or 59mV). However, since the cytoplasmic side is viewed as negative in this case, this would be -59mV.

The resting membrane potential of the β-cell is dominated by K+ channels. As a result, the major ionic movement across the plasma membrane is that of K+ out of the cell, powered by the concentration gradient. This creates a resting membrane potential of the cell is approximately -70mv. Although this value does not seem very large, given that the cell membrane is only ~3.5nm thick, this corresponds to ~200,000 volts per cm. To put this in context, high-voltage power lines generally use a 200,000 volt gradient over a kilometer.

Under low glucose conditions, ATP-sensitive K^+ channels (K_{ATP} channels) are open, allowing an outward flux of K^+ ions which effectively clamps the beta-cell membrane potential at the K^+ Nernst potential and produces a steady-state cell membrane potential of ~-70mV (Rorsman, 1997; Henquin, 2000). These channels are tetramers of a complex of two proteins: a high-affinity sulfonylurea receptor (SUR1) and an inwardly rectifying K+ channel (Kir 6.2). SUR1 provides the pore-forming KIR6.2 with sensitivity to sulfonylureas and diazoxide, which respectively close and open the channel. The closing action in response to an elevated ATP:ADP ratio is KIR6.2 –dependent (Henquin, 2000; Ashcroft & Gribble, 1998).

When the β-cell is exposed to glucose through the pancreatic vasculature, glucose enters the cell through GLUT2 transporters and increased cellular metabolism of the sugar through glycolysis (anaerobic) and oxidative phosphorylation (aerobic) leads to a rise in the ATP:ADP ratio. Increased levels of ATP bind to the KRI6.2 subunit of the K_{ATP} channel and cause it to close; stopping the influx of K^+ ions down their electrical gradient. This drives the membrane towards a more positive potential and once the K_{ATP} channels are almost all (>90%) inhibited, the K_{ATP} conductance is unable to balance the background depolarizing

influences and the beta cell depolarizes at around -45mV (Rorsman 1997; MacDonald & Rorsman, 2006; Drews et al., 2010; Misler et al., 1992). When this depolarization is large enough, L-type voltage-gated calcium channels (VDCC) become activated, allowing the influx of Ca2+ down the electrical gradient, further driving the membrane potential.

The predominant VDCC isoforms found in β cells are composed of four subunits. Each subunit is composed of six transmembrane α-helices, the fourth of which serves as the voltage sensors for activation. In response to membrane depolarization, VDCCs undergo an extremely rapid conformational shift, moving outward and rotating under the influence of the electric field and initiating a conformational change which opens a highly permeable pore (Yang & Berggren, 2006).

The resultant increase in $[Ca^{2+}]_i$ triggers direct interactions between the exocytotic proteins situated in the insulin-containing granule membrane and those localized in the plasma membrane. Eventually, the interaction between exocytotic proteins initiates the fusion of insulin-containing granules with the plasma membrane resulting in insulin exocytosis (Yang & Berggen, 2005a; Yang & Berggen, 2005b).

If glucose concentrations remain high, the β-cell undergoes oscillatory Vm activity. This is caused by oscillatory changes in ATP and activation of voltage-dependent inward rectifying K^+ (K_v) channels, whose opposing activity creates high frequency oscillations at high membrane potentials. As the levels of $[Ca^{2+}]_i$ increase, Ca^{2+}-activated K+ channels are opened which are responsible for the repolarizing curve of the V_m trace and reset the cycle (MacDonald, 2003).

Thus, the K_{ATP} channels can be viewed as the transducers of glucose-induced insulin secretion. This role is easily demonstrated by the use of agents which manipulate the

channels behavior. Opening of channels with diazoxide causes membrane repolarization, lowers $[Ca^{2+}]_i$ and inhibits insulin secretion (Henquin, 2000). Subsequent addition of tolbutamide or sulfonylureas to close the channels leads to a depolarization of the cell and a resumption in $[Ca^{2+}]_i$ -driven insulin release (Henquin, 2000). In addition, recent evidence has suggested that waves of depolarization through the entire islet originate in areas of high K_{ATP} inhibition (Rochelau et al., 2004).

If K_{ATP} are said to be the transducers of glucose-stimulated insulin secretion, then the VDCCs are the effectors because of their effect on insulin exocytosis. This is supported by a work in which a point mutation of human VDCC channel rendering constitutively active makes the β-cell secrete insulin excessively (Splawski et al., 2004).

A number of additional factors have been found to control β-cell electrophysiology, including Cl^- and non-selective cation channels, as well as electrogenic pumps such as the Na^+ / K^+ ATPase. While the role of these has not been extensively characterized, their activity has been found to be highly dependent on peripheral systems such as the protein-kinase C pathway and mitochondrial NADPH production (MacDonald, 2003). Though they may play an undiscovered critical role, the three channels which regulate the glucose-induced response (and were discussed above) are the main players in regulating glycemic control through insulin secretion.

Amplification Pathway and Exocytosis

Although much work has been done to show that insulin exocytosis is clearly Ca^{2+} -dependent, recent evidence suggests that increased intracellular $[Ca^{2+}]_i$ acts more as an initiator rather than a determinant of insulin release. For example, removal of extracellular

Ca^{2+} prevents action potential (Liu et al., 2004) and subsequent insulin secretion (Gopel et al., 2000; Gromada et al., 2004), however, the amplitude of the exocytotic response depends to a greater extent on the activity of kinases and phosphatases rather than purely $[Ca^{2+}]_i$ (Rorsman, 1997; Milser et al., 1992; Henquin, et al., 2000). This points to another, 'amplifying pathway' of insulin secretion that has been found to be mediated by cyclic adenosine monophosphate (cAMP).

A ubiquitous secondary messenger of most cell types in the body, cAMP is another critical factor in GSIS. Until recently, little was known about the spatiotemporal dynamics of cAMP signaling in β cells. With the recent advance of novel fluorescent biosensors, complex spatiotemporal patterns which are Ca^{2+} dependent and independent are beginning to emerge. Interestingly, glucose has been found to trigger concurrent oscillations of cAMP and $[Ca^{2+}]_i$ in individual MIN6 cells (Landa et al., 2005; Ni et al., 2010). Since cAMP enhances exocytosis predominantly via PKA, and is also influenced by hormonal factors (in addition to $[Ca^{2+}]_I$), it has been suggested that cAMP plays an amplifying role of the Ca^{2+} signal. In both humans and rodents, the glucose-induced oscillations in $[cAMP]_i$ resemble those of $[Ca^{2+}]_i$ with small initial lowering, followed by pronounced rise and slow oscillations with a period of 2-10 minutes (Dyachok et al., 2008). Although several studies have found that depolarization of the cell causes oscillations in $[cAMP]_i$ (Dyachok & Gylfe, 2004; Landa et al., 2005; Ni et al., 2010), the phase relationship between these two signaling factors seems to depend on the other conditions. Whereas cells stimulated with GLP-1 showed synchronous oscillations in $[cAMP]_i$ and $[Ca^{2+}]_i$ (Dyachok et al., 2006), TEA-induced elevations of $[Ca^{2+}]_i$ were associated with decreases of cAMP (Landa et al., 2005), which may be due to over-activation of Ca2+ -sensitive phosphodiesterase.

Glucose-induced generation of cAMP in β cells may potentiate insulin secretion by sensitizing the exocytosis machinery since inhibition of [cAMP]i oscillations markedly suppress pulsatile insulin secretion without affecting the underlying [Ca2+]i oscillations (Henquin, 2000). Agents which increase cytoplasmic levels of cAMP potentiate Ca^{2+} -stimulated insulin exocytosis almost 10-fold (through a protein kinase A (PKA)-dependent mechanism) without affecting Ca^{2+} influx or $[Ca^{2+}]_i$ (Ammala et al., 1993). This is thought to be due to PKA accelerating granule mobilization. Thus, when exocytosis is initiated by $[Ca^{2+}]_i$ a greater number of granules are available for release. Therefore, the Ca2+, ATP:ADP and cAMP dynamics may lead to triggering and amplification pathways of insulin secretion, which would explain why cAMP can oscillate even under steady Ca2+ levels.

The principal action of cAMP on exocytosis seems to be exerted at a step distal to the elevation of $[Ca^{2+}]_i$ (Ammala et al., 1993; Gillis and Misler, 1993), involving both PKA-dependent and -independent mechanisms, the latter most likely mediated by exchange proteins activated by cAMP (Epac) (Renstrom et al., 1997). Many exocytosis-related proteins have been identified as substrates for PKA (Seino and Shibasaki, 2005), and the subcellular targeting of PKA to its effectors via A-kinase anchoring proteins has been found to be critical for the stimulatory effect of cAMP-elevating agents on insulin secretion (Lester et al., 1997; Fraser et al., 1998). Capacitance recordings by Eliasson, et al. have indicated that PKA mediates the slower cAMP-dependent mobilization of insulin granules, while Epac accounts for the rapid cAMP-dependent potentiation of exocytosis in β-cells (Eliasson et al., 2003). Epac has also been reported to increase the number of granule fusion sites and along with PKA the number of granule-granule fusion events (Kwan et al., 2007).

Interestingly, both sulfonylureas and GLP-1 treatment have been found to improve in-vivo insulin pulsatility (Porksen, 2002), which is most likely due to the established ability

of these drugs to generate oscillations in $[Ca^{2+}]_i$ (Grapengeisser, 1990) and cAMP (Dyachok, 2006). Impairment of insulin pulsatility from β cells is central to the development of type 2 diabetes, and may reflect a degradation of synchronization in secretory activity rather than a deficit in β cells mass. In addition, since insulin has been suggested to be an important stimulus for β cell proliferation in states of insulin resistance (Henquin, 2000), loss of pulsatile insulin secretion in prediabetic and diabetic states may also impair the compensatory expansion of the β cell mass (Lang, 1981).

Despite the fact that much work has been done in regards to understanding the roles of cAMP and $[Ca^{2+}]_i$ in individual cells, how these cells come together to form a coordinated pulse of insulin remains unclear. Despite work in the role of gap junctions in coordinating electrical activity (Benninger et al., 2008; Benninger et al., 2011; Rochelau et al., 2004), how cAMP activity coordinates the 'amplifying pathway' remains unclear. In fact, there is a lack of data where cAMP and $[Ca^{2+}]_i$ were measured in anything but a single cell. If islets are ever to be reformed from primary cells or stem cells, these are important dynamics that need to be established to recreate a functional islet capable of overcoming diabetes.

The Insulin Response

Pancreatic β-cells respond to a step increase in the glucose concentration with a biphasic insulin secretory pattern. This biphasic pattern of insulin secretion was first observed in the perfused rat pancreas (Grodsky, 1966; Nesher, 1987). Later, it was also visualized in the portal vein and peripheral blood in human subjects in response to a rapid elevation of glucose (Cerasi et al., 1972). The response is characterized by a rapid initial

phase of insulin release, which is maintained for about 10 minutes, followed by a gradually increasing second phase, which reaches a plateau after another 25 to 30 minutes (Yang & Berggen, 2005a). Mouse islets subjected to an abrupt and sustained increase also secrete insulin biphasically. However, the second phase of insulin release from mouse islets is lower than that from human and rat islets (Jing, 2005). A loss of the first phase and a reduction of the second phase of insulin secretion occur in type 2 diabetes characterized by β-cell dysfunction (Rorsman & Renstrom, 2003).

This supports other evidence which shows that glucose-induced insulin secretion dynamics by human islets is very similar to that in rodents in terms of metabolic and Ca2+ dependencies (Ricordi et al., 1998; Grant et al., 1980; Misler, et al., 1992). Therefore, this supports the use of rodent models in the study of islet electrophysiology, pathology and diabetes.

Oscillatory Nature of GSIS

Insulin secretion occurs in a pulsatile fashion, which is driven by the underlying pulsatile nature of the cell voltage. The opening of Ca^{2+} channels is intermittent, oscillating with the membrane potential and therefore resulting in oscillations in $[Ca^{2+}]_i$ and in-turn, oscillations in insulin release (Gilon et al., 1992; Tornheim, 1997).These oscillations occur with a period of 2-8 minutes in humans (Land et al., 1979) and mice (Nunemaker et al., 2006), and reflect a balance between the VDCCs (depolarization) and the K_{Ca} channel activity (repolarization) (Ashcroft & Rorsman, 1989). The depolarizing Ca^{2+} component dominates at the beginning of the burst, but the Ca^{2+} influx rapidly leads to increased K_{Ca} channel activity. This occurs via a direct effect on Ca^{2+}-activated K_{Ca} channels (Zhang et al.,

2005) and also through indirect effect on K_{ATP} channels by lowering the cytoplasmic ATP:ADP ratio due increased Ca2+ ATPase activity (Kanno et al., 2002). Upon the buildup of Ca^{2+}, K_{Ca} channel activity repolarizes the β-cell, thereby readying the cell for another burst if intracellular metabolism remains high.

Glucose produces a concentration-dependent decrease in the period. At glucose concentrations beyond physiological levels (20mM), constant action potential spiking is seen, which may be due to a higher rate of glucose metabolism leading to such high intracellular ATP concentrations that Ca^{2+} ATPase cannot lower them to increase K_{Ca} conductance enough to lead to repolarization. This is supported by the use of the of K_{ATP} inhibitor tolbutamide, which has been used to treat diabetes for over 50 years. By blocking K_{ATP} channels, membrane potential is suppressed and results in continuous firing (MacDonald & Rorsman, 2006).

Cell-Cell Coupling in GSIS

In addition to proper electrophysiology in individual β cells, communication between cells is imperative for a proper insulin response. β-cells within the same pancreatic islet are electrically coupled by gap junctions (Santos et al., 1991; Eddlestone et al., 1984), such that the $[Ca^{2+}]_i$ oscillations within different parts of the islet occur in-phase – even though individual β-cells show a heterogeneous sensitivity to a given glucose concentration. This gap junction coupling coordinates the dynamics underlying GSIS and also mediates the suppression of electrical activity at low blood glucose concentrations. This synchronization of electrical activity produces coordinated bursts of insulin, which are imperative in glycemic control.

In contrast to continuous secretion, pulsatile insulin release has been shown to be more effective at lowering blood-glucose (Bratusch-Marrian et al., 1986; Matthews et al., 1983; Paolisso et al., 1988; Meier et al., 2005), and also maintaining peripheral tissue insulin sensitivity (Goodner et al., 1988). Several landmark studies have also shown that diabetic patients require less insulin to maintain normoglycemia if insulin is infused in an oscillatory manner as opposed to a constant rate. Pulsatile insulin infusion has also been implicated for use in patients with type 2 diabetes with positive results (Bratusch-Marrain et al., 1986; Matthews et al., 1987; Paolisso et al., 1988). These oscillations are disrupted in patients with type II diabetes (O'Rahilly et al., 1988; Porksen, 2002) as well as obese individuals (Peiris et al., 1992), and this has been proposed to play a pathogenic role in the progression of diabetes (O'Meara et al., 1993). Therefore, it can be reasoned that this is the result of downregultion of gap junctions as well as a reduction in β-cell to β-cell proximity due to infiltration of α-cells and other immune cells, which is known to occur in hyperglycemic conditions (Sorenson et al., 1997; Sheridan et al., 1988).

The gap junction channels which electrically couple β-cells are formed by six identical connexin-36 (Cx36) transmembrane proteins, which mediate ionic currents and the diffusion of small molecules (ref from 3). As a result, Cx36 gap junctions are the sole means of electrical coupling between β-cells in the islet (Benninger et al., 2008; Ravier et al., 2005), and in the absence of Cx36, isolated islets do not exhibit coordination in $[Ca^{2+}]_i$ oscillations (Benninger, 2011) or pulsatile insulin release (Benninger et al., 2011; Drews et al., 2010; Ravier et al., 2005). When islet architecture is altered, a concomitant impairment of insulin secretion and $[Ca^{2+}]_i$ is observed, which recovers as soon as contact among cells is re-established (Halban et al., 1982; Bertuzzi et al., 1999). Underscoring the importance of coupling, β-cells from intact islets exhibit several-fold the glucose-stimulated insulin secretion (GSIS) at elevated glucose compared to dispersed β-cells (Lernmark, 1974;

Halban et al., 1982). Recently, we have shown that the dimensionality of the coupling (2D vs. 3D) alone can explain the better response of highly coupled islets and have developed a novel simulation-based mathematical model to explain such behavior (Hraha, et al. 2013, in submission).

Similar to patients with type II diabetes, Cx36 knockout mice were glucose intolerant and had reduced peak amplitude of the insulin pulse as measured through plasma insulin levels (Benninger et al., 2008; Head et al., 2012). Since this effect was also found in the isolated islets ex-vivo, this pathology is thought to be islet-specific. Therefore, since Cx36 is also the sole means of coupling in humans islets (Serre-Beiner et al., 2009), a reduction in Cx36 gap junction conductance would help explain the symptoms seen in type 2 diabetics.

Using a model of Cx36 knockout mice, Head and colleagues found that in the absence of Cx36, the heterogeneity in $[Ca^{2+}]_i$ oscillations is indicative of some β-cells exhibiting transient repolarizing events even high glucose. This is in contrast to the sustained elevations in $[Ca^{2+}]_i$ in the presence of Cx36. This can help to explain the decrease in mean $[Ca^{2+}]_i$ concentration at high glucose stimulation in the absence of Cx36, and points to the role of gap junctions in maximizing the effectiveness of the GSIS (Head, et al., 2012).

Gap junction coupling has also been found to coordinate behavior at low blood-glucose concentrations by having a hyperpolarizing effect. This is a desirable characteristic because secreting insulin at levels of low blood glucose would drive the system into a deeper state of hypoglycemia. Benninger et al. has demonstrated a similar $[Ca^{2+}]_i$ response to glucose in $Cx36^{-/-}$ islets and isolated β-cells suggests gap junctions are the predominant mechanism present to suppress elevations in basal $[Ca^{2+}]_i$ that rise due to cellular heterogeneity in mice expressing a K_{ATP} transgene (Benninger et al., 2010). Therefore, an

understanding of coupling between β cells via gap junctions is imperative for understanding the pathogenesis of the disease as well as understanding the challenges of creating islets de novo.

β-Cell Heterogeneity

The unique feature of the beta cell, essential for its ability to serve as the body's fuel sensor, is the presence of K_{ATP} channels. As discussed previously, the activity of these channels sets the membrane potential of the β-cell and this determines its electrical sensitivity to blood glucose and therefore its secretory activity. For this reason, the K_{ATP} channel inhibitor sulphonylureas has been used for over 70 years to treat treat type 2 diabetes (Gerstein, 2008).

In contrast to the highly synchronized islet, isolated β-cells show a considerably variable glucose response. Isolated β-cells exhibit heterogenous and irregular responses to clucose for many variables, including NAD(P)H elevations (Bennett et al. 1996), $[Ca^{2+}]_i$ oscillations (Zhang et al. 2003) and the dynamic range of insulin release (Vanschravendijk, et al. 1992). This demonstrates that a high degree of electrical coupling exists between β-cells in the islet to create synchronous oscillations in $[Ca^{2+}]_i$ and insulin release. Recent evidence has actually suggested that the origin of $[Ca^{2+}]_i$ waves in intact islets is actually due to heterogeneity in β-cells population (Benninger et al. 2008). Heterogeneity in $[Ca^{2+}]_i$ oscillations occurs in both dissociated β-cells (Zhang et al. 2003) and islets lacking gap junctions (Ravier et al., 2005; Benninger et al., 2008). Therefore β-cells within the islet are intrinsically heterogeneous in terms of the electrical response to glucose, and gap junction acts to uniformly suppress any subthreshold response.

Overview of Relevant Mathematical Models of β-cell Electrophysiology

Mathematical modeling is useful in biology to unify theories, fit data to statistical models, identify mechanisms from disparate data, and to predict tests. Physicists have used modeling for centuries to explain phenomena, however most biologists are just recently beginning to employ detailed models to inform their research (Winters, 2012). Because of its complex dynamics as well as measurable outcomes, the electrophysiology of the β-cells lends itself quite readily to mathematical treatment and therefore much work has been done on the subject.

The Chay-Keizer model is a minimal mathematical model which describes the bursting behavior of 2-dimensional clusters of pancreatic β-cells. The model is minimal in that it includes only the basic set of processes that lead to burst oscillations: voltage-regulated K+ channels, Ca^{2+}-activated K^{+} channels, voltage-regulated Ca^{2+} channels, and glucose-stimulated efflux of Ca+2 from the cytosol. With these basic processes the model produces burst oscillations with features like those observed experimentally. The Chay-Keizer model also describes the evolution of the cytosolic Ca^{2+} concentration (Chay & Keizer, 1983).

Although commendable for its ability to simulate β-cell bursting using simple dynamics, the Chay-Keizer model is a bit too simplistic to capture all of the complex dynamics underlying membrane potential. One of the criticisms of the Chay-Keizer model is that in its original form, it is unable to account for some of the variation in calcium dynamics; namely that experimental evidence has suggested that calcium levels plateau quickly, rather than in the stepped fashion seen in the model. Also, it is unable to accurately account for both high and low frequency $[Ca^{2+}]_i$ components (Keizer et al., 1991). This has been somewhat remedied by the addition of an endoplasmic reticulum component to the

$[Ca^{2+}]_i$ dynamics. Another qualm was that it does not include a glycolytic component. Since the bursting patterns of $[Ca^{2+}]_i$ is due to intracellular ATP levels, Bertram et al. introduced a model in which the conductance of K_{ATP} channels varied with observed oscillation in glycolysis (Bertram et al., 2000).

Though the previous models are reported to fit experimental data nicely, they still do not include components of the model which (as we have seen) explain much of the behavior seen in β-cells: coupling, cAMP and heterogeneity. The Bertram group solved one of these by creating what is called the phantom burster model. The authors considered a mechanism which allows single cells to fire on both the slow (1-5 seconds) and fast (1-2 minutes) scales (as is seen in experimental data of single cells) (Bertram et al. 2000). Since there is no pacemaker cells initiating the burst, and instead it is a function of the collective behavior, it has been termed the phantom-burster.

To introduce coupling, Sherman et al. considered many Chay-Keizer-like cells coupled together, thereby creating a 'supercell' with a very high coupling conductance (Sherman & Keizer, 1990). Importantly, they demonstrated that coupling a silent cell with a cell undergoing periodic oscillations may result in bursting at the network level as the network passes between both solution types. However, the model did not account for any heterogeneity and needed values of conductance parameters that were much higher than what has been previously reported.

Heterogeneity in β-cells is an inherent physiological property that intercellular coupling must overcome. In their 2008 paper Benninger et al. studied coupled cells based on the previously mentioned phantom burster model. They introduced heterogeneity into their network by randomly distributing the electrical coupling strength between adjacent cells. Therefore, a given cells membrane potential is affected by its surrounding cells

potential as a function of heterogeneous coupling strength. Additional heterogeneity was introduced through K_{ATP} sensitivity and metabolic flux (ATP production). They found that the model predicts traveling waves of calcium levels amongst the network, which was consistent with experimental data. In addition, it was able to explain how large numbers of heterogeneous β-cells can couple to form a coordinated syncytium at both high and low glucose (Benninger et al., 2008).

Although the effects of gap junction coupling and $[Ca^{2+}]_i$ remain to be uncovered, cAMP nonetheless plays an important part in GSIS and deserves adequate mathematical treatment to help elucidate it's behavior. Recently, Ni, et al. published an extremely elegant model of cAMP dynamics based off of an $[Ca^{2+}]_i$-cAMP-PKA oscillatory / regulatory circuit. The model was able to predict the effects of numerous channel inhibitors for different endpoints, which were confirmed by experimental data (which was also not a trivial undertaking). However, as impressive as their model was, it was only in single cells and therefore misses much of the dynamics which underlie cAMP signaling.

Therefore, although the understanding of β-cell dynamics has been greatly enhanced from these models, a full working model of GSIS is still a far-off goal. To fully elucidate the mechanisms underlying GSIS and to create a set of endpoints for which engineered islets can be based, a full working model is needed.

Applications of Transgenic Mouse Models

In pancreatic β-cells, the K_{ATP} channel is a critical link in the pathway of glucose-induced insulin release. According to this paradigm, a high intracellular ATP/ADP ratio inhibits Katp channels, causing membrane depolarization. This induces Ca^{2+} entry though

VDCCs and initiates events leading to subsequent exocytosis. Conversely, a lower ATP/ADP ratio during a fasting state relieves inhibition of the Katp channels, resulting in membrane hyperpolarization and suppression of Ca2+ activity. The dependence of channel activity on intracellular ATP underlies the physiologic role of the K_{ATP} channel by coupling the metabolic status of a cell to electrical activity.

The recent discovery of numerous mutations in pancreatic K_{ATP} channel subunits (both the pore-forming Kir6.2 and SUR1) in human patients with persistent hyperinsulinemic hypoglycemia of infancy (PHHI) further establishes the link between suppressed K_{ATP} activity and the corollary metabolic disorder of *hyper*insulinism (Huopi, et al., 2002). PHHI-associated K_{ATP} mutations can be classified into two major categories: those which suppress channel activity without altering cell-surface expression, and biosynthetic or trafficking defects that reduce or abolish surface expression. In both cases, reduced K_{ATP} channel activity is expected to result in constitutive depolarization, persistently elevated $[Ca^{2+}]_i$, and unregulated insulin secretion (Huopio, et al., 2002). Although a few cases can be treated with the K_{ATP} channel opener drug diazoxide, but the majority of cases require surgical removal of almost all of the pancreas (de Lonlay, et al., 2002).

Genetic suppression of the K_{ATP} channel has been undertaken previously to better characterize its role by alteration of the KIR6.2 and SUR1 subunits. Miki et al. developed a transgenic model expressing a dominant-negative KIR6.2 mutant which perturbs the structure of the KATP pore forming unit which renders it non-functional (Miki, et al., 1998). Although these β-cells from these mice showed reduced K_{ATP} currents and an increase in resting membrane potential, they also showed no glucose-induced insulin secretion and therefore developed neonatal hyperglycemia and experience extensive β-cell apoptosis.

To circumvent this issue, Koster et al. developed another KIR6.2 mutant which showed suppressed pancreatic K_{ATP} currents as adults, in contrast to neonates (Koster, et al. 2001 PNAS; Koster et al., 2000). In their model, there was ~70% penetrance of the KIR6.2[AAA] mutation, meaning transgenic overexpression and incorporation of the nonfunctional KIR6.2 subunit in approximately 2/3 of β-cells in a particular islet will exhibit no measurable KATP channel activity. This reduction in overall K_{ATP} conductance lead to reduced resting membrane potential and a loss of hyperpolarizing. Therefore, these mice exhibit hypersecretion of insulin leading to a left-shift of the insulin dose-response curve (Koster, et al., 2000 & 2001). However, since this does not lead to a dominant negative phenotype with no K_{ATP} activity (like in other models), hyperinsulinemia and the onset of diabetes is markedly delayed.

In contrast to loss-of-function K_{ATP} mutants associated with hypersecretion of insulin, mutations in K_{ATP} subunits that reduce sensitivity to inhibitory ATP (gain of function) give rise to the corollary disease, diabetes. To test this, Koster et al. created mutants by truncating the 30 N-terminal amino acids (KIR6.2[ΔN2-30]), and combined this with a point mutation at amino acid 185 (KIR6.2[K185Q]), hence KIR6.2[ΔN2-30,K185Q]. This combination results in mutant subunits with a ~30-fold reduction of ATP sensitivity (Koster, et al., 2000). Since K_{ATP} channels are formed as tetramers, each with a SUR1 and KIR6.2 subunit, overexpression of the KIR6.2 will yield SUR1 as rate-limiting. Therefore, KIR6.2[ΔN2-30,K185Q] subunits will be incorporated accordingly and result in a partial 'functional knockin' of the transgenic product. The effects of transgenic expression were profound and included early onset diabetes characterized by reduced serum insulin levels and dramatically elevated blood glucose (Koster et al, 2000).

In addition to K_{ATP} transgenic models, Cx36 knockout mice have also lead to a greater understanding in how β-cells suppress and coordinate activity. For example, Benninger, et al. have found at sub-threshold glucose conditions Cx36-/- had spontaneous Ca2+ activity in ~50% of β-cells, whereas wild-type islets remained quiescent (Benninger, et al., 2011).

In intact Kir6.2[AAA] islets, β-cells exhibit essentially normal $[Ca^{2+}]_i$ and insulin secretion responses to glucose (Rocheleau et al. 2006). Therefore the maintained cell–cell contacts in these islets acts to suppresses the expected elevations in $[Ca^{2+}]_i$ and insulin release at low glucose due to the K_{ATP} mutation. These islets therefore allow us to quantify and further distinguish how gap junctions and other means of cell–cell communication can specifically regulate basal electrical activity and insulin secretion in the intact islet. They also allow us to verify and fit our models to better explain how cell–cell contact suppressed basal $[Ca^{2+}]_i$ dynamics and insulin release.

To test this, we can investigate islets in which electrical activity has been perturbed by the mosaic expression of a loss-of-function or gain-of-function mutations in K_{ATP} channels (Koster et al. 2000; Rocheleau et al. 2006), in addition to Cx36 knockout. In these mouse models, elevations of basal $[Ca^{2+}]_i$ and insulin secretion due to the K_{ATP} loss-of-function are suppressed by mechanisms dependent on cell–cell contact in the intact islet. These islets therefore allow us to specifically study how cellular differences in electrical activity in the intact islet are suppressed by gap junction coupling and other mechanism dependent on cell–cell contacts, as well as to understand how these mechanisms apply to mathematical modeling of the islet architecture.

Islet Transplantation

Currently, the best treatment option for patients with type 1 diabetes is islet transplantation from cadaveric donors. Since they are the only cells known to secrete insulin in response to elevated blood glucose, β-cells can be transplanted by a variety of methods to reduce insulin-dependence of diabetic patients. Partial pancreas transplants were first attempted in the early 1900's. However, it was not until the historic Edmonton study described 7 type I diabetics who became insulin-independent after as isolated islet transplant that this procedure initiated a new arena of research. In this study, patients were injected with isolated whole islet preparations into the portal vein, where the islets lodge in the vasculature. By being in a high-flow digestion-related system, graft islets are then capable of physiologically regulating insulin secretion. However, despite the wide-spread promise of this procedure, many complications remain with regards to its efficacy.

In the United States, it is estimated that there are 12,000 potential islet donors per year. However, when consent, time and isolation efficiencies are taken into account the number drops to 3,000 (Rother & Harlan, 2004). Barriers to the effectiveness of transplants include not only the availability number of donor islets, but also post-transplant graft viability. Normally, pancreatic islets have a dense capillary network that entails blood perfusion which is 10 times higher than that of the exocrine pancreas (Fung et al. 2007). This not only allows the islet to be sensitive to changes in blood glucose, but also maintains the high metabolic demand of the islets. However, during the process of isolation and in vitro culture pre-transplant, islet vasculature dedifferentiates or degenerates (Brissova & Powers 2008). Immediately after transplantation the pancreatic islets are supplied with oxygen and nutrients solely by diffusion. Therefore, in the early post-transplant setting of the portal vein the centers of larger islets can become hypoxic and necrotic. It is estimated

that 50-70% of the transplanted islets will be lost in the immediate post-transplantation period (Lehmann et al., 2007; MacGregor et al., 2006), with the hypoxic conditions of the portal vein combined with the energy status of the islets being major contributor (Ryan et al., 2002). Consequently, most patients require multiple transplants (2-4 in most instances), further reducing the number of available pancreata (MacGregor et al., 2006). Taken together, the statistics show that our current transplant protocols are only ~25% effective at using the ~6,000 available donors to treat the 1,000,000 type I diabetics in the United States (Hirshberg et al. 2003). However, by increasing the post-transplant viability of donor islets the efficacy can be increased.

Other than cadaveric islets, many other potential sources of β-cells have been discussed in scientific literature, though the chasm between promise and reality remains large. Three potential sources that have seen much discussion are expanding β-cells in-vitro, other-species transplantation (xenograph) and differentiation of stem cells into β-cells. Though research should be maintained, issues with each remain, for example: no group has been able to reliably propagate isolated islet cells; immunoreactivity and ethical questions remain around xenographs; and issues remain around the efficacy potential malignancy of differentiated stem cells (Rother & Harlan, 2004; Hirshberg, et al, 2003; Shaprio, et al.; 2000). In addition, none of these options address the complex cell architecture that will be necessary for a proper GSIS. Therefore, it can be argued that pursuing option which make human islet transplant more effective poses the highest immediate potential for addressing the islet deficiency.

It has historically been noted that large islets >200μm in diameter do not survive in culture as well as their smaller counterparts, developing necrotic cores while smaller islets showed little core damage (MacGregor et al., 2006). Recently, it has also been shown that

smaller islets show a much better insulin response (MacGregor et al., 2006; Chan et al., 1999), and perform better in hypoxic and normoxic culture (Lehmann et al., 2007).

Previous work has also demonstrated that large isolated islets have poor oxygen utilization, poor survivability following isolation, and secrete less insulin than small islets when normalized for the same volume (Williams et al. 2009). When diabetic rats were transplanted with a marginal mass of large islets, none of them became insulin independent. In contrast, when an equivalent mass of small islets was transplanted into diabetic rats, 80% became insulin independent and remained that way for the 2 month duration of the experiment (MacGregor et al., 2006).

Subsequently, Lehmann et al. determined that small human islets had a higher survival rate during both normoxic and hypoxic culture conditions with a preferential loss of large islets after 48 hours in hypoxic culture. Ultimately, they demonstrated better performance of human islet transplants with a higher percentage of small versus large islets (Lehman, et al. 2007).

A Japanese study (Kaihow et al., 1986) reported that small islets far outnumber large islets in the human pancreata, but constitute only a small percentage of the total islet volume. Since large islets make up the largest percentage of overall transplant mass, but also die with the highest probability, it stands to reason that transplants could be made far more efficient if the large islets could be re-aggregated into smaller islets of optimal size, or sizes, which allow for proper diffusion of nutrients and maximum insulin response.

Engineering Islets

Multiple methods have been reported for aggregating or re-aggregating pancreatic primary cells and other insulin-secreting tumor cells lines, however most have not given control of the aggregate size, thus preventing the issues discussed above. Recent work by Bernard, et al. has shown that using a novel hydrogel-based device, they were able to reform aggregates of mouse insulinoma cells (MIN6) of controlled sizes ranging from 100μm to 250μm in diameter with high precision. In addition, cell viability showed positive results using confocal imaging (Bernard, et al. 2012). Using photolithography to create high-density polyethylene glycol (PEG) microwells of defined precise diameters, cell aggregates can be formed from dissociated pancreata after culture for ~7 days. Our group has recently shown that these aggregates have similar Ca^{2+} dynamics, however caution must be taken.

Despite the promise that such advancements hold, when re-aggregating an organ as complex and reliant on cell-cell communication as the Islet of Langerhans, data must first prove that cell coupling and electrophysiology are similar to intact organs. Though popular, simply measuring insulin release can be a crude way to determine viability. Though accurate, it is impossible to simulate the different conditions of the transplant environment. However, if we can verify that the inner workings of these organs are intact, we can have more confidence in the procedure and its promise for the future. Therefore, this data needs to be backed by mechanistic and mathematical modeling to support further research into human applications.

Percolation Model

Complex network models describe a wide range of systems in nature, and are increasingly used to describe complex intra- and intercellular behaviors. In recent years, they have been used with some success to describe how interacting dynamical systems – be they neurons, power stations, weather or β-cells – behave collectively given their individual dynamics and coupling architecture (Strogatz, 2001).

Random graphs were first studied by famed mathematician Paul Erdos. In their model, Erdos and Albert Renyi define a random graph as N randomly positioned nodes (or points) which are connected by n edges (or lines). Two nodes are connected by an edge with a probability p, and a histogram of the edges per node (or degree distribution) follows a Poisson distribution (Erdos and Renyi, 1959; Bollobas, 1981). Although seemingly simple, this models probabilistic properties have led to many breakthroughs in the study of complex systems.

An interesting finding of random graph theory is the probabilistic clustering behavior of the nodes at different values of p. Specifically, percolation theory predicts the existence of a critical probability p_c such that below this probability the network is composed of isolated clusters of nodes, but above p_c a phase transition occurs and a giant cluster begins to span the network. See figure 12A for example of sub-p_c clustering and emergence of the infinite network. Above P_c, this cluster is called an infinite network since it diverges as the lattice size increases (Albert & Barabasi, 2002).

In contrast to random graph theory, percolation theory starts with a regular d-dimensional lattice of nodes which can only connect to adjacent nodes. Similar to random graphs, an edge is present between two adjacent nodes with a probability p and absent with

a probability 1-p. For example, in a 2-dimensional square lattice, a node can form edges with its 4 adjacent nodes and for the 3-dimensional cubic lattice 6 edges can be formed – all with a probability p. An alternative 'site percolation' model posits that all edges are present, but nodes are occupied with probability p. However, in applications to islet and cell coupling architecture, the bond percolation model is more appropriate since all nodes (cells) are present, but not electrically coupled (Benninger, et al. 2008).

Since islets are highly vascularized and contain ~20% non-excitable cells, two β-cells in close proximity (and potentially adjacent) may not be directly coupled via gap junctions. In addition, heterogeneity in connexin-36 coupling may lead to adjacent β-cells being in different coupling environments. Thus, these aspects of islet architecture lend themselves to description through a percolation model.

Percolation theory has previously described the properties of randomly coupled resistor networks and how these properties can alter the behavior of $[Ca^{2+}]_i$ in coupled systems of β-cells (Benninger, et al. 2008). For instance, the electrical conductance across an islet or cluster of β-cells is proportional to the number of unique paths that can traverse the network. Then a p=0.75 indicates a 75% chance of adjacent β-cell to β-cell connections, and a 25% reduction from maximum conductance of the cell network. As network connections are increased from some $p < p_c$, the number of paths increases until the system reaches criticality and an infinite percolating structures forms. Thus, in percolation pc is the probability below which no percolation can occur and is dependent on the lattice architecture and dimension.

A principle property of percolation theory is that even the most general percolation problem in any dimension obeys a scaling relation near the percolation threshold. These scaling laws are heavily dependent on the architecture and dimension of the node lattice.

For example, an element of the scaling hypothesis is that the correlation length (ξ) for a given cluster diverges near the percolation threshold according the following power law:

$$\xi(p) \sim |p - p_c|^{-v} \qquad as\ p \to p_c$$

Where the critical probability p_c is dependent on the lattice architecture and the critical exponent *v* is dimensional-dependent. The correlation length ξ is a measure of the mean cluster radius and scales with the power law given for cluster size (not shown). Thus, since their size does not scale with their radius to the dimensional power but rather a separate power law, finite percolation clusters have been proven to be fractals for $p \leq p_c$ (Kapitulnick, et al., 1983; Albert & Barbasi, 2002). Further, the percolation probability P, denoting the probability that a given node is part of the infinite cluster is given by

$$P \sim (p - p_c)^{\beta}$$

which scales as a positive power of $p - p_c$ for $p \geq p_c$. Therefore, it is 0 for $p = p_c$ and increases for all $p > p_c$. Conversely, the average size of finite clusters $\left(\langle s \rangle^f\right)$ within the percolation network can be calculated on either side of the p_c, and obeys

$$\langle s \rangle^f \sim |p - p_c|^{-\gamma}$$

diverging for $p \to pc$ (Stauffer & Aharony, 1994).

Although there are many elegant scaling laws which describe cluster size distributions, node correlation length, and intra-cluster coupling of percolation lattices – which have been successfully used to approximate islet electrical coordination (Benninger, et al. 2008) – these laws only hold for $p \to p_c$ (Stauffer & Aharony, 1994). Therefore, for discrete cellular networks with p away from pc, percolation-based simulations (which were historically used to find most of these scaling laws) offer the best mode of model fitting.

Percolation theory was first applied to model the synchronization of islet electrophysiology in a paper by Benninger, et al. Using connexin-36 homozygous knockout, heterozygous and wild type mice (which theoretically correspond to p = 0, 0.5 and ~1, respectively), they were able to demonstrate how disruptions in inter-cell connectivity can lead to erratic behavior of β-cells. In both experimental and computational models, a ~50% decrease in mean coupling conductance was able to disrupt wave propagation and reduce overall synchrony in β-cells.

Considering both wave velocity and proportion of cells in the islet showing synchronized $[Ca^{2+}]_i$ dynamics, they found experimental data fit a percolation model of cell coupling compared to an ohmic model which posits that all cells are coupled and overall coupling is mediated by individual differences in coupling conductance. Furthermore, their model found that p = 0.85 optimally fit experimental wild-type data, indicating that under normal physiological coupling, 85% of neighboring β-cells are electrically coupled, which is in sound agreement which previous data on islet coupling (Moreno, et al., 2005) and the proportion of non-β-cells in the islet (Brissova, et al. 2004).

Application of percolation theory to β-cell dynamics also predicts a phase-transition which can be characterized in both 2D and 3D. For example, since the theoretical Pc = 0.2488 for a 3D cubic lattice (which has been shown to appropriately match coupled β-cells in the islet), ~25% of normal physiological coupling will be insufficient to maintain a synchronized syncytium of β-cells. Therefore, Ca^{2+} would not be able to propagate across the whole islet to coordinate [Ca2+]i oscillations and insulin dynamics at $p<p_c$ would be similar to p = 0 or homozygous knockout Cx36 mice.

Since a loss in insulin pulsatility is often seen in type II diabetics and obese individuals (Porksen, et al. 2002 ; Peiris, et al. 1992) the effects of coupling probabilities and

phase transitions may play a previously understated role in the progression of diabetes as well as the underlying properties of multicellular dynamical systems in general. In addition, this model predicts that at alternative dimensions the differences in coupling alone (even at the same p) can explain the differences in synchronized $[Ca^{2+}]_i$ behavior.

CHAPTER II

MATERIALS & METHODS

Cell Culture and Aggregate Formation

Mouse insulinoma 6 (MIN6) cells (P28-36) were maintained in DMEM supplemented with 10% FBS, 1% penicillin-streptomycin, 0.2% fungizone, 1mM sodium pyruvate and 60μM 2-mercaptoethanol. Media was changed 3 times per week and cells were passaged at ~70% confluency. For passage and seeding, MIN6 cells were briefly washed in Hanks balanced salt solution (HBSS) and then treated with 0.05% trypsin/EDTA. The trypsin was deactivated with growth media. For 2-dimensional aggregates MIN6 cells were seeded at ~4,000cells/mm^2 in glass bottom dishes (MatTek) which aggregate over 5 days in culture.

Three-dimensional (3D) cell aggregates were formed using hydrogel microwell cell culture arrays as previously described (Bernard et al., 2012). Briefly, cell microwell arrays were formed from a prepolymer solution of 10.8 wt% polyethylene glycol (PEG) diacrylate (M_n~3,000 Da, synthesized as previously described (Lin et al., 2009), 4.2 wt% PEG monoacrylate (M_n~400 Da), 0.5 wt% 4-(2-hydroxyethoxy)phenyl-(2-hydroxy-2-propyl)ketone (Irgacure 2959), and HBSS (Figure 1A). Hydrogel microwells were polymerized to glass slides treated with (3-acryloxypropyl)-trimethoxysilane (Gelest) by chemical vapor deposition (Kloxin et al., 2010). Well dimensions were defined by photoinitiation of the prepolymer solution through chrome photomasks (Photo Sciences, 100 μm x 100 μm (w100), 200 μm x 200 μm (w200), and 300 μm x 300 μm (w300) wide.

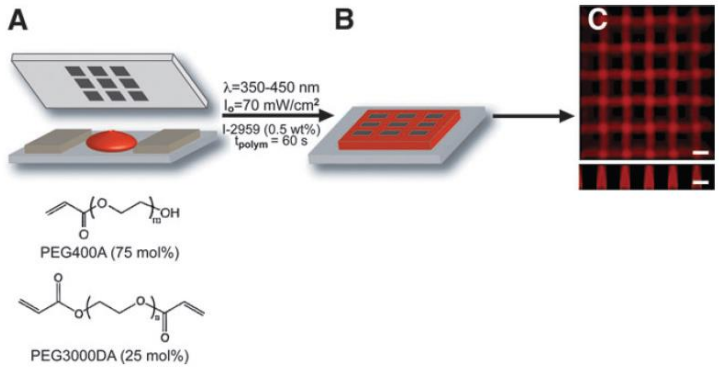

Figure 1: Formation of hydrogel devices for aggregating MIN6 cells. **A)** Photocrosslinkable prepolymer solution (red) consisting of 15 wt% macromere (75mol% PEGA0.4kDa, 25mol% PEGDA3 kDa), 0.5 wt% photoinitiator I2959, and 300 mM methacryloxyethyl thiocarbonyl Rhodamine B in Hank's balanced salt solution was placed between a glass slide and a chrome photomask separated by spacers (tan) of defined thickness. **B)** Microwells formed after ultraviolet light exposure (350–450 nm) for 60 s had been covalently attached to the functionalized glass slide. **C)** Representative confocal image of a microwell device (width and height = 100 mm) in both the x-y plane (top) and x-z plane (bottom). Scale bars represent 100 μm. PEGDA, poly(ethylene glycol) diacrylate.

Inc., Torrance, CA) to form wells (Figure 1B & C) that were approximately 100 μm deep and MIN6 cells were seeded into the wells at a density of 520,000 cells/cm^2 in w100 devices and 940,000 cells/cm^2 in w200 and w300 devices using centrifugation as described previously (Bernard et al., 2012). The devices were rotated on an orbital shaker for 2 hours and then cultured under static conditions in growth media for 5 additional days. 3D aggregates were removed from the microwell devices using a gentle flow of media and selected for experiments using a Leica SL30 dissection microscope (Figure 2).

Prior to the formation of primary cell 3D aggregates, fresh isolated islets were incubated overnight in RPMI (Invitrogen) supplemented with 10% FBS, 1% penicillin-streptomycin, and 0.2% fungizone. To disperse individual cells, islets were twice digested in a solution HBSS with 0.05% trypsin for 30 minutes and centrifuged to collect the cells. The final cell suspension was then seeded on to preformed 100 μm x 100 μm (w100), 200 μm x 200 μm (w200) devices and aggregates were formed as explained above.

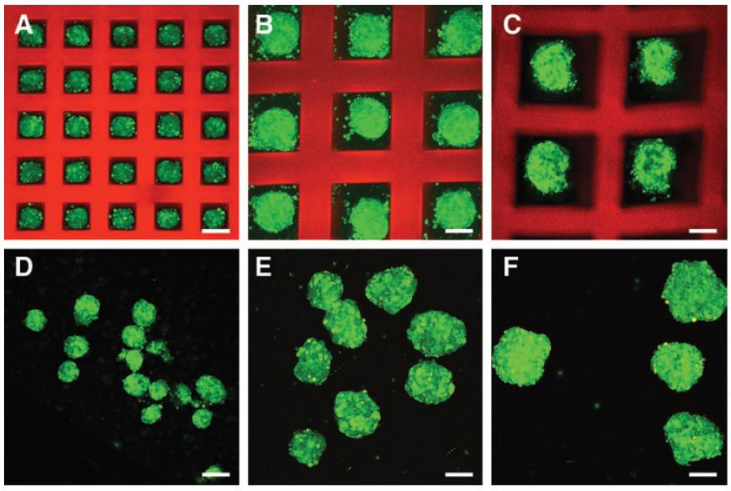

Figure 2: Formation of MIN6 aggregates. Aggregates of MIN6 cells in poly(ethylene glycol) microwell devices. Cells were seeded at a density of $3x10^6$ cells / ml followed by centrifugation. To visualize, cells were stained with CellTracker Green before seeding and confocal images were taken 5 days after seeding **(A-C)** and after removal **(D-F)**. Well widths are 100μm **(A, D)**, 200μm **(B, E)** and 300μm **(C, F)**.

Insulin Secretion

Cumulative, static insulin secretion was measured in order to investigate correlations with the $[Ca^{2+}]_i$ behavior. Two and three-dimensional cell aggregates were formed as described above and cultured for 5 days. MIN6 cell clusters were conditioned in Krebs-Ringer Buffer (KRB, 128.8 mM NaCl, 5 mM $NaHCO_3$, 5.8 mM KCl, 1.2 mM KH_2PO_4, 2.5 mM $CaCl_2$, 1.2 mM $MgSO_4$, 10 mM Hepes, 0.1% BSA) containing 2 mM glucose for 1 hour prior to the glucose stimulation assay. Aggregates were then incubated in KRB containing either 2 mM glucose (low glucose), 20 mM glucose only (high glucose), or 20 mM glucose and 20 mM TEA (+TEA) for one hour. Supernatant from each sample was collected and stored at -70°C until testing. Supernatant samples were tested using a sandwich ELISA per the manufacturer's instructions (Mercodia). Total insulin secreted was normalized to basal secretion levels.

Microscopy

To measure $[Ca^{2+}]_i$ dynamics, 2- and 3-dimensional aggregates were stained with 4μM Fluo4-AM in imaging medium (125mM NaCl, 5.7mM KCl, 2.5mM $CaCl_2$, 1.2mM $MgCl_2$, 10mM Hepes, 2mM glucose, and 0.1% BSA, pH 7.4) at room temperature for 60-90 minutes before imaging. 2D aggregates were imaged in glass-bottom dishes, and 3D aggregates were imaged in polydimethylsiloxane (PDMS) microfluidic device, the fabrication of which has been previously described (Rocheleau, et al., 2004). Real-time imaging was performed on a Nikon Eclipse Ti equipped with a humidified environmental chamber maintained at 37°C. Fluo4 fluorescence was imaged with a 20x 0.8NA objective, using a Xenon-arc lamp light source (Sutter) and 470/20 filter for excitation and 525/36 filter and a CCD camera (Andor Clara) for fluorescence detection. Aggregates were allowed to equilibrate after each treatment for 10 minutes before imaging at 1 frame/s for 15 minutes, with negligible photobleaching observed.

Matlab Analysis

In signal processing, cross correlation is the measure of similarity between two waveforms with a time-lag, or phase shift, applied to one of them. To calculate $[Ca^{2+}]_i$ coordination of a cell cluster, a cross correlation function was used to determine the level of similarity of the waveforms generated by the fluorescent intensity of the imaging time course. The average fluorescent intensity of a selected area of the cell cluster or aggregate was used as the reference waveform and then the cross correlation was performed between this reference waveform and the fluorescent intensity waveform of each pixel in the cluster (Figure 3A). The cross correlation function measures waveform similarity by sliding one

wave function across the other and calculating the integral of the overlapping area. At each interval a cross correlation coefficient is calculated in this way, with 1 indicating perfect overlap and 0 indicating none. For example, a cross correlation coefficient of 1 would indicate that a certain pixel is in perfect synchronization with the reference area, whereas a coefficient of 0 means there is no similarity. The maximum cross correlation coefficient was used as a measure of similarity and a value above 0.75 was used as a threshold as to whether a certain cell was correlated with the cell cluster or aggregate as a whole. Therefore, the total area of the cluster with a cross correlation coefficient above 0.75 was used as a measurement for the overall correlation, or synchrony.

The information describing cell synchronization and areas of coordination is represented as a false color hue-saturation-value image where the hue (color) represents the cross correlation coefficient or period of oscillation, saturation (the amount of color) is set to one and value (intensity) represents the average fluorescence intensity in order visualize cell localization.

Based on the presumption that the cumulative standard deviation of the fluorescent intensity of a silent cell will be much less than that of an active cell, the mean and plus three times the standard deviation of the 'silent cell' fluorescent intensity was compared to the total standard deviation of the measured fluorescence intensity of each pixel in the rest of the cluster. If the standard deviation in fluorescence of a pixel was higher, it was deemed to be active. This was accomplished by a custom-written program which would calculate the standard deviation of the fluorescent intensity across the entire time course of a selected a silent cell, then compare that with every pixel within the entire cell cluster. Silent cells were selected by looking at a cells fluorescent waveform in a software package (Nikon Elements).

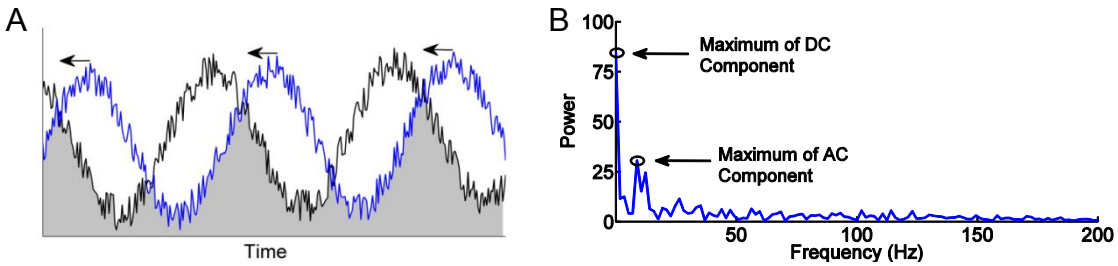

Figure 3: Explanations of computational methods. **A)** Cross correlation analysis calculates a sliding integral of the overlap between the test wave (blue) and the stationary reference wave (black). The maximum cross correlation coefficient is achieved at the point of maximum overlap. **B)** Sample power spectrum from experimental data. Power robustness was calculated by normalizing the maximum value of the AC component with the maximum value of the DC component.

Only cells with relatively flat responses were used as the silent cell reference. The size of each cluster or aggregate, as well as the regions of coordination within them, was determined by manually tracing the boundaries in a custom written Matlab program, which then tabulated the pixels within the boundaries. Average cell size in both two dimensional aggregates and three dimensional clusters were also determined and found to be approximately 14μm in diameter, which is in agreement with previous work (Ni, et al. 2010). To determine aggregate cell number, the radius was found from the area and then used to calculate volume using a spherical formula, which was then divided by the volume of a single cell. Two dimensional cell cluster area was found by dividing the total area of the cluster by the area of a cell.

To determine whether there is a maximum distance over which cells are coupled, a Matlab program was written to calculate the Euclidian distance of over which cells in a cluster were coordinated. A cell within a cluster was isolated by tracing its boundaries and the average fluorescent intensity was calculated over the entire time course to give a representative waveform of that cells. A cross correlation was performed between that

reference waveform and each other pixel in the cell cluster and a value higher than 0.75 indicated that that pixel was correlated with the reference cells. Therefore, the distance over which the pixels maintained a coefficient higher than 0.75 was used as a measure of the correlation distance of the cells.

To extract data regarding phase and period, a Fourier Transform was performed on the fluorescent intensity profile of each pixel. The power spectrum from the Fourier Transform tells us how much of the fluorescent signal is at a particular frequency. For example, in a sine wave where there is one frequency, there would be a single impulse. In a noisier signal of the same average fluorescence intensity there may be multiple peaks corresponding to multiple frequencies in the signal, though the area under the spectrum will be the same. The 'DC' component of the power spectrum, located at the zero frequency, corresponds to the average value of the signal (Figure 3B), and is typically removed (Najarian & Splinter, 2012). To measure the robustness, or regularity, of the period in $[Ca^{2+}]_i$ oscillations, the maximum value of the power spectrum with the DC component removed was normalized to the maximum value of the power spectrum with the DC not removed to normalize for the variability in fluorescent signal (Figure 3B). The maximum value of the power spectrum was also used to find the period of oscillation for each pixel, which was then mapped (using the HSV format explained above) to investigate coordination in frequency of $[Ca^{2+}]_i$ oscillations.

Wave propagation was determined by selecting two cells within a two dimensional cluster or three dimensional aggregate which were separated by approximately 100μm and measuring the temporal offset between successive identical parts of a $[Ca^{2+}]_i$ wave. The velocity is calculated in the direction of the wave propagation by dividing the exact spatial separation by the temporal offset of the $[Ca^{2+}]_i$ wave.

All statistics were performed in Matlab (Mathworks, Natick, MA). For comparison of two means, Student's t test was utilized. For comparison of multiple means, ANOVA was utilized. To compare determine whether linear relationships existed between a variable and cell number, a linear regression model was used.

Development of KIR2.1 and Connexin-36 Knockout Mice

Mutant KIR6.2[AAA] constructs containing green fluorescence protein (GFP) were generated by replacing the tripeptide sequence 132GFG134 of the ion selectivity filter KIR6.2 with nonpolar alanine residues. After verifying functional expression in a β-cell lines through transient transfection, constructs were purified and microinjected into fertilized mice eggs. Transgenic mice were identified through PCR on using GFP-specific primers (Koster et al., 2000; Koster et al., 2001). To establish a stable line, one KIR6.2[AAA] founder was identified and bred back to littermates.

Bond Percolation Simulations for Size-Scaling and Dimensionality Comparisons

Bond percolation is a sub-model of percolation theory in which for a given lattice of nodes (cells) adjacent nodes are connected (coupled) with a probability p, or not connected with a probability $(1-p)$. This is in contrast to site percolation, in which all edges are present but nodes only exist with a probability p. In a 2D or 3D aggregate all cells are present; however, whether the cells are coupled varies according to size-scaling and dimensionality laws. Therefore, a bond percolation model was established to model cellular coordination on a 2D square lattice or 3D cubic lattice where each node (cell) is capable of establishing connections with its 4 or 6 adjacent neighbors, respectively. The bond percolation lattice

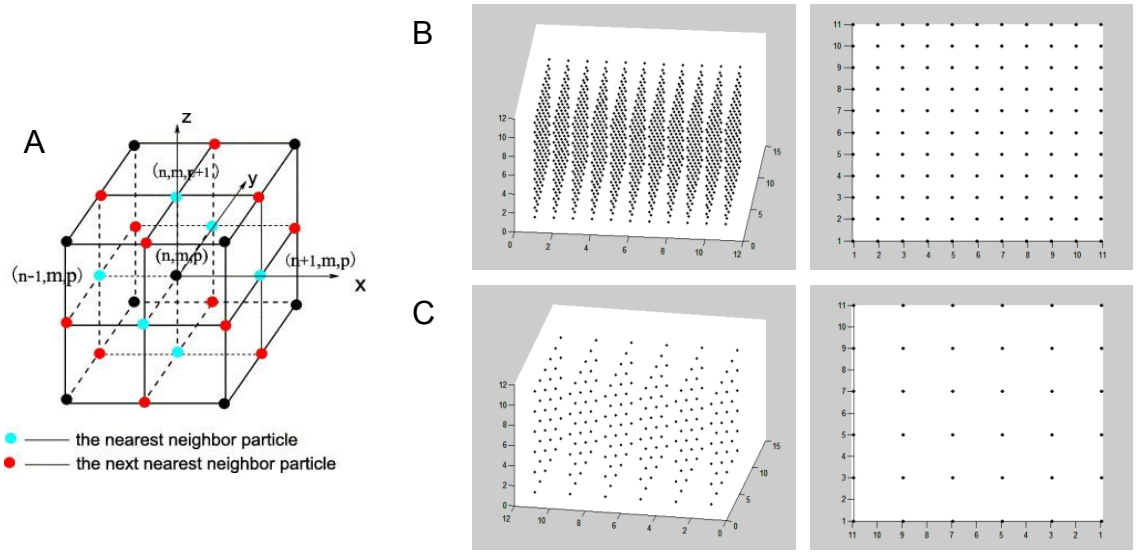

Figure 4: Overview of bond percolation lattice. **A)** Visual representation a cubic lattice with bonds to all 6 nearest neighbors, representing a p = 1. **B)** Visualization of the 11x11x11 lattice created for the percolation model in Matlab at p = 0, representing the nodes only without cells. The left panel is a top view demonstrating the equal spacing for edges, which are not present. **C)** Visualization of the 5x5x5 lattice created for the percolation model in Matlab at p = 0, representing the nodes only without cells. The left panel is a top view demonstrating the equal spacing for edges, which are not present.

was developed in Matlab with a matrix of alternating values of 1 (node) and 0 (site for potential edge bond). Probabilities were randomly assigned to each edge bond point. If the probability was less than or equal to the assigned percolation probability (p), an edge was established and the 2 neighboring nodes were deemed coupled. An identification number was assigned to each individual cluster formed from coupled edges, and the edges were then removed to establish clusters based solely on node coupling (Figure 4A, second panel).

<u>High Glucose (Synchronization) Simulations</u>

Simulations of high glucose coupling were carried out with a custom MATLAB routine based on a previously published method (Kapitulnik, et al. 1983). Two dimensional clusters of 25x25 nodes were populated with edge probabilities based on a Gaussian

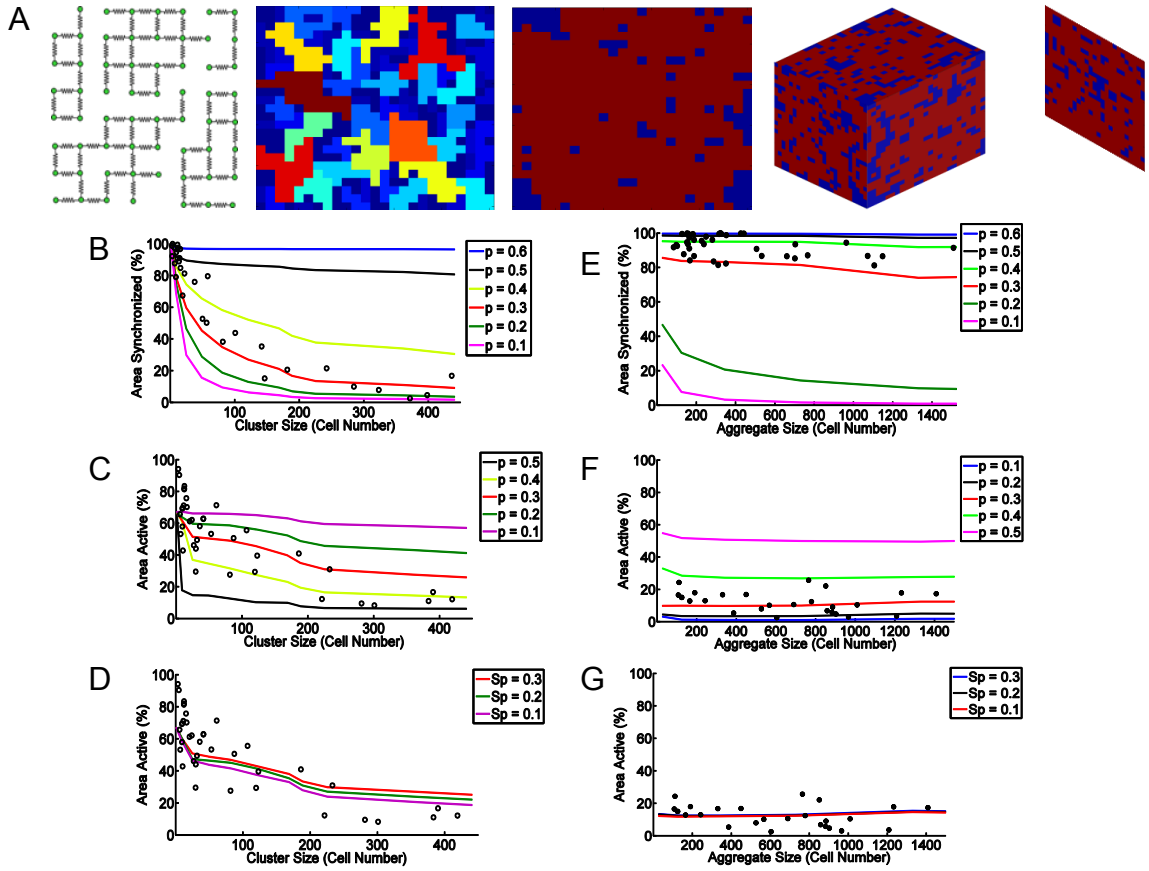

Figure 4: Summary of resistor network model. **A)** False-color simulation of cluster size for bond percolation with p below (left) and above (middle) the critical probability. (Right) Resistor network showing behavior above the critical probability. **B)** Simulations and experimental data of oscillation synchronization for values of p at high glucose in 2D. **C)** Simulations and experimental data of $[Ca^{2+}]_i$ activity for values of p at low glucose in 2D. **D)** Simulations and experimental data of $[Ca^{2+}]_i$ activity for values of the percent of cells within a cluster necessary to suppress $[Ca^{2+}]_i$ activity of the entire cluster (Sp) in 2D. **E)** Simulations and experimental data of oscillation synchronization for values of p at high glucose in 3D. **F)** Simulations and experimental data of $[Ca^{2+}]_i$ activity for values of p at low glucose in 3D. **G)** Simulations and experimental data of $[Ca^{2+}]_i$ activity for values of the percent of cells within a cluster necessary to suppress $[Ca^{2+}]_i$ activity of the entire cluster (Sp) in 2D.

distribution and clusters were formed based on a whether adjacent connections had assigned probabilities greater than, or equal to, the critical probability (Figure 5A). We next identified the largest cluster on each of the simulated lattices and selected only those in which the central lattice site belonged to the cluster. The mass of the percolating area, or

M(L), was determined by summing the connected nodes to the central cluster within squares of area L^2 around it. By averaging these over the area of the simulated cluster sizes, we found the percolation density

$$\rho(L) = \frac{M(L)}{L^2}$$

We then deemed that if any two cells were coupled to the same network, they were synchronized. Therefore the percolation density is analogous to the synchronized area of each cluster. For each value of p, 1,000 simulations were run (Figure 5B) and best fit to experimental data was determined by a chi-square test.

Low Glucose (Suppression) Simulations

In contrast to modeling high glucose $[Ca^{2+}]_i$ activity, where all cells within a network are deemed synchronized, low glucose modeling was based on the principle that a certain percentage of non-responsive cells can hyperpolarize and suppress the activity of all other cells in a coupled network. A linear fit to the experimental low glucose data showed a y-intercept value of 67%, indicating that that there is approximately a 2/3 probability that a given cell will be active. We then used this probability in a binomial model, which describes the number of successes k (active cells) in a number of trials n (total cells in a cluster), with each success having a probability p (67%). Or,

$$\Pr(X = k) = \binom{n}{k} p^k (1-p)^{n-k}, \text{ where}$$

$$\binom{n}{k} = \frac{n!}{(n-k)!\,k!}$$

After establishing bond percolation clusters as in the high glucose model, the cell number of each cluster (n) was then determined and the probability of the cell being active was calculated using the binomial model. For each value of p and k, 2,000 simulations were run, and best fit to experimental data was determined by a chi-square test (Figure 5B).

Bond Percolation Simulations for Discrete Modeling of Islet Connectivity

To examine how our mathematical model can predict islet $[Ca^{2+}]_i$ and insulin behavior when the system is perturbed through transgenic mutation of the K_{ATP} channel or Cx36 gap junctions, the simulations of high glucose were run to calculate percent synchronization as a function of p for varying cell diameters. In addition, the level of suppression was simulated in the low glucose model for varying levels of p and the probability of a cell being active for varying network diameters.

CHAPTER III

RESULTS: DIMENSIONALITY AND SIZE-SCALING OF COORDINATED Ca^{2+} DYNAMICS IN PANCREATIC β-CELL NETWORKS

$[Ca^{2+}]_i$ Dynamics and Insulin Secretion Under Two- and Three-Dimensional Coupling

Under normal physiological conditions at high glucose, β-cells within the islet of Langerhans undergo robust oscillations in $[Ca^{2+}]_i$. These individual $[Ca^{2+}]_i$ oscillations are synchronized through cell-cell gap junctions and results in a transverse Ca2+ wave across the islet which coordinates pulsatile insulin secretion (Head, et al., 2012; Macdonald & Rorsman, 2006). However, the underlying architecture and coupling has been shown to have large impacts on this synchronized behavior.

In order to investigate how the underlying cellular architecture and electrical coupling affects the robustness and synchronization of $[Ca^{2+}]_i$ dynamics in β-cells, we analyzed $[Ca^{2+}]_i$ time-courses in 2D cell clusters and 3D aggregates of defined size and shape. Under 2D coupling, cell clusters generally exhibited irregular bursts of $[Ca^{2+}]_i$ at high glucose, which became more regular upon addition of the K_{ATP} channel inhibitor TEA (Figure 6A) . As quantified from the robustness of the Fourier power spectrum, TEA at high glucose was found to significantly increase the robustness of the oscillation period compared to high glucose alone ($p<0.01$) (Figure 6C). This increase in regularity of the period was expected given that blockage of the K_{ATP} channels has previously been shown to increase resting membrane potential and therefore render β-cells more sensitive to changes in V_m and inter-cellular coupling (Bokvist, et al., 1990)

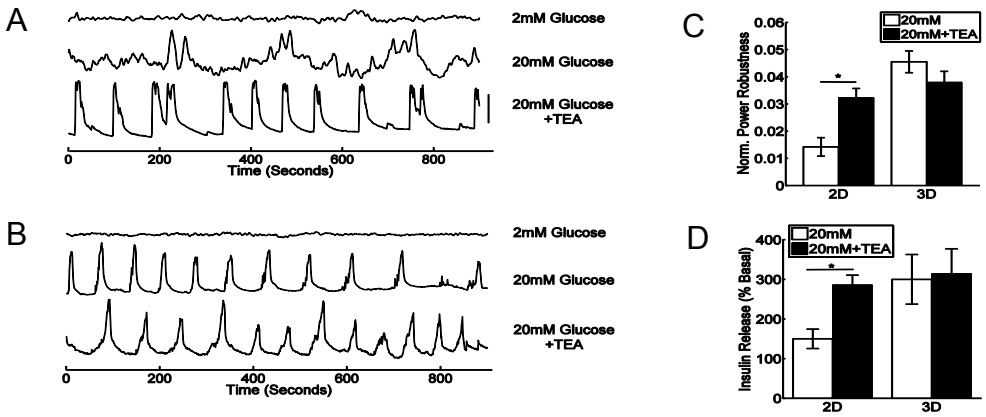

Figure 6: Robust $[Ca^{2+}]_i$ oscillations and insulin release in 3D aggregates. **A)** Representative $[Ca^{2+}]_i$ oscillations, measured from Fluo-4 fluorescence, averaged over a 2D aggregate. **B)** As in A, averaged over a 3D aggregate of comparable size. Time-courses are offset for clarity and vertical scale bar represents 50% change in fluorescence. **C)** Mean (±s.e.m.) power robustness at 20mM glucose and 20mM glucose +20mM TEA. **D)** Mean (±s.e.m.) insulin release as % of content, normalized to release at 2mM glucose. Data in C averaged over n=28 (2D) and n=22 (3D) aggregates, and data in D averaged over n=6 (2D) and n=12 (3D) aggregates. * in C, D indicates significant difference between glucose and glucose+TEA for power robustness ($p=0.00015$) and insulin release ($p=0.0166$).

In contrast, under 3D coupling aggregates exhibited highly regular $[Ca^{2+}]_i$ oscillations both in the presence and absence of TEA (Figure 6B). The robustness of the 3D oscillations showed no significant differences ($p>0.05$) upon addition of TEA and was significantly more robust compared to 2D clusters under high glucose alone, but not 2D under high glucose with TEA (Figure 6C).

Similarly, the insulin secretion response demonstrated a similar pattern to the $[Ca^{2+}]_i$ oscillation robustness. In 2D aggregates, high glucose with TEA stimulated a significantly greater insulin secretion compared to high glucose alone. However, the addition of TEA was not found to have an effect on 3D insulin secretion at high glucose (Figure 6D). Therefore, this data demonstrates that the aggregation of β-cells into

structures which allow for 3D coupling increases the robustness of the oscillatory $[Ca^{2+}]_i$ response and leads to higher levels of insulin secretion at high glucose.

Dimension and Size-Dependence of $[Ca^{2+}]_i$ Synchronization

To investigate the spatial variation of $[Ca^{2+}]_i$ dynamics, we next measured the synchronization of $[Ca^{2+}]_i$ oscillations in 2D and 3D under high glucose with and without TEA. In 2D aggregates at high glucose with TEA, oscillations were found to be synchronized within distinct sub-regions of the cell cluster (Figure 7A). Compared to the oscillations in a specific cell, the synchronization of the oscillations in other cells decreased as a function of increasing distance. Using a cross correlation function, we found that these oscillations were highly synchronized within a radius of approximately 5 cells. However, at greater distances there was a sharp decrease with little synchronization observed. The change was sudden, with adjacent cells showing different oscillatory $[Ca^{2+}]_i$ patterns suggesting they are part of different electrophysiological coupling environments (Figure 7B). In contrast, 3D aggregates at high glucose with TEA showed synchronization that was consistent across the entire cell mass (Figure 7C). Most cells showed synchronized oscillations, independent of separation distance and position with in the aggregate (Figure 7D).

Given that cells were only synchronized within a limited Euclidean distance (~5 cells) in 2D, we anticipated that smaller 2D aggregates with less than a 5 cell radius would show a greater proportion of cells that were synchronized. Indeed, 2D cell clusters consisting of <20 cells were highly synchronized (Figure 7F), with a percentage of synchronized cells that was not different compared to 3D aggregates ($p<0.05$) (Figure 7E).

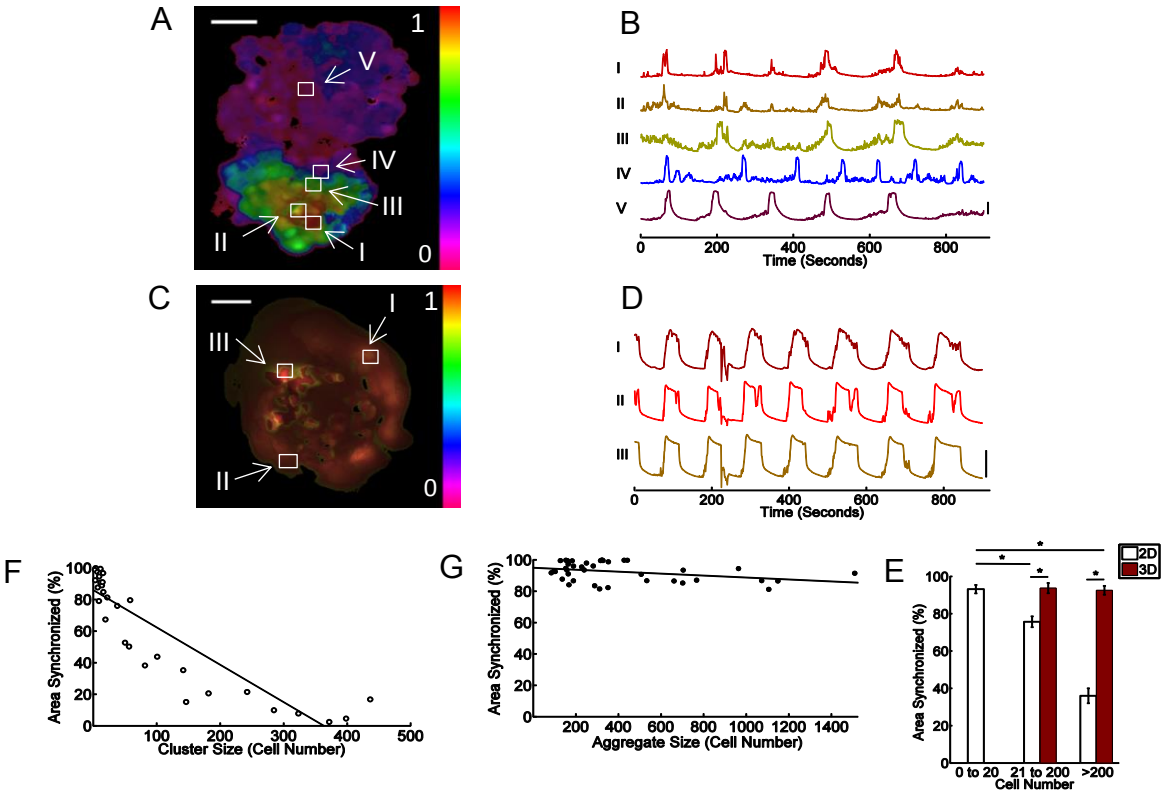

Figure 7: Size scaling and dimensionality of $[Ca^{2+}]_i$ oscillation synchronization. **A)** False-color map of the cross-correlation coefficient in a 2D aggregate, relative to a reference cell (I). **B)** Fluo4 time-courses in cells at increasing distance from the reference cell (II-V). **C)** False-color map of the cross-correlation coefficient in a 3D aggregate, relative to a reference cell (I). **D)** Fluo4 time-courses in cells well separated from the reference cell in 3D (II, III). **E)** Mean (±s.e.m.) area of aggregate showing synchronized $[Ca^{2+}]_i$ oscillations, in 2D and 3D aggregates of different size ranges at 20mM glucose +20mM TEA. **F)** Scatterplot of synchronization versus aggregate size, for 2D aggregates at 20mM glucose +20mM TEA. **G)** As in F for 3D aggregates. * in E indicates significant difference in synchronization of larger 2D aggregates (21-200 and >200) compared to small aggregates (<20), and a significant difference in synchronization comparing 2D and 3D aggregates ($p<0.001$). Linear regression in F, G indicated by solid line, with significant size dependence in F and G ($p < 0.0001$).

However, larger 2D aggregates above the critical size showed a significant reduction in synchronization with increasing size compared to 3D aggregates containing an equivalent number of cells ($p>0.01$) (Figure 7E). Interestingly, in larger 2D cell clusters above the critical size there were multiple clusters of cells which were highly synchronized,

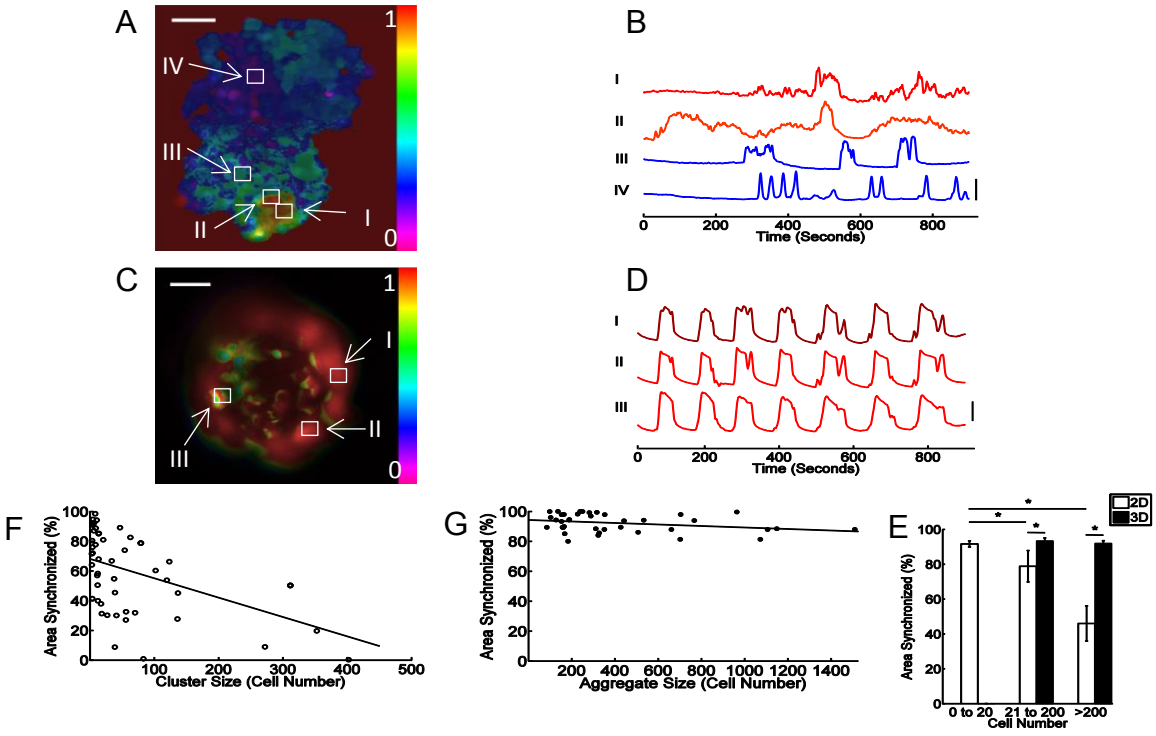

Figure 8: Size scaling and dimensionality of $[Ca^{2+}]_i$ oscillation synchronization at 20mM glucose. **A)** False-color map of the cross-correlation coefficient in a 2D aggregate, relative to a reference cell (I). **B)** Fluo4 time-courses in cells at increasing distance from the reference cell (II-V). **C)** False-color map of the cross-correlation coefficient in a 3D aggregate, relative to a reference cell (I). **D)** Fluo4 time-courses in cells well separated from the reference cell in 3D (II, III). **E)** Mean (±s.e.m.) area of aggregate showing synchronized $[Ca^{2+}]_i$ oscillations, in 2D and 3D aggregates of different size ranges at 20mM glucose +20mM TEA. **F)** Scatterplot of synchronization versus aggregate size, for 2D aggregates at 20mM glucose +20mM TEA. **G)** As in F for 3D aggregates. * in E indicates significant difference in synchronization of larger 2D aggregates (21-200 and >200) compared to small aggregates (<20), and a significant difference in synchronization comparing 2D and 3D aggregates ($p<0.01$).

supporting the notion of a defined distance over which cells can coordinate.

Synchronization in 3D aggregates also showed a size-dependence up to the 300μm diameter, however the slope of the line was much more shallow (Figure 7G). Similar results were seen in 2D and 3D aggregates under high glucose alone. However, the radius of synchronization was found to be far less (~2 cells) (Figure 8).

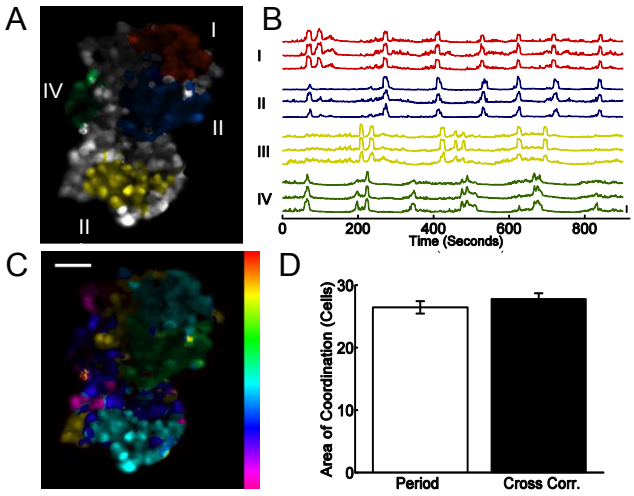

Figure 9: Localization of synchronized $[Ca^{2+}]_i$ oscillations to discrete regions in 2D. **A)** False-color map of regions of high cross-correlation coefficient in a 2D aggregate, with respect to different reference cells. **B)** Fluo4 time-courses of cells within each area of synchronization in A. **C)** False-color map of $[Ca^{2+}]_i$ oscillation period in same 2D aggregate as A. **D)** Mean (±s.e.m.) area of oscillation period (Period) and area of high cross-correlation coefficient (Cross corr). Data averaged over n=28 clusters. No significant difference is observed (p=0.3147).

Therefore, this data indicates that not only can cells coordinate over a defined region, but the size of 2D β-cell clusters can have a significant impact on [Ca2+]i synchronization. In addition, the dimensionality of the coupling is critical to properly synchronize an entire syncytium of electrically excitable cells.

Sub-Regions of Synchronization in Two-Dimensional Cell Clusters

To further investigate the limiting range over which 2D cell clusters can synchronize $[Ca^{2+}]_i$ oscillations, we measured the extent of synchronization at different positions within cell clusters. Qualitatively, multiple non-overlapping areas of synchronized $[Ca^{2+}]_i$ oscillations and similar period were observed within large cell clusters (Figure 9A).

Importantly, regions with similar oscillation period as found from the Fourier power spectrum overlapped strongly with regions of synchronization as found by our methods. There was not found to be a difference between the area of synchronization as found by either method (Figure 9D), validating the 0.75 cross correlation coefficient threshold. Within the cell cluster, the largest area of synchronization was similar to the largest region with similar oscillation period, with a mean size of ~28 cells (Figure 9D). In addition, regions of similar period as defined through Fourier mapping produced similar results compared to cross correlation mapping independent of which cell within the area was chosen as the reference (Figure 9 A & C). This indicates that areas of synchronization are well-defined through local interactions in 2D.

Wave Velocity Under Two- and Three-Dimensional Coupling

Calcium dynamics are synchronized within the islet through intercellular coupling, where elevations in $[Ca^{2+}]_i$ propagate across the islet from regions of higher glucose sensitivity (Benninger, et al., 2008; Aslanidi et al., 2001; Bertuzzi, et al., 1999). The velocity of the Ca^{2+} wave propagation has been linked to β-cell coupling where reduced coupling across the islet results in slower waves and less overall $[Ca^{2+}]_i$ coordination (Benninger, et al., 2008). To further characterize the effects of dimensionality on the coupling behavior of β-cells, we measured the propagation velocity in 2D and 3D. In 2D aggregates, Ca2+ waves were confined to the sub-regions of synchronization (~100μm). As characterized by the temporal offset of peak $[Ca^{2+}]_i$ between two cells ~100μm apart, the mean wave velocity was found to be significantly higher in 3D aggregates compared to the 2D sub-regions (Figure 10A-C). The distribution of wave velocities was also biased to waves >50μm/s in 3D aggregates compared to a bias towards <50μm/s waves in 2D (Figure 10D).

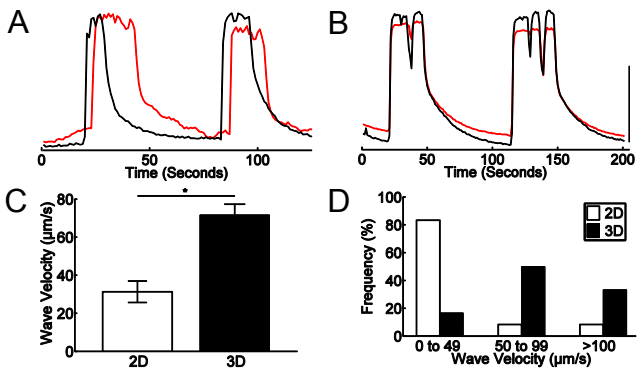

Figure 10: Dimensionality affects wave propagation velocity. **A)** Fluo4 time-course for two cells within a 2D aggregate separated by ~100μm, at the wave start (black) and wave end (red). **B)** As in A, for time-course at the wave start and end within a 3D aggregate. **C)** Mean (±s.e.m.) wave velocity in 2D and 3D aggregates. **D)** Histogram of measured wave velocities in 2D and 3D aggregates. Data averaged over n = 18 (2D) and n=12 (3D) aggregates. * in C indicates significant difference in wave velocity ($p<0.001$).

Therefore, 2D aggregates show slower propagating Ca2+ waves compared to 3D aggregates, which further suggests that 2D cells are less coupled and that dimensionality plays an important role in β-cell synchronization.

Dimension and Size-Dependence of Basal $[Ca^{2+}]_i$ Suppression

Intact islets area also characterized by a uniformly quiescent $[Ca^{2+}]_i$ at low/basal glucose as a results of the suppressive hyperpolarizing effect of β-cell coupling (Benninger, et al., 2011; Speier, et al., 2007). Therefore, given the dependence of $[Ca^{2+}]_i$ dynamics on size and dimensionality of the cellular architecture, we next measured whether $[Ca^{2+}]_i$ suppression had a similar dependence at low glucose. Under low glucose conditions (2mM), 2D cell clusters generally exhibited spontaneous, transient $[Ca^{2+}]_i$ activity, whereas 3D aggregates remain quiescent. Interestingly, large 2D cell clusters consisting of >200 cells were mostly quiescent, showing similar activity to that measured in 3D aggregates

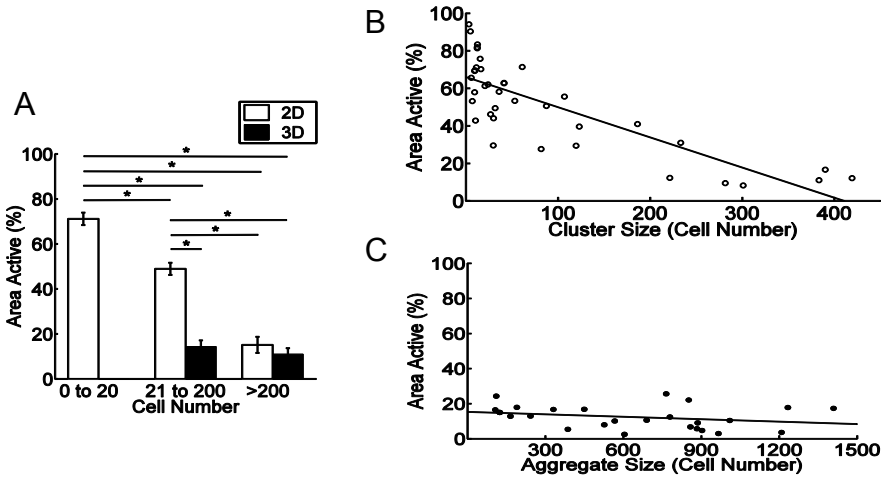

Figure 11: Size scaling and dimensionality of $[Ca^{2+}]_i$ suppression at low glucose. **A)** Mean (±s.e.m.) area of aggregate showing transient $[Ca^{2+}]_i$ elevations in 2D and 3D aggregates of different sizes at 2mM glucose. **B)** Scatterplot of transient $[Ca^{2+}]_i$ elevations versus aggregate size, for 2D aggregates. **C)** As in B for 3D aggregates. * in A indicates significant difference in transient $[Ca^{2+}]_i$ elevations of small 2D aggregates (<20) compared to larger aggregates (20-200, >200), and a significant difference in elevation comparing 2D and 3D aggregates at moderate size (20-200, $p<0.001$), but not very large clusters (>200, $p>0.05$). Linear regression in B,C indicated by solid line, with significant size dependence in B ($p < 0.001$), but not in C ($p > 0.05$).

($p<0.001$)(Figure 11A). However, smaller 2D cell clusters were found to be more active compared to 3D aggregates of similar cell number and larger 2D cell clusters ($p<0.001$).

In the smallest 2D aggregates, 67% of the cells showed a transient $[Ca^{2+}]_i$ elevation with a progressive decrease in activity with increasing cluster size, suggesting that β-cell suppression is size-dependent 2D (Figure 11B). In contrast, 3D aggregates showed a size-independent suppression with ~20% active cells over the entire range of sizes measured, up to 300μm diameter (Figure 11C).

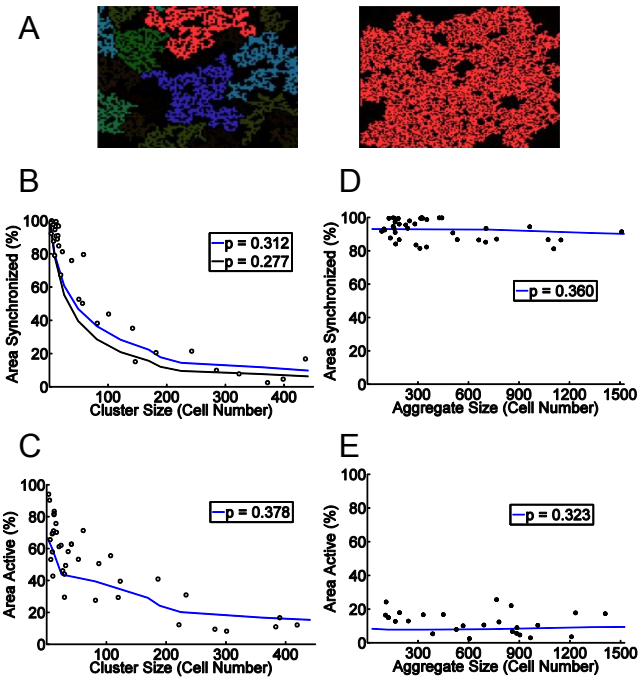

Figure 12: Coupled resistor network model of size scaling and dimensionality. **A)** Simulated networks for different probabilities of resistive coupling connections (*p*), where low numbers of connections give sub-critical behavior with multiple sub regions of connected units (left) but high numbers of connections give super-critical behavior with connecting units spanning the entire network (right). **B)** Simulation and experimental data of oscillation synchronization for 2 values connection probability *p.* Circle represents experiment, solid blue line represents p=0.27 (χ^2 = 8.01) and solid red line represents p=0.32 (χ^2 = 3.89). **C)** Simulation and experimental data of transient elevations with p=0.32 (χ^2 = 12.31). Each line represents an average over n=2000 simulations.

Network Lattice Model of $[Ca^{2+}]_i$ Dynamics

As previously outlined, a lattice resistor model has been used to accurately describe the dependence of $[Ca^{2+}]_i$ dynamics on coupling strength between β-cells (Benninger, et al., 2008). Therefore, we next set out to put our results in mathematical context by testing whether such a model could describe the size and dimensional-dependence of synchronized $[Ca^{2+}]_i$ oscillations and suppression. Our initial methodology centered on using established power laws which describe the average size of a cluster, the average correlation distance

and percolation probability of a random percolation network. However, using this approach we could not accurately reproduce our experimental results, especially in the 3D case. This is most likely due to the fact that these power laws only obey the scaling relation near the percolation threshold, which is p_c=0.5 for 2D square and p_c=0.2488 for 3D cubic lattices.

Therefore, to circumvent the scaling relations, we simulated partially coupled resistor networks covering different sizes over 2D and 3D for a given proportion of node (cell) connectivity. In a 2D network for sub p_c ($p<0.5$) connectivity, multiple small clusters of connected nodes were generated which were similar to the sub-regions of synchronized oscillations measured in 2D aggregates (Figure 12A). For higher connectivity ($p>0.5$) in 2D and 3D, a single cluster of connected nodes emerged which spanned the whole network.

This network-spanning behavior was similar to the uniform synchronization seen in 3D aggregates at high glucose and suggests that the network model simulations can be related to $[Ca^{2+}]_i$ oscillation synchronization: β-cells are synchronized if their corresponding nodes belong to the same connected cluster, with an unbroken path traced between the nodes.

We next tested whether this network model could quantitatively describe the $[Ca^{2+}]_i$ oscillations synchronization, as well as reconcile the differences seen with regards to dimension and size. We initially simulated low connectivity 2D networks for varying p. As predicted by previous percolation work, as p decreases from p_c multiple fractal clusters begin to form (Kapitulnick, et al., 1983). A p=0.32±0.005 generated multiple synchronized clusters with a mean size of 28 nodes, which is similar to the experimentally determined number of cells in the largest synchronized cluster in 2D networks. Following Kapitulnick, et al. we then measured the proportion of nodes in the largest synchronized cluster relative to the total network for varying network sizes (9 to 441 nodes on a square lattice). A

p=0.312 (95% CI: 0.284-0.337) generated a size variation which best fit the experimental 2D synchronization data (Figure 12B)and is in close agreement with the p describing the number of cells in a 2D synchronized region.

The scaling laws of percolation theory are proven for infinite networks and therefore become more applicable as the network size becomes very large ($n \to \infty$). Based on the power law concerning characteristic cluster size

$$\langle n_s \rangle = |p - p_c|^{-\gamma}$$

a p=0.253 was found to generate an average cluster size of 28 cells, which is outside of the 95% confidence interval bounds found by simulation. However, when the simulation was run to best fit data for >250 cells, a p=0.277 generated a best fit. Therefore, as cluster size increase in the 2D model the behavior may better converge to that of the scaling laws.

In the 3D model, a p=0.369 (95% CI: 0.334-0.423) generated a size variation which best fit the experimental synchronization data (Figure 12D), which is in sound agreement with the 2D model as demonstrated by the overlapping 95% confidence intervals. Therefore, taken together this data shows that the size dependence of multiple independent parameters representing $[Ca^{2+}]_i$ oscillations at high glucose can be quantitatively described by the lattice resistor network model. Of note is the fact that both cases generated similar p, indicating the probability of coupling may be conserved across dimensions. However, this value of p corresponds to sub-critical, fractured percolation in 2D and super-critical percolation in 3D.

We next tested whether this same network model could also describe the suppression of spontaneous $[Ca^{2+}]_i$ elevations at low glucose. Inexcitable β-cells can suppress the activity in excitable β-cells through gap junctions electrical coupling (Head, et

al., 2012), and therefore also lends itself to description through the percolation model. To determine whether cells were active or silent within the model, we defined a rule were a threshold proportion of the inexcitable cells within a connected cluster can suppress activity in all cells in the connected cluster. Based on our experimental measurement that 67% of single cells are active, binomial statistics were used to determine whether there were sufficient inexcitable cells to reach the suppression threshold. Naturally, as n becomes large the probability of the entire cluster being quiescent increases.

In both 2D and 3D there was a strong agreement between experimental data and network model with a threshold of 15% inexcitable cells, whereas the data was best fit by p=0.378 (95% CI:0.354-0.398) in 2D (Figure 12C) and p=0.323 (95% CI:0.302-0.346) in 3D (Figure 12E). Therefore, not only can the size-dependence of spontaneous $[Ca^{2+}]_i$ suppression can be quantitatively described by a lattice network architecture, but the values of the percolation probability were found to be similar to those that describe high glucose $[Ca^{2+}]_i$ oscillations.

CHAPTER IV

RESULTS: REAGGREGATION OF PRIMARY ISLET CELLS INTO 'PSEUDO-ISLETS' OF DEFINED SIZE BY MICROWELL CELL CULTURE

Primary Islet Cells Uniformly Aggregate to Defined Sizes in 3D PEG Microwell Arrays

Islet transplant is currently the best option in the treatment of type I diabetes. However, recent work has shown that even though large islets make up the majority of the transplant mass, limited post-transplant diffusion often causes the islet centers to become necrotic, which leads to reduced transplant efficacy. Therefore, a method to disperse and then re-aggregate large primary islets into 'pseudo-islets' of smaller dimensions, as well as similar cellular composition and function, could drastically increase the efficacy of islet transplants.

Towards this goal, primary murine islets were dispersed by trypsin digestion and seeded into square PEG microwells with diameters of 100μm and 200μm. After 5 days of in-vitro culture seeded cells naturally formed tight aggregates within the microwells (Figure 13A). The 3D structure was verified through nuclear staining followed by confocal microscopy (Figure 13B). Primary cells clustered were relatively uniform in size and with dimensions that scaled with the microdevice well dimensions. To assess the uniformity and scalability of primary cell aggregates formed using microwell devices, the aggregate diameter was measured using confocal laser scanning microscopy combined with further image analysis. The average aggregate diameters were found to

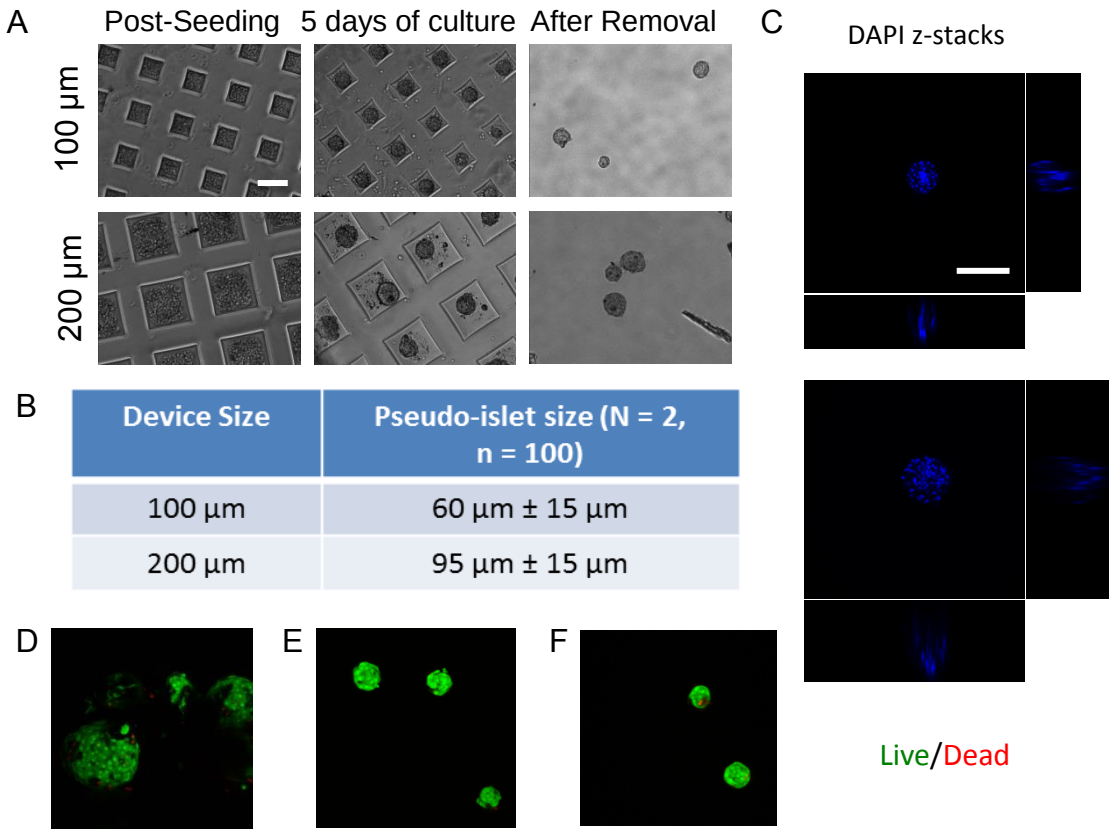

Figure 13: Primary islet cells form viable 3D pseudo-islets of defined size in PEG microwells. **A)** Formation of pseudo-islests. Bright field images taken 1 day after seeding, 5 days in culture and after removal from the devices. **B)** Table of pseudo-islet sizes for each PEG microwell diameter. **C)** Confocal images of pseudo-islets stained with the fluorescent nucleic acid stain DAPI to demonstrate 3D structure. **D-E)** Live/Dead staining of D) whole islets as well as E) 100µm and F) 200µm pseudo-islets on day 7. Green fluorescent cells are live while dead are red. All scale bars represent 100µm.

depend on the cross sectional area of the microwells, with w100 aggregates having a diameter of 60±15µm and w200 aggregates w200 aggregates having a diameter of 100±15µm (Figure 13C). Therefore, the diameter of the aggregates was 50-60% of the microwell diameter. The mean diameter of all normal islets analyzed was 153±21µm (n = 21).

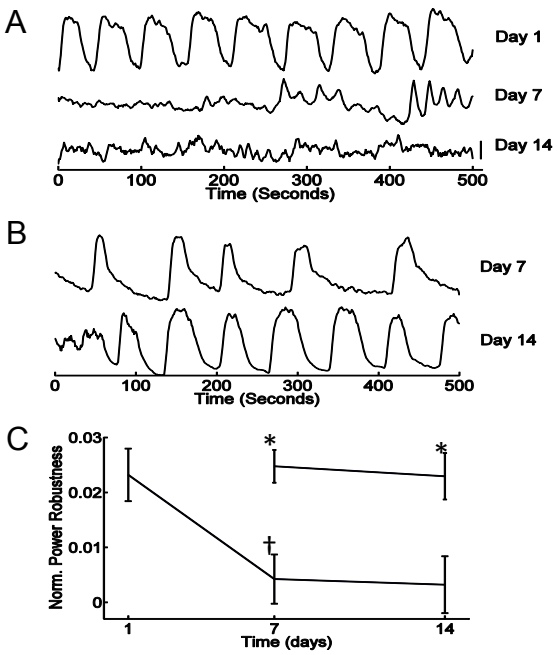

Figure 14: Pseudo-islets show more robust $[Ca^{2+}]_i$ oscillations compared to age-matched normal islets. **A)** Representative $[Ca^{2+}]_i$ oscillations, measured from Fluo-4 fluorescence, averaged over entire normal islets for on day 1, 7 and 14. **B)** Representative $[Ca^{2+}]_i$ oscillations, measured from Fluo-4 fluorescence, averaged over pseudo-islets on day 7 and 14, which are days 1 and 7 removed from the microwell devices, respectively. **C)** Normalized power robustness for normal islets (bottom line) and pseudo-islets (top line) on days 1, 7 and 14. Error bars represent SEM, * indicates a significant difference between groups at the same time point and † indicates a significant difference within the same group compared to the previous time point.

Pseudo-Islets Show Comparable Viability and Functionality to Fresh Islets

Islets exist in a unique, highly vascularized environment in-vivo, and generally do not show optimal function or viability after long-term in-vitro culture. Since the re-aggregation procedure takes 7 days, the post-aggregation function and viability is of concern. After 7 days in culture, both the w100 and w200 sized pseudo-islets demonstrated similar viability to day 1 normal islets (Figure 14 A, B & C). As a percentage of total cells, w100s and w200s comparable viability to day 1 normal islets ($p<0.05$)(Figure 14D).

Therefore, the re-aggregation procedure was not found to have a significant effect on the overall viability of primary islet cells.

To examine the function of the pseudo-islets, we used a similar procedure to the MIN6 aggregates. Time courses of $[Ca^{2+}]_i$ dynamics were analyzed for overall synchronization across the entire cell mass as well as robustness of the oscillation period. Activity at low glucose was also examined to determine if there was proper electrical suppression.

At 11mM glucose, the $[Ca^{2+}]_i$ dynamics of the pseudo-islets was highly synchronized (~88.35±4.02%). This was very similar to control Day 1 normal islets (~84.05±6.03%), suggesting that functionality and proper gap junction coupling was properly re-established after 7 days in culture. When grouped by well size, the W200s were found to have a higher area of synchronization compared to the W100s ($P<0.05$) (Figure 16D), although neither group was significantly different compared to normal islets ($P>0.05$). The area of synchronization for normal islets at day 1 at 11mM was also in agreement with previous results using an analogous method (Benninger, et al.). Pseudo-islets had very regular $[Ca^{2+}]_i$ oscillations which mimicked Day 1 normal islets; when quantified, day 7 pseudo-islets had a normalized power robustness that was not found to be different than Day 1 normal islets (0.0248±0.0003 vs. 0.0232±0.0048, respectively)($p>0.05$)(Figure 15C). Taken together, this data indicates that after 7 days in culture the islet re-aggregation procedure was able to maintain proper islet dynamics, comparable to freshly harvested islets.

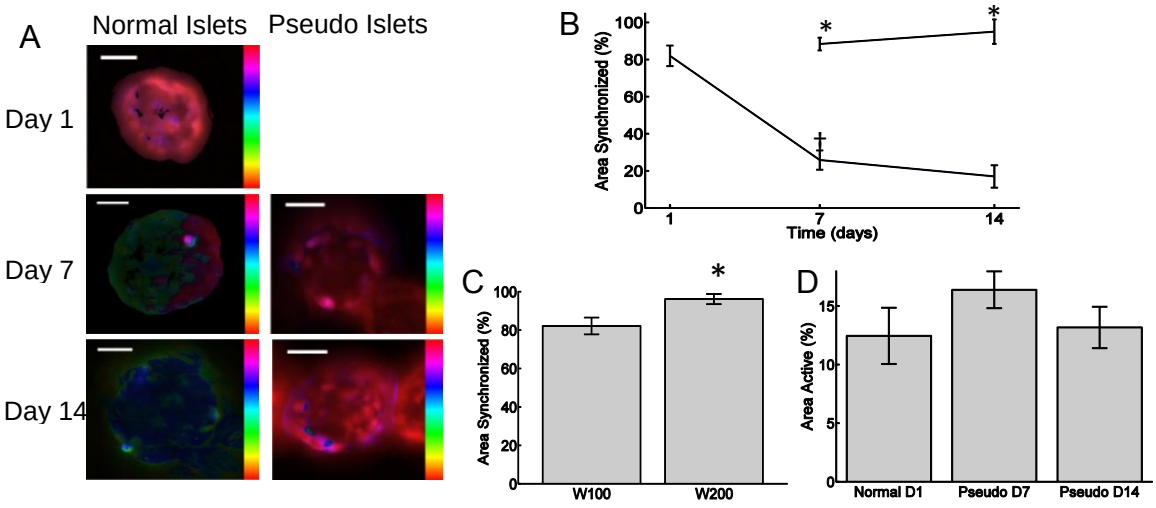

Figure 15: Pseudo-islets show better superior functionality over time. **A)** False-color map of the cross-correlation coefficient in a 3D aggregates, relative to a reference cell. **B)** Area with synchronized $[Ca^{2+}]_i$ dynamics (as defined as the area with a cross correlation coefficient > 0.75) for normal islets (bottom line) and pseudo-islets (top line) on days 1, 7 and 14. Error bars represent SEM, * indicates a significant difference between groups at the same time point and † indicates a significant difference within the same group compared to the previous time point. **C)** Area synchronized found as in B for W100 and W200 pseudo-islets. * indicates a significant difference between groups. **D)** Islet area active at low glucose.

Day 7 and 14 Pseudo-Islets are Better Than Age-Matched Normal Islets

A major concern in islet transplantation is post-transplant graft survival. It has been reported that ~50% of islets become necrotic after transplantation. Since this is the issue we intend to address with this procedure, long-term function is of concern. Therefore, we compared $[Ca^{2+}]_i$ endpoints for Day 7 (1 day removed from the microwell device) pseudo-islets to batch-matched normal islets which were cultured in parallel for 7 days. We then did the same comparison on Day 14.

When compared to normal islets one day post-harvest, pseudo-islets one day removed from the microwell device (day 7) showed much more robust and coordinated $[Ca^{2+}]_i$ oscillations despite the fact that both groups had spent 7 days in culture. At 14 days, the oscillatory behavior of the pseudo-islets remained synchronized while the normal islets

maintained their deteriorated behavior (Figure 15). Indeed, when the robust of the oscillations were quantified a significant reduction in robustness was seen in day 7 normal islets compared to day 1 normal islets ($p<0.05$). In contrast, day 7 and 14 pseudo-islets were not found to be different from day 1 normal islets ($p<0.05$).

After 7 days in culture, normal islets were found to have a significantly reduced area of synchronization compared to Day 1 normal islets (84.05±6.03% vs. 25.85±5.82%, respectively) ($p<0.001$) (Figure 16B). However, day 7 pseudo-islets were found to function similar to normal day 1 islets, with significantly higher synchronization ($p<0.001$) (Figure 16B). After 14 days in culture, normal islets were still unresponsive with overall synchronization not significantly different from the normal day 7 islets, which was poor ($p>0.05$). Surprisingly, pseudo-islets were found to have comparable synchronization to Day 7 pseudo-islets and remained markedly better than the normal islets ($p<0.001$).

At 2mM glucose, Day 7 normal islets had higher transient $[Ca^{2+}]_i$ activity compared to Day 1 normal islets (data not shown). Pseudo-islets at day 7 and 14 were also found to be comparatively quiescent, showing similar activity at low glucose to normal day 1 islets ($p>0.05$) (Figure 17C). Taken together, the high and low glucose data indicates that while the normal islets were decreasing in function pseudo-islets were maintaining or increasing functionality. In addition, the low glucose data specifically indicates that gap junctional conductance may be leading to greater suppression of transient $[Ca^{2+}]_i$ activity.

Summary of Results

We found that using precision-controlled PEG microwells to reaggregate normal islets resulted in viable pseudo-islets with defined shape and size. We then tested their

viability by analyzing the synchronization and robustness of their $[Ca^{2+}]_i$ dynamics. While day 1 normal islets demonstrated viability that was in line with previously published results, day 7 and 14 normal islets showed a significant deterioration in viability. Conversely, day 7 pseudo-islets (which are one day removed from the microwells) showed viability and functionality which resembled day 1 normal islets. Pseudo-islets from 100μm sized wells were also found to be slightly less synchronized than those from 200μm sized wells. Surprisingly, pseudo-islets continued to show high levels of viability and functionality at day 14, suggesting that the reaggregation procedure impacts the long-term behavior of islet cells in some way.

Chapter V

RESULTS: PERCOLATION MODELING PREDICTS LOW-GLUCOSE BEHAVIOR OF K_{ATP} CHANNEL GENETIC MUTANTS

In pancreatic β-cells, the K_{ATP} channel is provides a link between cellular metabolism (intracellular ATP concentration) and membrane potential. In a low glucose state, the channel is open allowing the outflow of K+ ions. Increased intracellular ATP causes the K_{ATP} channel to close and the accumulation of K^+ ions creates an increase in membrane potential which, when large enough, will activate voltage-gated Ca^{2+} channels. This rapid influx of Ca^{2+} ions causes the membrane to depolarization. At low glucose, the intracellular concentration of ATP in commonly not sufficient to deactivate enough KATP channels to sufficiently increase membrane potential, however a heterogeneous distribution of these channels makes some β-cells more excitable at a given glucose concentration than others. Over activity of the highly active cells is overcome by a hyperpolarizing effect of cell-cell coupling through gap junctions.

As we have previously shown, an increase in gap junction coupling (whether through larger 2D structures or increasing dimensionality to 3D) produces lower $[Ca^{2+}]_i$ activity at low glucose. We also demonstrated how percolation modeling combined with binomial statistics can predict how active a given cluster will be. Using genetic mutations which can decrease

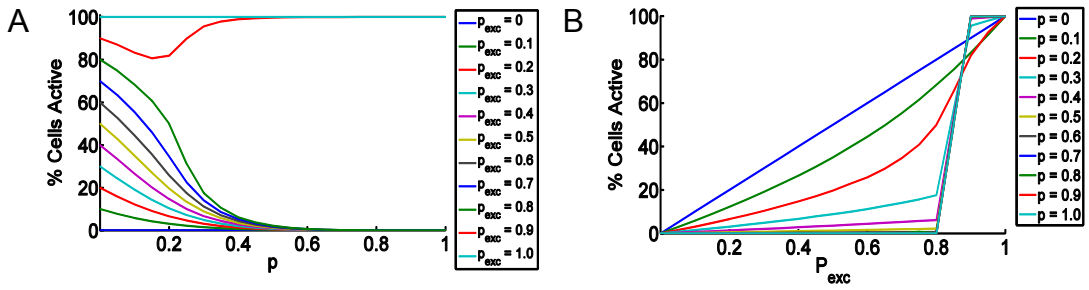

Figure 17: Percolation model predictions for transgenic mouse models. **A)** Percent of islet cells active at low glucose as a function of p (g_{coup}) for variable percentage of excitable cells in the islet (p_{exc}). **B)** Percent of islet cells active at low glucose as a function of p_{exc} for variable p. For both simulations the step size was 0.05 with an n=500 and the percentage of cells necessary to suppress the entire islet was 15%.

(loss-of-function) or increase (gain-of-function) K_{ATP} function, we set to further test the percolation model by using a forward model[2].

Model Predictions

Using previously acquired data from mice expressing transgenes for Cx36 and the K_{ATP} channel, we were able to compared perturbed experimental systems to our theoretical model. As previously shown, mosaic expression of the KIR6.2[AAA] transgene, which renders the pore-forming subunit of the K_{ATP} channel non-functional, makes 70% of the cells functional knockouts (Koster et al. 2001). In terms of our model this means 70% of cells will be active at low glucose. These mice were crossed with Cx36 knockout mice to yield different levels of gap junction conductance (g_{coup}), which is represented by the percolation probability p in our model.

[2] A forward model is based on prediction, in contrast to the reverse paradigm where the model is fit to the data retrospectively. Since the reverse model was used in chapter 1 to fit the model parameters, we now use the same tool to predict the behavior when the wild type system is perturbed.

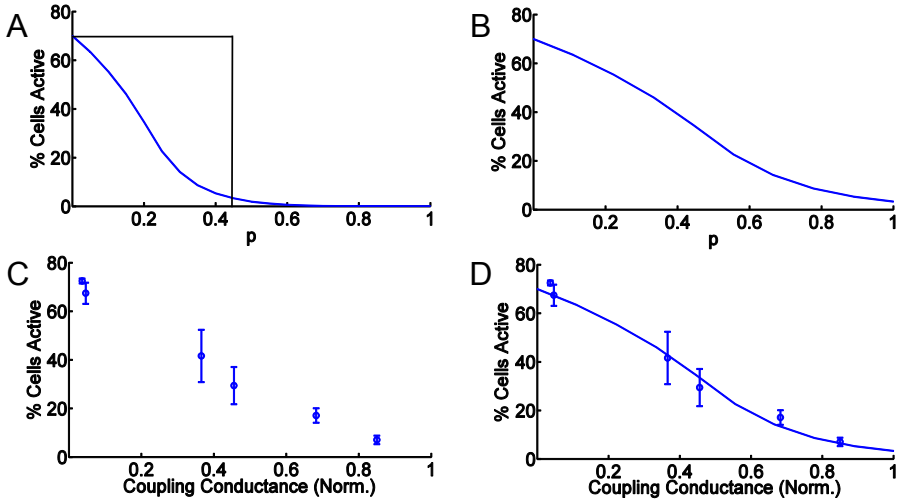

Figure 18: Percolation modeling fits experimental data from K_{ATP} loss-of-function islets. **A)** Plot of percent cells active versus p for p_{exc} = 0.7, corresponding to the theoretical cells active for KIR6.2[AAA] islets. The data was normalized to a wild type p = 0.45, represented by the area within the box. **B)** Normalized model plot. **C)** Scatterplot of percent of cells active at low glucose in mice as a function of coupling conductance (g_{coup}) from Cx36 knockout mice with further gap junction inhibition. **D)** Fit of model to experimental data. For C and D, points represent the mean ± SEM.

Predictive activity of the KIR6.2[AAA] knockout islets from these mice at different levels of coupling conductance (or levels of Cx36 knockout) were simulated through the low glucose percolation model using a 3D cubic lattice of diameter 11. This diameter was chosen based off the average islet having a diameter of ~150μm and the average cell having a diameter of ~10-20μm. Therefore, an average islet is 10 cells across, but since the model requires there to be a central cell in each lattice 11 was chosen. The threshold of quiescent cells to silence a cluster was set at 15%, which was previously found to provide the best fit for the MIN6 data. Although the effect of this parameter was not found to have a very substantial effect on parameter fit, it is within the 10-30% range as previously reported. For each simulation on this lattice the predictive activity was found for each p (g_{coup}) at different levels of cell excitability (p_{exc}). Since incorporation of the KIR6.2[AAA] trangsgene renders 70% of cells in the islet active, p_{exc} = 0.7 for this transgenic model. The resolution (or step

size) for each variable was 0.05 and simulations were run for n=500. The standard deviation of the predictions for each simulation was low, varying by less than 10% of the mean (corresponding to <1% SEM).

For a given p_{exc} below 85%, the model showed the percent active cells in the islet would also decrease as a function of p (Figure 17A). However, when p_{exc}>0.85 there are not enough quiet cells to suppress the activity (since 15% are required) of the overactive β-cells and the islets become constitutively active. In our experimental model where p_{exc} = 0.7, this predicts that when g_{coup} = 0 the islet will be 70% active and this will decrease as g_{coup} is increased.

The model was then run as a function of p_{exc} for variable p to describe the behavior of a gain-of-function K_{ATP} mutant. In mice expressing the KIR6.2[ΔN2-30,K185Q]-GFP transgene, the K_{ATP} channel becomes ~30 times less sensitive to ATP and is therefore overactive. This creates a hyperpolarizing current in expressing β-cells so that membrane potential never increases enough to activate the voltage-dependent Ca^{2+} channels. This inhibits $[Ca^{2+}]_i$ activity and renders them under-active. The expression of the KIR6.2[ΔN2-30,K185Q]-GFP transgene is inducible and dependent on the dosage of the inducing agent tamoxifen and can be quantified by GFP penetrance. Therefore, this gives us a model to predict low glucose activity as a function of p_{exc} for a given p.

For levels of p (or g_{coup}) below p_c the percent of active cells at low glucose increased linearly as p_{exc} was increased. This is expected given that the many small clusters seen when $p<p_c$ will not do much to suppress activity. However, when p > pc = 0.2488 the behavior becomes

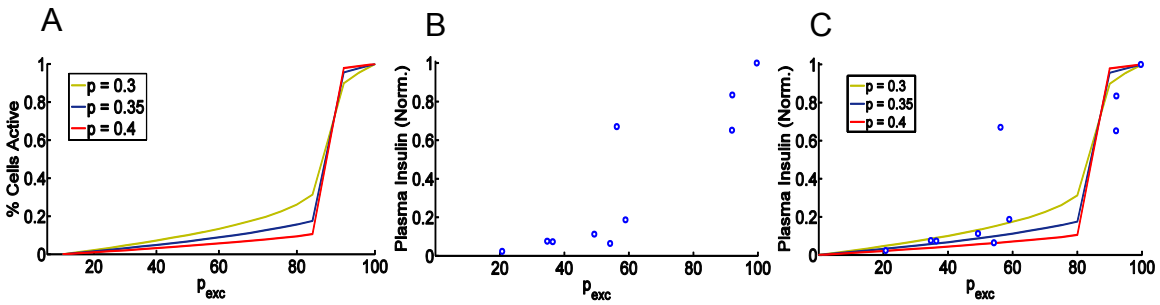

Figure 19: Percolation modeling fits experimental data from KATP gain-of-function islets. **A)** Theoretical plot of percent cells active at low glucose as a function of percent of cells excitable for previous estimations of p for wild type islets. **B)** Scatterplot of plasma insulin versus the fraction of excitable for KIR6.2[ΔN2-30,K185Q] expressing islets. **C)** Fit of model to experimental data.

markedly different. The percent active cells remain relatively quiescent at low p_{exc} and critical behavior appears at $p_{exc} \rightarrow 0.8$, where above this level of activity the islets overcome any suppressive effects and become highly active. For p = 0.3-0.4, there were still enough uncoupled cells to increase the percent cells active as Pexc was increased up to the critical point, but for p > 0.4 the percent cells active remained very low until $p_{exc} \sim 0.8$ (Figure 17B).

Cell Activity as a Function of Coupling Conductance in KIR6.2[AAA] Mice

In KIR6.2[AAA] mice ~70% of β-cells are constitutively active and therefore a model parameter from our simulations of $p_{exc} = 0.7$ should fit the experimental data best (Figure 18A). However, since wild type islets do not have a p = 1, but a value somewhere between 0.3-0.4 as was shown in MIN6 aggregates and previously for high glucose synchronization (Benninger et al. 2008), the simulation data is normalized to wild type conductance (Figure 18B). A wild type conductance of p = 0.45 was found to best match the experimental data and if plotted in Figure 18B. When plotted, percent cells active at low glucose follows a trend very similar to that of the normalized simulation plot (Figure 17C), and when plotted

with the theoretical data they match very closely (Figure 17D). Only one data point was found to have a SEM which did not include the theoretical line. The model was also able to capture the behavior of the experimental system at low g_{coup} (p) and high. In addition, it nicely explains the rapid drop in percent cells active follows by more asymptotic behavior.

Cell Activity as a Function of Excitability in KIR6.2[ΔN2-30,K185Q] Mice

Simulations of g_{coup} for varying percent cells active found that for a p within the range of what was previously found (p = 0.3-0.4), there would be low activity in the islet up to the point where ~80% of the cells are active. However, when activity goes beyond that point there will be a transition accompanied by a rapid increase in the percent cells active (Figure 19A). This increase corresponds to the number of cells required to suppress transient activity at low glucose (15% in our model), and the simulations will therefore be very sensitive to this parameter. For instance, if this threshold was set to 25% instead of 15% the critical point would occur around 70-75% instead. As the number of active cells increases, there will be a point above which there are not enough quiescent cells by percentage to suppress. In our model this point was 85% (100%-15%). When using plasma insulin in fasting mice as a measure of islet activity at low glucose, the data was found to follow a similar patter as that described by the model for p between 0.3 and 0.4 (Figure 18B). Though incomplete in the 60-90% range, as activity of the β-cells increases through reductions of inducible KIR6.2[ΔN2-30,K185Q] expression plasma insulin normalized to wild type levels shows low levels of activity combined with a sudden increase. When plotted with the theoretical data, there is sound agreement at low percent cells active and the location of the phase transition (Figure 19C).

Summary of Findings

After fitting our model of islet connectivity to the MIN6 2D/3D data retrospectively, we wanted to test if we could predict the behavior of wild type islets as parameters of the model were perturbed. The model found that for increasing values of p (when $p_{exc} = 0.7$) there would be a sigmoidal-like decrease in the percent cells active at low glucose. Using data acquired from transgenic variants we were able to fit data from K_{ATP} loss-of-function KIR6.2[AAA] (which have ~70% of cells active) very well when normalizing to a p = 0.45. When simulations were run as a function of p_{exc} for variable p, the range of p values which were found to approximate MIN6 aggregates had a small size dependent increase in activity up to a critical point at ~80%, above which the islets became highly active. Similarly, the experimental data was found to fit the theoretical data. Taken together, these results demonstrate that the experimental data from transgenic mice can be fit using the same percolation model, albeit with a p for wild type conductance which was slightly higher than the MIN6 aggregates.

CHAPTER VI

DISCUSSION AND FUTURE DIRECTIONS

Dimensionality and Size-Scaling of Coordinated $[Ca^{2+}]_i$ Dynamics in β-cells

The importance of cell-cell communication is a recurring theme in physiology and is integral to the proper function of multiple biological systems. In the pancreas, the islets of Langerhans show coordinated $[Ca^{2+}]_i$ oscillations and propagating Ca2+ waves at elevated glucose mediated by Cx36 gap junctions. These electrical dynamics are critical for the underlying dynamics of insulin release and glucose homeostasis. In addition, gap junction coupling also coordinates a suppressive effect at low glucose, preventing non-essential insulin release which has been shown to be a contributing factor to the progression of type II diabetes (Benninger, et al. 2011; Tisch et al. 1996).

Utilizing a hydrogel microwell array to generate 3D β-cell aggregates of defined size, we examined the dependence of $[Ca^{2+}]_i$ dynamics on size and dimension by comparing the $[Ca^{2+}]_i$ dynamics to 2D cell cluster sheets. Previous work has modeled the islet architecture as a partially coupled lattice resistor network to quantify the dependence of these dynamics on the level of gap junction coupling. Since this model was established for multiple network mesh sizes and dimensions, we were able to take it a step further to quantify multiple aspects of size-scaling and dimensionality of β-cell $[Ca^{2+}]_i$ dynamics.

Insufficient β-cell Coupling in Two-Dimensions

In our model, when MIN6 β-cells were coupled within a 3D architecture, they showed significantly more robust $[Ca^{2+}]_i$ dynamics compared to a 2D architecture. This included more robust oscillations, increased oscillation synchrony between cells and faster Ca2+ wave propagation across the cell structure. Within this 3D architecture, MIN6 cells showed similar responses to previously reported values for intact islets, with similar wave velocities (72μm/s±6 vs. 69μm/s±5, respectively) and oscillation synchronization (96±2% vs. 91±2%, respectively) (Benninger, et al., 2008). Since the MIN6 aggregates are composed of solely coupled β-cells, compared to intact islets which are ~80% β-cells and ~20% non-coupled cells, this could explain the increase in both wave velocity and synchronization. However, the closeness of the two values can be reconciled with our percolation mode. Since both systems would be estimated to have behavior above the critical probability, a 20% reduction in resistors or cells would have a negligible effect on total synchronization. This is exhibited by figure 5E, in which there is a distinct transition from p=0.2 to p=0.3 (p_c=0.2488) and with only a ~15% change over a range of p=0.3-1.0. The closeness of the values also indicates that MIN6 aggregates can serve as a sufficient model system in which to examine the effects of coupling.

When the coupling architecture is reduced to 2D, the behavior of the cell cluster becomes qualitatively similar to islets showing a loss of coupling. There is a marked reduction in synchronized oscillations which are restricted to defined sub-regions, propagating Ca2+ waves slow (Benninger, et al., 2008), and basal $[Ca^{2+}]_i$ activity is elevated (Benninger, et al., 2011). In intact islets, patch-clamp data has shown β-cells are electrically coupled to ~6 neighboring cells (Zhang, et al., 2008). Since this the degree of connectivity for each node in a simple cubic lattice, this architecture is suitable to model islets.

Therefore, by reducing the dimensionality from 3D to 2D there is a ~33% decrease in total coupling to adjacent neighbors by reducing each node degree from 6 to 4. However, this effect becomes magnified when considering the range of which cells can couple. We experimentally determined that MIN6 cells can couple over a 5 cell radius. Therefore, over this range 2D allows for 5 times fewer cells with which a given cell can interact over this range (5^2=5 vs. 5^3=125).

This is supported by the percolation model, in which the critical probability is ~25% less in 3D than in 2D (p_c=0.2488 vs. p_c=0.5, respectively), meaning that 25% more connections can be uncoupled to have a fully coupled electrical syncytium. This may also help to explain why a disproportionately low reduction in synchronization is seen in 3D islet networks following a >50% reduction in coupling (Benninger et al. 2008). If the p falls further below pc in an islet through gap junction knockout and/or inhibition, there will be a sharp decrease in overall synchronization.

In MIN6 cells, the K+ channel inhibitor TEA is conventionally used to increase resting membrane potential, which creates more regular oscillation patterns. In fact, this cell line was developed primarily for these properties. Therefore, we also measured size and dimensionality scaling under treatment with high glucose alone as a control condition. Since $[Ca^{2+}]_i$ patterns were similar in the presence and absence of TEA, this suggests that the size-scaling and dimensional behavior seen is more a function of intercellular dynamics rather than intracellular events. However, upon increasing the dimension from 2D to 3D with glucose alone, we found that there was a significant increase in period robustness of the oscillations. This indicates that the 3D coupling architecture is vital affects MIN6 cells in such a way where they becomes more sensitized to adjacent depolarizations at high glucose.

At low glucose, 3D aggregates showed suppression of transient $[Ca^{2+}]_i$ activity which was size invariant. In contrast, suppression improved with increasing cell number in 2D aggregates, which is opposite to the size-scaling seen at high glucose. Therefore, there is not an ideal size at which 2D aggregates can form a proper balance between high glucose synchronization and low glucose suppression: as the cluster increases in size it becomes better able to suppress transient $[Ca^{2+}]_i$ activity but loses overall synchronization. This can be qualitatively explained by considering the mechanisms of gap junction-mediated suppression and synchronization. To be show similar synchronization behavior, cells must be effectively coupled. In 2D aggregates cells at opposite ends of a cluster are very unlikely to be within the same coupling environment. However, for cells in an aggregate to be suppressed, the must only be in contact to a sufficient number of inactive cells. Cells at opposite ends of a large cluster do not themselves need to be connected to be quiescent. As the cluster increases in size, the proportion of inactive cells increases and the network dynamics allow for suppression to propagate over larger distances. This reveals a fundamental and unexpected difference in the way in which cell-cell connections play a role in the suppression of $[Ca^{2+}]_i$ at low glucose compared to the synchronization of $[Ca^{2+}]_i$ oscillations at high glucose.

Network Model Describes Dimension and Size-Scaling of $[Ca^{2+}]_i$ dynamics

To gain a better theoretical understanding of how these different behaviors emerge from the coupling architecture, we simulated β-cell coupling within a lattice resistor network model. By examining network properties based on the probability of adjacent coupling, these simulations could describe multiple aspects of the size-scaling of $[Ca^{2+}]_i$ dynamics, including the size of synchronized regions in 2D and 3D, the effect on dimension

on synchronization and the change in suppression in 2D and 3D. Importantly, these models were fit with one network connectivity parameter (p) to describe the proportion of functional cell-cell interactions. The suppression utilized an additional parameter (S_p) to describe the percent of inactive cells necessary to suppress the connected cluster.

In percolation theory, there are a critical percentage of connections (defined by p_c) for which a phase transition occurs and overall coupling spans the full network. This critical probability p_c=0.2488 for 3D cubic networks and p_c=0.5 for 2D square networks. In our simulation models, a phase transition is clearly visible for finite size networks >100 cells, where there is a sharp jump in synchronization when $p>p_c$ (Figure 5). Given the similar p which fit the 2D and 3D experimental data best (p=0.312 vs. p=0.369, respectively), 3D β-cell networks are 'super-critical' where coupling spans the entire network and 2D β-cell networks are 'sub-critical', where coupling is localized to defined sub-regions which do not span the network. This further explains how 3D aggregates are able to show high levels of synchronization and propagating Ca^{2+} waves over the entire cell structure, but large 2D clusters show very low synchronization. The fractal clustering behavior of random percolation networks in the sub-critical phase closely mimics that of coupled β-cell clusters, which further supports the use of the network model (compare Figures 5E and 9C). In addition, the model supports the idea that through the coupling architecture, a characteristic probability alone can explain the coupling and synchronization behavior of electrically coordinated cellular networks.

Overall, these model results demonstrate how separating details of cellular dynamics from the system architecture can be used to discover general properties by which cellular interactions govern the behavior of multicellular systems, which could be broadly applicable.

Physiological Importance of Dimensionality and Size-Scaling in Cellular Network Architecture

Size and dimensionality play an integral role in the regulation of electrical activity in β-cell aggregates. Aggregates with higher dimensionality show a more coordinated $[Ca^{2+}]_i$ response at high glucose and enhanced suppression of $[Ca^{2+}]_i$ activity at low glucose. This can therefore explain the higher insulin secretion in 3D aggregates in our model, and also explain the higher dynamic range of non-diabetic islets. Although we did not investigate the size-dependence of insulin secretion, it has been shown to be size invariant in the 3D aggregates (Bernard, Lin & Anseth, 2013). Furthermore, previous studies have shown that confluent MIN6 cells (large cell clusters) show reduced insulin compared to non-confluent MIN6 (small cell clusters) (Konstantinova, et al., 2007). In context of our data of $[Ca^{2+}]_i$ dynamics and insulin secretion, this indicates a key role that the underlying cellular architecture plays in determining the efficacy of the glucose-stimulated insulin response.

The 3D aggregates we created through hydrogel microwells behave very similarly to intact islets, which demonstrate the utility of the 3D architecture. Compared to 2D cell clusters, 3D aggregates were able to show robust and synchronized oscillations without the addition of TEA. Human islets have been proposed to have a number of different architectures (Cabrera, et al., 2006; Bosco, et al., 2010), however defects which alter the systems architecture and reduce the dimensionality over which coupling occurs would be expected to lead to dysfunction that is similar to a loss of gap junction coupling (Head, et al., 2012). Indeed, a loss in insulin pulsatility is often seen in type II diabetics (O'Rahilly et al. 1988; Porksen et al. 2002; Menge et al. 2011) and obese individuals (Periris et al. 1992), which could potentially be the result of downregulation of gap junction proteins as well as a reduction in cell-cell contact through inflammation and α-cell infiltration. These events are known to occur in hyperglycemic conditions which are associated with the symptoms of

type II diabetes (Rahier et al. 1983; Allagnat et al. 2005). Furthermore, it has been shown that during pregnancy, an increase in gap junctional coupling is observed in islets, coinciding with increased islet size and enhanced insulin secretion (Sorenson et al. 1997; Sheridan et al. 1988).

Excitable cells in the human body have a small finite conductance that is dictated by the coupling architecture of the gap junctions. Through this architecture, cells are able to synchronize behavior across large distance through these low-conductance channels. For example, electrical synchronization allows for our hearts to beat, muscles to move and glucose levels to be maintained. These findings add insight into how the body is able to achieve the optimal cellular architecture for life.

Currently the most promising treatment for type I diabetes is islet transplant and these results are also important to consider for generating alternate sources of β-cells for islet transplantation. While cellular coupling will be important to enhance insulin release, our data suggests that the architecture will also be important. Transplantation of 2D sheets of β-cells, as has been recently suggested, will provide insufficient coupling for well-regulated insulin dynamics. Rather, a robust 3D architecture is necessary. This also has important implication when seeding β-cells onto scaffolds (Pedraza et al. 2012; Kodama et al. 2009), since those scaffolds which promote the formation of higher-dimensional structures will likely show enhance function. It will also be important to consider if other factors such as revascularization, nutrient diffusion and hypoxia are dependent on architecture. For example, it has been shown that transplanting smaller 3D islets better reverses diabetes compared to large 3D islets in both mouse and human models (Lehman et al. 2007). Nevertheless, our method of controlled aggregation to generate 3D aggregates of

controlled size (Bernard, Lin & Anseth, 2013) could be used to re-aggregate primary islets to optimal sizes or creating islets from differentiated stem cells.

Intercellular coordination via $[Ca^{2+}]_i$ oscillation is not unique to the islet and applies to other neuroendocrine cell systems. For example, robust and enhanced pulsatile growth-hormone (GH) secretion results from the coupling between GH cells and the coordination of $[Ca^{2+}]_i$ (Bonnefort et al. 2005; Hodson et al. 2012); where remodeling of the coupling architecture regulates GH release in puberty (Bonnefort et al. 2005). Gap junctions couple chromaffin cells in the adrenal medulla which synchronize $[Ca^{2+}]_i$ transients and regulate catecholamine release (Martin et al. 2001); where stress responses evokes a remodeling of electrical coupling to enhance chromaffin cell excitability (Colomer et al. 2008; Hill et al. 2012). Therefore, our findings are not only applicable for the islet and may have the ability to predict architecture and gap junction coupling changes in the pathology of other diseases.

Re-Aggregation of Primary Islet Cells into Functional Pseudo-Islets

In the transplant environment, whole pancreas grafts are not realistic because of rejection and functionality issues, and islet isolation procedures are thus necessary. In addition, time delays to engraftment make culture inevitable. It has previously been shown that the unique architecture of islets cells and vasculature is not maintained in cultured or transplanted islets (Bosco, et al., 2010). This is not surprising given the insults sustained during isolation, digestion, shaking and subsequent culture. Therefore, to improve the quality to transplant tissue methods are needed to avoid these pitfalls. Here, we have shown that long-term viability and functionality of normal islets is poor (to which the isolation procedure may have contributed), but show that using PEG microwells to re-

aggregate primary cells results into pseudo-islets of defined sizes leads to long-term functionality and viability resembling freshly isolated islets.

Efforts to improve islet transplantation have begun to focus more on improved survival rates of the transplanted islets as an adjunct to isolation techniques and immunosuppression (Lehman, et al. 2008). It is estimated that ~50% of whole islet transplants become necrotic, with a larger proportion of larger islets being affected. Despite high numbers of transplanted islets, the functional capacity of the graft remains around 20-40% (Ryan et al. 2001). Normally, pancreatic islets have a blood perfusion that is 10 times higher than in exocrine pancreas, resulting in a significantly higher oxygen tension (Fung et al. 2007). During the process of isolation and *in vitro* culture the islet vasculature dedifferentiates or degenerates, rendering nutrient and oxygen availability to be based solely on the limits of diffusion. Even islets which revascularize show oxygen tension that is 10 times lower that in native pancreas (Carlsson et al. 2004).

We propose a new, previously neglected parameter to improve islet function: islet size. Islet size has been shown to be of importance for *in vitro* and *in vivo* function (Lehman et al. 2007), and may also influence many other factors such as higher percentages of β-cells, higher insulin secretion per unit mass, better oxygenation and more favorable outcomes (Lehman et al. 2007; MacGregor et al. 2006; Fung et al. 2007). Smaller islets have also been shown to have a significantly reduced diffusion barrier, easing the effects of hypoxia and nutrient accessibility (Mattsson et al. 2002; O'Sullivan et al. 2010). This is supported by previous work showing that smaller islets have a more robust insulin response and had better outcomes after engraftment (Macgregor et al. 2006). Therefore, by re-aggregating larger islets into pseudo-islets of optimal islet size, the efficacy of transplants can be significantly improved.

Primary Islet Cells Readily Aggregate Form 3D Pseudo-Islets of Defined Size

Primary mouse islet cells have been shown to reaggregate after dispersion, however these methods have mostly been cumbersome and inaccurate (Cavalleri et al. 2007; O'Sullivan et al. 2010; Ramachandran et al. 2013). Here, we show that using photolithography to form precisely sized PEG microwells, we can repeatedly form pseudo-islets of defined size (Figure 14A). For both the 100μm and 200μm well diameters, pseudo-islets were found to have a diameter which was ~50% of the microwell diameter (Figure 14B). This is expected given one of the mechanisms through which the wells create pseudo-islets of defined size by limiting and evenly distributing the number of cells within the well. These cells then create 3D aggregates of lesser diameters, which are similar to the diameters of MIN6 aggregates formed using the same method (Bernard, Lin & Anseth, 2012). More importantly, the standard error for both well diameters was only found to be 15-25% of the pseudo-islet diameter (Figure 14B), indicating a high level of control regarding size. This size control is comparable with the diameters of MIN6 aggregates using the same method (Bernard, Lin & Anseth, 2012) and superior to flat culture aggregation (O'Sullivan et al. 2010), hanging drop aggregation (Cavalleri et al. 2007) and other micromold-guided techniques (Hwang et al. 2011; O'Sullivan et al. 2010). Although the optimal size for transplanted islets still needs to be addressed, given the emphasis on islet size in transplant viability control over this aspect will be of high importance for *in-vivo* trials.

Pseudo-Islets Show Superior Viability and Functionality Compared to Age-Matched Islets

Directly removed from the microwells, pseudo-islets were found to have a defined 3D shape (Figure 14C) and high levels of viability (Figure 14D-F). Importantly, they also had coordinated (Figure 16A & B) and robust (Figure 15A-C) $[Ca^{2+}]_i$ dynamics which were similar to freshly isolated islets (Figure 15C), indicating that 5 days in culture was sufficient for intercellular gap junction coupling to develop. Gap junction coupling plays an important role not only in coordinating insulin secretion at high glucose, but also suppressing insulin secretion at low glucose – which can also have a detrimental effect (Benninger et al. 2011). As shown by $[Ca^{2+}]_i$ activity at low glucose (Figure 16C), pseudo-islets were found to have similar suppression to freshly isolated islets.

Interestingly, we found that pseudo-islets continued to maintain highly synchronized and robust $[Ca^{2+}]_i$ dynamics up to two weeks (day 14) in culture, while cultured normal islets continued to deteriorate (Figure 15C; Figure 16B). In addition, the suppression of $[Ca^{2+}]_i$ activity was found to be similar to both fresh islets and day 7 pseudo islets (Figure 16C). This is surprising given normal islets 7 days post-harvest showed deteriorated dynamics, but pseudo-islets 7 days post-removal from the microwells showed no such deterioration of their $[Ca^{2+}]_i$ dynamics.

Although we were not able to determine whether the improvements seen in pseudo-islets were based solely on changes in islet size, this could possibly explain some of the differences seen between the two groups at day 7. While control normal islets remained in culture under potentially hypoxic and nutrient-poor conditions, cells from pseudo-islets were dissociated and therefore under more optimal culture conditions. This notion is supported by the fact that even small normal islets exhibited poor viability and functionality

after 7 days. In addition, pseudo-islets were then aggregated to smaller sizes, allowing for better nutrient diffusion and higher oxygen tension when functionality was assessed through $[Ca^{2+}]_i$ imaging.

However, size differences do not seem to explain the high viability and function of the pseudo-islets at day 14. At this time point the pseudo-islet cells had been in culture for 14 days, and were 7 days post-removal from the microwell devices – the same timeframe over which the normal islets of comparable size were found to deteriorate (data not shown). This suggests that some aspect of the dispersion / aggregation procedure is increasing function and viability. Future work will aim to elucidate this mechanism, but two probable explanations are either molecular switching or a reworking of the islet architecture into a more beneficial organization.

In rodents, dissociated islet cells have previously been shown to reaggregate in culture to form pseudoislets with a core-mantle organization similar to that of normal mouse islets (Cavalleri et al. 2007; Ramachandran et al. 2013). This indicates that in rodents, information that decides the islet architecture is foremost provided by islet cells themselves (Cirulli et al. 1993; Rouiller et al. 1991). Therefore, the intracellular mechanism which controls cell aggregation may also be causing the cells to circumvent the cell death seen in normal islets in culture. Indeed, a study by Beattie et al. found that dedifferentiation of human fetal pancreatic cells is reversed by reaggregation (Beattie et al. 2000).

As supported by previous work in the literature as well as this thesis, islet architecture plays a hugely important role in islet behavior, and a relative increase in alpha-cells present in the central core of the islet has been reported in many animal models of type 2 diabetes, pregnancy and obesity (Epstein et al. 1989; Bates et al. 2008; Rahier et al. 1983; Clark et al. 1988). This is often described as “disorganized islet architecture” based on

"the prototype" structure (Kharouta et al. 2009). However, it is also thought that the architecture accompanied with increased α-cell fractions may lead to more efficient cell-cell communication resulting in enhanced endocrine function such as increased sensitivity to changes of external glucose concentrations (Cabrera et al. 2006 ; Kharouta et al. 2009). This is supported by mouse islets containing β-cells over expressing the glucagon receptor were found to have increased β-cell mass (Gelling et al. 2009).

Therefore, this offers an alternate explanation for the increased function and viability: the reaggregation procedure may allow the incorporation of α-cells into the β-cell mantle thereby increasing content without disrupting gap junction connections between β-cells. Since the cells were taken from healthy mice, an increase in the α-cell:β-cell ratio associated with obesity and diabetes will not be seen. In addition, if we assume that normal islets have a similar coupling environment to MIN6 aggregates, our percolation model can still explain how there would not be a reduction in overall $[Ca^{2+}]_i$ synchronization. For example, if there was a theoretical 20% decrease in β-cell coupling from the infiltration of α-cells (since α-cells constitute ~20% of the islet), this would only reduce the p to 0.36*(1-0.2)=0.288, which is still well above the critical threshold

Applications to Human Work

Although our findings in a mouse model are promising, there is currently not an epidemic of murine diabetes in the United States. To realize its full potential, our work needs to be applied to human transplant islets. As in the murine model, the architecture of the human pseudo-islets will prove to play an important role in defining their function, viability and behavior.

Recent evidence has shown marked differences in the cellular organization of islets in humans compared to mice. In addition to human islets having a lower percentage of β-cells, Cabrera, et al. have demonstrated that mice have a β-cell core surrounded by an α-cell mantle (mantle-core), while human islets may have a higher proportion of these cells that are intermixed. Therefore, human islets may have much lower β-cell coupling and may be characterized by a lower p. For example, the Cabrera, et al. study also showed that synchronization of $[Ca^{2+}]_i$ dynamics was absent in human islets, but present in isolated sub-regions. Conversely, the study has not been repeated with human islets and a ~30% reduction in β-cell coupling would not be enough to justify a phase-transition to sub-critical percolation according to our model (corresponding to a $p = 0.252 > p_c = 0.2488$).

However, observations by Bosco, et al. in the only statistically well-powered study to date have found that small human islets (40-60μm) do indeed show a segregated mantle-corer architecture with α-cells localized to the mantle and β-cells predominantly forming the core (Bosco, et al., 2010). In larger islets (60+μm) α-cells were found in the mantle, but also within the islet adjacent to vascularized areas. They therefore proposed a model in which β-cells exist as sheets with α-cell edges, which fold around the vasculature of the islet as it becomes larger than the defined sheet diameter (Bosco et al. 2010). Since smaller islets have diameters less than the sheet diameter, the mantle-core architecture is conserved.

It is interesting to note that islets obtained from older patients in many under-powered architecture studies (Cabrera, et al. 2005; Brissova, 2005) have shown similar architectures to murine models of diabetes (Kim et al. 2009), and smaller islets from the same patients often have mantle-core structures. Indeed, it has been suggested that the heterogeneous architecture seen in older humans may represent a reorganization of the architecture over time – one that potentially contributes to diabetes (Butler et al. 2003).

This suggests that the architecture seen in older human islets (which is the most widely available tissue for both research and transplant) may be an effect of aging rather than normal composition. Therefore, reaggregating donor tissue may not only create smaller, more viable islets, but reassembling the cyto-architecture to a more non-diseased state may also serve to further improve outcomes.

Therefore, if the reaggregation procedure is found to reorganize the islet architecture in a way which makes transplant tissue from older patients function better, this could pose to greatly increase the effectiveness of the donor-recipient matching. Future experiments in both human and mouse models are currently being planned to test this. However, even if reaggregation is unable to increase function in islets cells from aged donors, the increase in smaller islets with higher viability as reported here may increase the grafts chance of surviving the hypoxic insult of the portal vein.

Percolation Modeling Predicts Low-Glucose Behavior of K_{ATP} Channel Genetic Mutants

In pancreatic β-cells, the K_{ATP} channel provides a link between cellular and membrane potential. In a low glucose state, the channel is open allowing the outflow of K^+ ions. Increased intracellular ATP causes the K_{ATP} channel to close and the accumulation of K^+ ions creates an increase in membrane potential which, when large enough, will activate voltage-gated Ca^{2+} channels and cause a membrane depolarization. Conversely, at low glucose the intracellular concentration of ATP is not sufficient to inhibit enough K_{ATP} channels to adequately increase membrane potential. However, a heterogeneous distribution of these channels makes some β-cells more excitable at a given glucose

concentration than others. Over-activity of the highly active cells is overcome by a hyperpolarizing effect of cell-cell coupling through gap junctions.

As we have previously shown, an increase in gap junction coupling (whether through larger 2D structures or increasing dimensionality to 3D) produces lower $[Ca^{2+}]_i$ activity at low glucose. We also demonstrated how percolation modeling combined with binomial statistics can predict how active a given cluster will be given a threshold number of inexcitable cells being able to suppress the activity of the cluster. To better understand this important mechanism and further validate our model, we used transgenic mice expressing altered or deficient pancreatic K_{ATP} channels that exhibit β-cell dysfunction.

Transgenic mice with overactive K_{ATP} channels (KIR6.2[ΔN2-30,K185Q] transgene) show neonatal diabetes due to permanent hyperpolarization of the cell membrane, demonstrating the K_{ATP} channels ability to suppress insulin secretion (Koster et al. 2000). These mice demonstrate a particularly accelerated progression from hyperinsulinemia to diabetes as might occur in the most severe (i.e., completely K_{ATP} channel deficient) versions of human hyperinsulinemia. Conversely, KIR6.2[AAA] mice differ significantly from the knockout mice in that whereas K_{ATP} channels are essentially absent from ≈70% of beta cells, they are present at near-normal density in the remainder. Thus, the phenotype is a partial (i.e., cell-by-cell) knockout. Because of a partial syncytium in the islet (cells are electrically coupled to one another), these mice should still exhibit a K_{ATP} dependence of insulin secretion, but with the set point of electrical activity, and hence secretion, shifted toward lower glucose concentration (Koster et al. 2002).

Previously, we have shown that in a single β-cell (or very small group of β-cells) were coupling can be considered negligent, heterogeneity of glucose sensitivities leads to a 67% probability that a given MIN6 cell in 2D will be active at low glucose. However, when

coupling was incorporated by analyzing larger 2D cell clusters a marked size-scaling effect was seen. Elevation of the dimension was also shown to have a highly suppressive effect given the same probability of being active. Given the unique architecture of the islet, extrapolation of our MIN6 findings is difficult without knowing a set point of K_{ATP} activity. Therefore, using KIR6.2[AAA] mutant mice provides a model in which it is known that ~70% of cells do not have functioning K_{ATP} channels and will thus be active at low glucose. The use of KIR6.2[DN30K185Q] provides a more thorough model because the level of K_{ATP} function can be varied and also quantified by GFP penetrance.

Percolation Modeling Accurately Predicts the Increase in Low Glucose Activity of KIR6.2[AAA] Islets as a Function of Gap Junction Coupling

In the absence of gap junction coupling, our model showed that KIR6.2[AAA] islets will theoretically have 70% activity. Being that there will be no gap junction coupling to suppress excitable cells at low glucose, this makes sense. For Cx36-/- islets expressing the KIR6.2[AAA] transgene, this was the approximate case. Since Cx36-/- still have small levels of gap junction conductance (Benninger et al. 2008), the lowest values g_{coup} will theoretically have percent of cells active at low glucose that is slightly less than 70%. Indeed, there was less of a reduction than a linear trend might suggest, but was in agreement with the model with $p_{exc} = 0.7$.

Normalizing the coupling conductance to a p=0.45 was found to provide the optimal fit for the KIR6.2[AAA]/Cx36 data. This was higher than the optimal p=0.36 seen in the MIN6 low glucose model, but may have been inflated by the large step size of the simulation. For example, a step size of 0.01 instead of 0.05 will lead to a better approximation and may lower the p of optimal fit. In addition, differences would be expected between MIN6

aggregates and intact islets given they have different development and cellular composition. This might also suggest an approximation for the true p of a WT islet as being between 0.4 and 0.45.

Our model was able to predict how a loss in gap junction coupling can lead to elevated $[Ca^{2+}]_i$ activity at basal glucose levels in KIR6.2[AAA] mice. These results show that the coupling of K_{ATP} activity via gap junctions results a suppressive activity at low glucose which is similar to wild-type islets, even though up to ~70% are constitutively active. Furthermore, we were also able to predict a critical point of excitable cells (~80%), above which suppressive coupling becomes nonexistent islets become constitutively active. This further supports that glucose control of $[Ca^{2+}]_i$ activity is gap junction dependent and validates them as means by which cells suppress a state of hyperinsulinemia in a fasting state.

Percolation modeling predicts critical behavior in fasting insulin secretion in KIR6.2[ΔN2-30,K185Q] mice

In KIR6.2[ΔN2-30,K185Q] transgenic mice, the level of expression can be induced by tamoxifen injections and quantified through GFP fluorescence. This ability to variably make levels of the K_{ATP} channels in β-cells insensitive to ATP gives us a model in which we can study the effect of variable percent of excitable cells (p_{exc}). The transgene is tagged with GFP and higher levels of GFP fluorescence indicate greater expression of the KIR6.2[ΔN2-30,K185Q] transgene and therefore a lower p_{exc}. The percent of excitable cells (x-axis in Figures19A-C) compared to a wild-type islet thus represents one minus the fraction of GFP fluorescence. At zero fluorescence, the islet is wild-type, and at maximal fluorescence the islet is maximally suppressed.

In ranges of p (or in this case, lattice connectivity) which were found to approximate MIN6 aggregates (0.3-0.4), the model predicted that at low levels of p_{exc} (high GFP fluorescence), there would be slight increases in the percent of cells active at low glucose up to $p_{exc} \sim 0.6$ (Figure 19A). However, as p_{exc} approaches 85% there are not enough quiescent cells in the system to suppress the other active cells and the model shows a sharp increase in low glucose activity. The plasma insulin data agreed nicely with this predication, showing a rapid increase in this area. However, a lack of data in the range of pexc = 0.6-0.9 made the true critical point difficult to predict. Since the dose-response of KIR6.2[ΔN2-30,K185Q] can be tailored to focus on this region, we hope to gain more data and better approximate this threshold in the future. Nonetheless, the existence of a critical point in the experimental data, which we were able to predict with relative accuracy, further verifies that the true threshold of quiescent cells necessary to suppress the entire islet is between 10-40%.

The diabetic phenotype is characterized by an increase in non-β-cells in the islet core combined with a decrease in β-cell mass, which could explain the decrease in gap junction coupling and insulin sensitivity. Indeed, development of overt diabetes (chronic hyperglycemia) is a long process has been found to occur when the overall functional beta-cell mass drops below a threshold necessary to maintain euglycemia (10–30% of total beta-cell mass in various species; Gepts 1965; Kjerns et al. 2001; Larsen et al. 2003; Sreenan et al. 1999; Bonner-Weir et al 1983). This is supported by previous from Rochelau et al, which showed that within intact KIR6.2[AAA] islets, β-cells exhibit essentially normal $[Ca^{2+}]_i$ activity and insulin release. This suggests that the maintained cell-cell contact suppresses the expected elevations in these two factors at low glucose given the K_{ATP} mutation (Rochelau et al. 2006). Since it is known that 70% of these cells are constitutively active, we can state that the level of quiescent cells necessary to suppress the coupled islet it <30%,

which is consistent with our data. Combined with our current findings, we can therefore further tailor the approximation of cells necessary to suppress coupling to 10-30%.

Using the same model of KIR6.2[AAA]/Cx36 mice as the present work, Benninger et al. found that despite elevations in $[Ca^{2+}]_i$ activity at low glucose following complete knockout of Cx36, there was not a concomitant increase in insulin secretion (Benninger et al. 2010). This suggests supports the work by Rochelau et al. suggesting that some level of gap junctional coupling is preventing activity at low glucose. Our model of KIR6.2[ΔN2-30,K185Q] mice shows that this is most likely because 70% penetrance of the transgene still corresponds to sub-critical suppression, meaning that there were sufficient quiescent cells to suppress the increase insulin secretion. However, our data predicts that if this level of penetrance was increased to >80% there would be a concomitant increase in insulin release.

In the KIR6.2[ΔN2-30,K185Q] model we used fasting plasma insulin as an approximation to low glucose activity of the islets, which is represented as percent of cells active in our model. However, the model was built and validated to predict $[Ca^{2+}]_i$ activity in isolated islets. Therefore, although the plasma insulin data was found to correlate well with model predictions at an experimentally predicated range of p, we suspect that when $[Ca^{2+}]_i$ activity is quantified there will be better agreement. More specifically, plasma insulin can vary even with maximal $[Ca^{2+}]_i$ activity and the experimental data will show a sharper increase in activity compared to the plasma insulin.

Implications of the Model for Overactive K_{ATP} Channels

The ability of cells to communicate with one another via gap junctions in the intact islet of Langerhans is important for the enhancement and coordination of glucose-stimulated insulin secretion as well as for uniform suppression of insulin secretion at low glucose. While isolated β-cells exhibit transient $[Ca^{2+}]_i$ activity which is thought to be based on a heterogeneous distribution of K_{ATP} channels, intact islets (some with up to 70% basal activity) show uniform quiescence at low glucose. Although this behavior has been shown to be a gap junction-dependent (Benninger et al. 2010), we have further explored this mechanism by applying a model based on percolation theory.

These results have implication in the understanding of diabetic phenotypes resulting from K_{ATP} dysfunction. Neonatal diabetes is caused from overactive K_{ATP} channels and leads to an inability to secrete insulin. Our data shows that cell-cell coupling can create a hyperpolarized state in all cells if K_{ATP} activity is low enough in a small percentage of cells. More ambitiously, our model predicts that when less than 15-30% of β-cells exhibit K_{ATP} hyperactivity, the entire islet becomes overactive and may potentially lead to a diabetic phenotype. Furthermore, our model predicts that when g_{coup} falls below ~25% of wild type levels, the reduction in coupling abolishes this suppressive effect (Figure 17B). Thus, normal percentages of active cells as found from our model (~67%) can lead to a several-fold increase in basal plasma insulin. For example, our model predicts that when coupling falls to 20% of wild type, ~67% excitable cells will secrete four times the insulin as the 35% coupling conductance which fit the model. If coupling falls to 10% of wild type, this insulin secreted will be ~6.5 fold higher.

It has previously been reported that elevating cAMP under low glucose conditions cause a rise in insulin secretion in Cx36-/- mice, but has a negligible effect in Cx36+/+ mice.

This result demonstrates that gap junctions can robustly suppress elevations in basal insulin secretion induced by secretagogues that act independently of Ca^{2+} (Benninger et al. 2010). Since plasma insulin was found to scale approximately with our model of $[Ca^{2+}]_i$ activity, evaluating the effects of cAMP on insulin secretion by the model's approximation will be an active area of research by our group. In addition, these data suggest that glucagon-like peptide 1 based treatments (which elevate cAMP and therefore prime insulin secretion) will be less effective at low levels of gap junction coupling since the elevated basal release will decrease the dynamic range of GSIS.

This mechanism may also explain an evolutionary drive to organize these secretory cells into a unique electrical syncytium. Such a mechanism provides a protective effect against hypoglycemia if individual cell properties change under pathological or physiological stimuli. Since elevations in basal insulin and a decrease in β-cell coupling have been shown to occur in obese individuals as well as type II diabetics (Bonner-Weier & Turner, 2008; Rahier et al. 2003; Porksen et al. 2002), our model further supports these pathological changes as occurring in-tandem and also makes clinically-relevant predictions about how a pathological phenotype can rapidly progress as regions of criticality are approached.

Future Directions

Given the surprising results seen in day 14 pseudo-islets, this gives promise to the potential for increasing the efficacy of human transplants. Future work in this arena needs to focus on not only further validating the procedure through application to a mouse model of diabetes, but also reaggregating human transplant islets to determine if function can

indeed be increased. A major part of this work is revealing the mechanism through which the increased viability was achieved.

Increase in contact between α- and β-cells could help to explain the differences seen. Glucagon (which is secreted by α-cells) has been known to potentiate glucose induced insulin secretion through what is thought to be a cAMP-dependent effect (Huypens et al 2000; Pipeleers et al. 1985; Samols, Marri & Marks 1965; Kawai et al. 1995). Insulin release from human β-cells at high glucose has also been found to be significantly diminished by the addition of a glucagon-receptor antagonist (Huypens et al. 2000). This has been thought to explain why patients with type 2 diabetes commonly have a mutation in the glucagon receptor gene (Hager et al. 1995). Taken together, this suggests that there is a minimal threshold of paracrine glucagon is required to keep β-cells in a glucose competent state.

Glucagon binding in β-cells causes an increase in cAMP levels and factors which increase intracellular cAMP have been found to increase β-cell survival and avoid apoptosis (Drucker 2003). In a mouse model with knockout glucagon receptor, mice showed β-cell destruction (Lee et al. 2011). Furthermore, cAMP promotes beta cell survival via a process mediated through the transcription factor CREB (Jhala et al. 2003).

Under in-vivo conditions, a significant portion of the vasculature flows from the α-cell containing mantle into the predominantly β-cell core, resulting in a paracrine pathway for glucagon interactions (Jansson 1994; Nyman et al. 2008). However, isolated islets do not have such vasculature and therefore the glucose-potentiating and anti-apoptotic properties of glucagon may not be fully realized and that may be leading to the deterioration of the normal islets at day 7. By reorganizing the islet cells in a heterogeneous manner, we may therefore be increasing the relative proximity between any given α-cell and β-cell and thus increasing viability and function. To investigate this effect, future experiments will first

need to identify the pseudo-islet architecture as being heterogeneous or mantle-core through staining for α- and β-cells. Then, the expression of cAMP with regards to glucagon-binding will need to be established in ex-vivo normal islets as well as pseudo-islets. Expression of cAMP can be accomplished through cAMP biosensors (Kim et al. 2010; Dyachok et al. 2006) and correlated with glucagon levels through ELISA or immunofluorescence.

While the aggregation procedure poses to greatly improve transplant outcomes, it can also give us a platform to continue to apply our model to the pathogenesis of diabetes. As previously stated, the diabetic phenotype is characterized by an increase in non-β-cells in the islet core combined with a decrease in β-cell mass, which could explain the decrease in gap junction coupling and insulin sensitivity. Indeed, development of overt diabetes (chronic hyperglycemia) is a long process has been found to occur when the overall functional beta-cell mass drops below a threshold necessary to maintain euglycemia (10–30% of total beta-cell mass in various species; Gepts 1965; Kjerns et al. 2001; Larsen et al. 2003; Sreenan et al. 1999; Bonner-Weir et al 1983). By incorporating inert microbeads or defined fractions of $Cx36^{-/-}$ islet cells, we can test this hypothesis and determine the true critical fraction of functional β-cells necessary to maintain insulin homeostasis. Also, since human islets have been reported to have distinct areas of $[Ca^{2+}]_i$ coordination, which may be the result of islet reorganization, we can also use this model to explain whether a different architecture is responsible for the differences seen between species or the progression of a diabetic phenotype as humans age.

Transgenic KIR6.2[AAA] mice allow us to look at an islet where 70% of the cells are active at low glucose. We show that in our low glucose model with a probability of being excitable of pexc = 0.7, the predicted p (or g_{coup}) fits the experimental data quite nicely.

Importantly, it is very accurate at the high and low ranges. However, this system can only shed light on the 70% activity for varying levels of p, which are created through Cx36 transgenic knockout combined with inhibitors. By reaggregating KIR6.2[AAA]/Cx36 mice with Cx36 mice lacking the KIR6.2 mutation we can achieve variable levels of pexc<0.7. This will allow us to further characterize and validate the model with higher level perturbations.

This model can also be added upon by incorporating a simple model of intracell electrodynamics combined with a coupling term to model how decreasing p affects the overall $[Ca^{2+}]_i$ dynamics at physiological levels of coupling. This model could also predict changes in gap junction conductance with the progression of diabetes. In addition, if the percolation model holds, it predicts that the clustering of coupled β-cells follows a fractal pattern, which is partially supported by the Bosco, et al. paper describing the islet as being based on a repeated unit of cell architecture. Using our model, we could possibly explain this behavior and the effects of dimensionality.

Not much is known about the topology of the β-cell network or about the conditions which underlay their synchronization. Our model can shed light on the topology of the β-cell network and help to understand how changes in cytoarchitecture can affect the coordination of $[Ca^{2+}]_i$ dynamics. Multiple papers have described how synchronized and chaotic behavior can emerge in coupled-oscillator networks, with many predicting coupling conditions and specific predictions regarding topology (Huang et al. 2008; Sherman 2011). For example, a paper by Huang et al. predicts that optimal synchronization in complex clustered networks evolves from many weak coupling of highly coupled clusters, which may explain why human islets have a different architecture from mice (Huang et al. 2008) – which is not surprising given that their islets are generally the same size despite the huge differences in metabolic demands. Some groups have also applied β-cell oscillatory

behavior; however none have had the proper experimental models to validate theoretical predictions. Since we have a variety of mouse models with ion channel mutations as well as a method for aggregating different proportions of these cells into functional pseudo-islets, we have the unique capability to test many of our complex mathematical models.

In our simulations, we model a heterogeneous and spherical organ (in terms of cellular composition) as a homogenous cube. Since we have proven that small perturbations in architecture can have significant impacts on behavior, this is an area where the model can be improved. Using a spherical lattice may impact behavior around the boundaries since the surface area of the cube is ~125% that of a sphere. Site percolation can be included to account for the presence of non β-cells, which are currently incorporated into the model by further reductions in p. Also, using site percolation also might allow us to predict some of the effects of cellular reorganization on $[Ca^{2+}]_i$ dynamics. Pseudo-islets were found to behave differently in long-term culture and a reorganization of cellular dynamics may be a cause. If this is indeed the case, the combined site/bond percolation model may be able to account for the behavior through decreased vasculature and other architectural effects.

Application of complex network theory in biology is a new and emerging field which is allowing us to understand structural properties and functional behavior of systems at scales inaccessible to classical approaches which explain behavior as the summation of its individual components. For example, a recent paper has already described that the network architecture of the islet follows scale-free principles, which predicts that there are highly connected cells which dominate the behavior of the whole cluster (Hastings et al. 2013), while another paper posits that the network follows a small-world architecture which is defined by many connected small clusters (Stozer et al. 2013). However informative, neither

model used validated techniques for measuring cell-cell coupling and both studies where done in 2D. By utilizing our model with confocal microscopy or other 3D techniques and genetic variants, we can build a working model of islet connectivity and provide compelling evidence for the true network topology.

REFERENCES

Albert, R., & Barabási, A. L. (2002). Statistical mechanics of complex networks. *Reviews of modern physics*, *74*(1), 47.

Ämmälä, C., Ashcroft, F. M., & Rorsman, P. (1993). Calcium-independent potentiation of insulin release by cyclic AMP in single β-cells. *Nature, 363,* 356-358

Allagnat, F., Martin, D., Condorelli, D. F., Waeber, G., & Haefliger, J. A. (2005). Glucose represses connexin36 in insulin-secreting cells. *Journal of cell science*, 118(22), 5335-5344.

Ashcroft FM, Rorsman P (1989) Electrophysiology of the pancreatic beta-cell. *Prog Biophys Mol Biol* 54: 87–143.

Ashcroft, F. M., & Gribble, F. M. (1999). ATP-sensitive K+ channels and insulin secretion: their role in health and disease. *Diabetologia*, *42*(8), 903-919.

Barabási, A. L., & Albert, R. (1999). Emergence of scaling in random networks. *Science,* 286(5439), 509-512.

Bates, H. E., Sirek, A. S., Kiràly, M. A., Yue, J. T., Montes, D. G., Matthews, S. G., & Vranic, M. (2008). Adaptation to mild, intermittent stress delays development of hyperglycemia in the Zucker diabetic Fatty rat independent of food intake: role of habituation of the hypothalamic-pituitary-adrenal axis. *Endocrinology*, 149(6), 2990-3001.

Beattie, G. M., Leibowitz, G., Lopez, A. D., Levine, F., & Hayek, A. (2000). Protection from cell death in cultured human fetal pancreatic cells. *Cell transplantation*, 9(3), 431.

Benninger, R. K., Zhang, M., Head, W. S., Satin, L. S., & Piston, D. W. (2008). Gap junction coupling and calcium waves in the pancreatic islet. *Biophysical journal*, *95*(11), 5048-5061.

Benninger, R. K., Head, W. S., Zhang, M., Satin, L. S., & Piston, D. W. (2011). Gap junctions and other mechanisms of cell–cell communication regulate basal insulin secretion in the pancreatic islet. *The Journal of physiology*, *589*(22), 5453-5466.

Bratusch-Marrain, P. R., Komjati, M., & Waldhäusl, W. K. (1986). Efficacy of pulsatile versus continuous insulin administration on hepatic glucose production and glucose utilization in type I diabetic humans. *Diabetes*, *35*(8), 922-926.

Bertram, R., Previte, J., Sherman, A., Kinard, T. A., & Satin, L. S. (2000). The Phantom Burster Model for Pancreatic β-Cells. *Biophysical journal*,*79*(6), 2880-2892.

Bertuzzi, F., Davalli, A. M., Nano, R., Socci, C., Codazzi, F., Fesce, R., ... & Grohovaz, F. (1999). Mechanisms of coordination of Ca2+ signals in pancreatic islet cells. *Diabetes*, *48*(10), 1971-1978.

Bosco, D., Armanet, M., Morel, P., Niclauss, N., Sgroi, A., Muller, Y. D., ... & Berney, T. (2010). Unique arrangement of α-and β-cells in human islets of Langerhans. *Diabetes*, 59(5), 1202-1210.

Bollobás, B. (1981). Degree sequences of random graphs. *Discrete Mathematics*, 33(1), 1-19.

Bokvist, K., Rorsman, P., & Smith, P. A. (1990). Block of ATP-regulated and Ca2 (+)-activated K+ channels in mouse pancreatic beta-cells by external tetraethylammonium and quinine. *The Journal of physiology*, 423(1), 327-342.

Bonner-Weir, S., Trent, D. F., & Weir, G. C. (1983). Partial pancreatectomy in the rat and subsequent defect in glucose-induced insulin release. *Journal of Clinical Investigation*, 71(6), 1544.

Brissova, M., Fowler, M., Wiebe, P., Shostak, A., Shiota, M., Radhika, A., ... & Powers, A. C. (2004). Intraislet endothelial cells contribute to revascularization of transplanted pancreatic islets. *Diabetes*, 53(5), 1318-1325.

Brissova, M., Fowler, M. J., Nicholson, W. E., Chu, A., Hirshberg, B., Harlan, D. M., & Powers, A. C. (2005). Assessment of human pancreatic islet architecture and composition by laser scanning confocal microscopy. *Journal of Histochemistry & Cytochemistry*, 53(9), 1087-1097.

Butler, A. E., Janson, J., Bonner-Weir, S., Ritzel, R., Rizza, R. A., & Butler, P. C. (2003). β-Cell deficit and increased β-cell apoptosis in humans with type 2 diabetes. *Diabetes*, 52(1), 102-110.

Cabrera, O., Berman, D. M., Kenyon, N. S., Ricordi, C., Berggren, P. O., & Caicedo, A. (2006). The unique cytoarchitecture of human pancreatic islets has implications for islet cell function. *Proceedings of the National Academy of Sciences of the United States of America*, *103*(7), 2334-2339.

Cerasi, E., Luft, R., & Efendic, S. (1972). Decreased sensitivity of the pancreatic beta cells to glucose in prediabetic and diabetic subjects: a glucose dose-response study. *Diabetes*, *21*(4), 224-234.

Clark, A., Wells, C. A., Buley, I. D., Cruickshank, J. K., Vanhegan, R. I., Matthews, D. R., ... & Turner, R. C. (1988). Islet amyloid, increased A-cells, reduced B-cells and exocrine fibrosis: quantitative changes in the pancreas in type 2 diabetes. *Diabetes research* (Edinburgh, Scotland), 9(4), 151.

Chan, C. B., & Surette, J. J. (1999). Glucose refractoriness of β-cells from fed fa/fa rats is ameliorated by nonesterified fatty acids. *Canadian journal of physiology and pharmacology*, *77*(12), 934-942.

Chay, T. R., & Keizer, J. (1983). Minimal model for membrane oscillations in the pancreatic beta-cell. *Biophysical Journal*, *42*(2), 181-189.

Cirulli, V., Halban, P. A., & Rouiller, D. G. (1993). Tumor necrosis factor-alpha modifies adhesion properties of rat islet B cells. *Journal of Clinical Investigation*, 91(5), 1868.

Drews, G., Krippeit-Drews, P., & Düfer, M. (2010). Electrophysiology of islet cells. In *The Islets of Langerhans* (pp. 115-163). Springer Netherlands.

Drucker, D. J. (2003). Glucagon-like peptide-1 and the islet β-cell: augmentation of cell proliferation and inhibition of apoptosis. *Endocrinology*, 144(12), 5145-5148.

Dyachok, O., & Gylfe, E. (2004). Ca2+-induced Ca2+ release via inositol 1, 4, 5-trisphosphate receptors is amplified by protein kinase A and triggers exocytosis in pancreatic β-cells. *Journal of Biological Chemistry*, *279*(44), 45455-45461.

Dyachok, O., Isakov, Y., Sågetorp, J., & Tengholm, A. (2006). Oscillations of cyclic AMP in hormone-stimulated insulin-secreting β-cells. *Nature*, *439*(7074), 349-352.

Dyachok, O., Idevall-Hagren, O., Sågetorp, J., Tian, G., Wuttke, A., Arrieumerlou, C., ... & Tengholm, A. (2008). Glucose-induced cyclic AMP oscillations regulate pulsatile insulin secretion. *Cell metabolism*, *8*(1), 26-37.

Eddlestone, G. T., Goncalves, A., Bangham, J. A., & Rojas, E. (1984). Electrical coupling between cells in islets of Langerhans from mouse. *The Journal of membrane biology*, *77*(1), 1-14.

Eliasson, L., Ma, X., Renström, E., Barg, S., Berggren, P. O., Galvanovskis, J., ... & Rorsman, P. (2003). SUR1 regulates PKA-independent cAMP-induced granule priming in mouse pancreatic B-cells. *The Journal of general physiology*,*121*(3), 181-197.

Erdős, P., & Rényi, A. (1959). On random graphs. *Publicationes Mathematicae Debrecen*, *6*, 290-297.

Epstein, P. N., Overbeek, P. A., & Means, A. R. (1989). Calmodulin-induced early-onset diabetes in transgenic mice. *Cell*, 58(6), 1067-1073.

Fraser, I. D., Tavalin, S. J., Lester, L. B., Langeberg, L. K., Westphal, A. M., Dean, R. A., ... & Scott, J. D. (1998). A novel lipid-anchored A-kinase anchoring protein facilitates cAMP-responsive membrane events. *The EMBO journal*,*17*(8), 2261-2272.

Fung, M. A., Warnock, G. L., Ao, Z., Keown, P., Meloche, M., Shapiro, R. J., ... & Thompson, D. M. (2007). The effect of medical therapy and islet cell transplantation on diabetic nephropathy: an interim report. *Transplantation,* 84(1), 17.

Gerstein HC, Miller ME, Byington RP, Goff DC, Bigger JT, Buse JB, Cushman WC, Genuth S, Ismail-Beigi F, Grimm RH, Probstfield JL, Simons-Morton DG, Friedewald WT (2008). "Effects of intensive glucose lowering in type 2 diabetes". *N. Engl. J. Med.* **358** (24): 2545–59.

Gepts, W. (1965). Pathologic anatomy of the pancreas in juvenile diabetes mellitus. *Diabetes*, 14(10), 619-633.

Gillis, K. D., & Misler, S. (1993). Enhancers of cytosolic cAMP augment depolarization-induced exocytosis from pancreatic B-cells: evidence for effects distal to Ca2+ entry. *Pflügers Archiv*, *424*(2), 195-197.

Gilon, P., & Henquin, J. C. (1992). Influence of membrane potential changes on cytoplasmic Ca2+ concentration in an electrically excitable cell, the insulin-secreting pancreatic B-cell. *Journal of Biological Chemistry*, *267*(29), 20713-20720.

Goodner, C. J., Sweet, I. R., & Harrison, H. C. (1988). Rapid reduction and return of surface insulin receptors after exposure to brief pulses of insulin in perifused rat hepatocytes. *Diabetes*, *37*(10), 1316-1323.

Gromada, J., Ma, X., Høy, M., Bokvist, K., Salehi, A., Berggren, P. O., & Rorsman, P. (2004). ATP-sensitive K+ channel–dependent regulation of glucagon release and electrical activity by glucose in wild-type and SUR1−/− mouse α-cells. *Diabetes*, *53*(suppl 3), S181-S189.

Göpel, S. O., Kanno, T., Barg, S., Weng, X. G., Gromada, J., & Rorsman, P. (2000). Regulation of glucagon release in mouse α-cells by KATP channels and inactivation of TTX-sensitive Na+ channels. *The Journal of physiology*, *528*(3), 509-520.

Grant AM, Christie MR, Ashcroft SJH. (1980). Insulin release from human pancreatic islets in vitro. *Diabetologia, 19*, 114-17

Grapengiesser, E., Gylfe, E. R. I. K., & Hellman, B. (1990). Sulfonylurea mimics the effect of glucose in inducing large amplitude oscillations of cytoplasmic Ca2+ in pancreatic beta-cells. *Molecular pharmacology*, *37*(3), 461-467.

Head, W. S., Orseth, M. L., Nunemaker, C. S., Satin, L. S., Piston, D. W., & Benninger, R. K. (2012). Connexin-36 gap junctions regulate in vivo first-and second-phase insulin secretion dynamics and glucose tolerance in the conscious mouse. *Diabetes*, *61*(7), 1700-1707.

Hager, J., Hansen, L., Vaisse, C., Vionnet, N., Philippi, A., Poller, W., ... & Froguel, P. H. I. L. I. P. P. E. (1995). A missense mutation in the glucagon receptor gene is associated with non–insulin–dependent diabetes mellitus. *Nature Genetics*, 9(3), 299-304.

Halban, P. A., WOLLHEIM, C. B., BLONDEL, B., Meda, P., NIESOR, E. N., & MINTZ, D. H. (1982). The possible importance of contact between pancreatic islet cells for the control of insulin release. *Endocrinology*, *111*(1), 86-94.

Henquin, J. C. (2000). Triggering and amplifying pathways of regulation of insulin secretion by glucose. *Diabetes*, *49*(11), 1751-1760.

Huypens, P., Ling, Z., Pipeleers, D., & Schuit, F. (2000). Glucagon receptors on human islet cells contribute to glucose competence of insulin release. *Diabetologia*, 43(8), 1012-1019.

Jansson, L. (1994). The regulation of pancreatic islet blood flow. *Diabetes/metabolism reviews*, 10(4), 407-416.

Jing, X., Li, D. Q., Olofsson, C. S., Salehi, A., Surve, V. V., Caballero, J., ... & Renström, E. (2005). CaV2. 3 calcium channels control second-phase insulin release. *Journal of Clinical Investigation*, *115*(1), 146-154.

Jhala, U. S., Canettieri, G., Screaton, R. A., Kulkarni, R. N., Krajewski, S., Reed, J., ... & Montminy, M. (2003). cAMP promotes pancreatic β-cell survival via CREB-mediated induction of IRS2. *Genes & development*, 17(13), 1575-1580.

Kaihow T, Masuda T, Sasano N, and Takahashi T. (1986). The size and number of Langerhans islets correlated with their endocrine function: a morphometry on immunostained serial sectioned adult human pancreases.*Tohoku J Exp Med* 149: 1–10.

Kawai, K., Yokota, C., Ohashi, S., Watanabe, Y., & Yamashita, K. (1995). Evidence that glucagon stimulates insulin secretion through its own receptor in rats. *Diabetologia*, 38(3), 274-276.

Kanno T, Rorsman P, Gopel SO (2002) Glucose-dependent regulation of rhythmic action potential firing in pancreatic β cells by KATP-channel modulation. *J Physiol, 545,* 501–507.

Keizer, J., & Smolen, P. (1991). Bursting electrical activity in pancreatic beta cells caused by Ca (2+)-and voltage-inactivated Ca2+ channels. *Proceedings of the National Academy of Sciences*, *88*(9), 3897-3901.

Kjems, L. L., Kirby, B. M., Welsh, E. M., Veldhuis, J. D., Straume, M., McIntyre, S. S., ... & Butler, P. C. (2001). Decrease in β-cell mass leads to impaired pulsatile insulin secretion, reduced postprandial hepatic insulin clearance, and relative hyperglucagonemia in the minipig. *Diabetes*, 50(9).

Kilimnik, G., Zhao, B., Jo, J., Periwal, V., Witkowski, P., Misawa, R., & Hara, M. (2011). Altered islet composition and disproportionate loss of large islets in patients with type 2 diabetes. *PloS one*, 6(11), e27445.

Kloxin, A. M., Tibbitt, M. W., & Anseth, K. S. (2010). Synthesis of photodegradable hydrogels as dynamically tunable cell culture platforms.*Nature protocols*, 5(12), 1867-1887.

Konstantinova, I., Nikolova, G., Ohara-Imaizumi, M., Meda, P., Kucera, T., Zarbalis, K., ... & Lammert, E. (2007). EphA-Ephrin-A-mediated β cell communication regulates insulin secretion from pancreatic islets. *Cell*, 129(2), 359-370.

Komatsu, M., Schermerhorn, T., Noda, M., Straub, S. G., Aizawa, T., & Sharp, G. W. (1997). Augmentation of insulin release by glucose in the absence of extracellular Ca2+: new insights into stimulus-secretion coupling. *Diabetes*,*46*(12), 1928-1938.

Koster, J. C., Marshall, B. A., Ensor, N. E. A., Corbett, J. A., & Nichols, C. G. (2000). Targeted Overactivity of β Cell K< sub> ATP</sub> Channels Induces Profound Neonatal Diabetes. *Cell*, *100*(6), 645-654.

Koster, J. C., Remedi, M. S., Flagg, T. P., Johnson, J. D., Markova, K. P., Marshall, B. A., & Nichols, C. G. (2002). Hyperinsulinism induced by targeted suppression of beta cell KATP channels. *Proceedings of the National Academy of Sciences*, *99*(26), 16992-16997.

Kwan, E. P., Xie, L., Sheu, L., Ohtsuka, T., & Gaisano, H. Y. (2007). Interaction Between Munc13-1 and RIM Is Critical for Glucagon-Like Peptide-1–Mediated Rescue of Exocytotic Defects in Munc13-1–Deficient Pancreatic β-Cells. *Diabetes*, *56*(10), 2579-2588.

Landa, L. R., Harbeck, M., Kaihara, K., Chepurny, O., Kitiphongspattana, K., Graf, O., ... & Roe, M. W. (2005). Interplay of Ca2+ and cAMP signaling in the insulin-secreting MIN6 β-cell line. *Journal of Biological Chemistry*, *280*(35), 31294-31302.

Lang, D. A., Matthews, D. R., Peto, J., & Turner, R. C. (1979). Cyclic oscillations of basal plasma glucose and insulin concentrations in human beings. *The New England journal of medicine*, *301*(19), 1023.

Lang, D. A., Matthews, D. R., Burnett, M., & Turner, R. C. (1981). Brief, irregular oscillations of basal plasma insulin and glucose concentrations in diabetic man. *Diabetes*, *30*(5), 435-439.

Larsen, M. O., Rolin, B., Wilken, M., Carr, R. D., & Gotfredsen, C. F. (2003). Measurements of insulin secretory capacity and glucose tolerance to predict pancreatic β-cell mass in vivo in the nicotinamide/streptozotocin Göttingen minipig, a model of moderate insulin deficiency and diabetes. *Diabetes*, 52(1), 118-123.

Lee, Y., Wang, M. Y., Du, X. Q., Charron, M. J., & Unger, R. H. (2011). Glucagon receptor knockout prevents insulin-deficient type 1 diabetes in mice. *Diabetes*, 60(2), 391-397.

Lehmann, R., Zuellig, R. A., Kugelmeier, P., Baenninger, P. B., Moritz, W., Perren, A., ... & Spinas, G. A. (2007). Superiority of small islets in human islet transplantation. *Diabetes*, *56*(3), 594-603.

Lernmark, Å. (1974). The preparation of, and studies on, free cell suspensions from mouse pancreatic islets. *Diabetologia*, *10*(5), 431-438.

LeRoith, D. (2002). β-cell dysfunction and insulin resistance in type 2 diabetes: role of metabolic and genetic abnormalities. *The American journal of medicine*,*113*(6), 3-11.

Lester, L. B., Langeberg, L. K., & Scott, J. D. (1997). Anchoring of protein kinase A facilitates hormone-mediated insulin secretion. *Proceedings of the National Academy of Sciences*, *94*(26), 14942-14947.

Lin, C. C., & Anseth, K. S. (2009). Controlling Affinity Binding with Peptide-Functionalized Poly (ethylene glycol) Hydrogels. *Advanced functional materials*, 19(14), 2325-2331.

Liu, Y. J., Vieira, E., & Gylfe, E. (2004). A store-operated mechanism determines the activity of the electrically excitable glucagon-secreting pancreatic α-cell. *Cell calcium*, *35*(4), 357-365.

MacDonald, P. E., & Wheeler, M. B. (2003). Voltage-dependent K+ channels in pancreatic beta cells: role, regulation and potential as therapeutic targets. *Diabetologia*, *46*(8), 1046-1062.

MacDonald PE, Rorsman P (2006) Oscillations, Intercellular Coupling, and Insulin Secretion in Pancreatic β Cells. PLoS Biol 4(2): e49. doi:10.1371/journal.pbio.0040049

MacGregor, R. R., Williams, S. J., Tong, P. Y., Kover, K., Moore, W. V., & Stehno-Bittel, L. (2006). Small rat islets are superior to large islets in in vitro function and in transplantation outcomes. *American Journal of Physiology-Endocrinology And Metabolism*, *290*(5), E771-E779.

Matthews, D. R., Naylor, B. A., Jones, R. G., Ward, G. M., & Turner, R. C. (1983). Pulsatile insulin has greater hypoglycemic effect than continuous delivery. *Diabetes*, *32*(7), 617-621.

Mattsson, G., Jansson, L., & Carlsson, P. O. (2002). Decreased vascular density in mouse pancreatic islets after transplantation. *Diabetes*, 51(5), 1362-1366.

Meier, J. J., Veldhuis, J. D., & Butler, P. C. (2005). Pulsatile insulin secretion dictates systemic insulin delivery by regulating hepatic insulin extraction in humans. *Diabetes*, *54*(6), 1649-1656.

Mellitus, D. (2006). Diagnosis and classification of diabetes mellitus. *Diabetes care*, *29*, S43.

Menge, B. A., Grüber, L., Jørgensen, S. M., Deacon, C. F., Schmidt, W. E., Veldhuis, J. D., ... & Meier, J. J. (2011). Loss of inverse relationship between pulsatile insulin and glucagon secretion in patients with type 2 diabetes. *Diabetes*, 60(8), 2160-2168.

Misler, S., Barnett, D. W., Pressel, D. M., Gillis, K. D., Scharp, D. W., & Falke, L. C. (1992). Stimulus-secretion coupling in β-cells of transplantable human islets of langerhans: evidence for a critical role for Ca2+ entry. *Diabetes*,*41*(6), 662-670.

Moreno, A. P., Berthoud, V. M., Pérez-Palacios, G., & Pérez-Armendariz, E. M. (2005). Biophysical evidence that connexin-36 forms functional gap junction channels between pancreatic mouse β-cells. *American Journal of Physiology-Endocrinology And Metabolism*, 288(5), E948-E956.

Najarian, K., & Splinter, R. (2012). Biomedical signal and image processing. CRC press.

Ni, Q., Ganesan, A., Aye-Han, N. N., Gao, X., Allen, M. D., Levchenko, A., & Zhang, J. (2010). Signaling diversity of PKA achieved via a Ca2+-cAMP-PKA oscillatory circuit. *Nature chemical biology*, *7*(1), 34-40.

Nunemaker, C. S., Wasserman, D. H., McGuinness, O. P., Sweet, I. R., Teague, J. C., & Satin, L. S. (2006). Insulin secretion in the conscious mouse is biphasic and pulsatile. *American Journal of Physiology-Endocrinology And Metabolism*, *290*(3), E523-E529.

Nyman, L. R., Wells, K. S., Head, W. S., McCaughey, M., Ford, E., Brissova, M., ... & Powers, A. C. (2008). Real-time, multidimensional in vivo imaging used to investigate blood flow in mouse pancreatic islets. *The Journal of clinical investigation*, 118(11), 3790.

O'Meara, N. M., Sturis, J., Van Cauter, E., & Polonsky, K. S. (1993). Lack of control by glucose of ultradian insulin secretory oscillations in impaired glucose tolerance and in non-insulin-dependent diabetes mellitus. *Journal of Clinical Investigation*, *92*(1), 262.

O'Rahilly, S., Turner, R. C., & Matthews, D. R. (1988). Impaired pulsatile secretion of insulin in relatives of patients with non-insulin-dependent diabetes.*The New England journal of medicine*, *318*(19), 1225.

O'sullivan, E. S., Johnson, A. S., Omer, A., Hollister-Lock, J., Bonner-Weir, S., Colton, C. K., & Weir, G. C. (2010). Rat islet cell aggregates are superior to islets for transplantation in microcapsules. *Diabetologia*, 53(5), 937-945.

Peiris, A. N., Stagner, J. I., Vogel, R. L., Nakagawa, A., & Samols, E. (1992). Body fat distribution and peripheral insulin sensitivity in healthy men: role of insulin pulsatility. *Journal of Clinical Endocrinology & Metabolism*, *75*(1), 290-294.

Paolisso, G., Sgambato, S., Torella, R., Varricchio, M., Scheen, A., D'onofrio, F., & Lefebvre, P. J. (1988). Pulsatile insulin delivery is more efficient than continuous infusion in modulating islet cell function in normal subjects and patients with type 1 diabetes. *Journal of Clinical Endocrinology & Metabolism*,*66*(6), 1220-1226.

Pipeleers, D. G., Schuit, F. C., Van Schravendijk, C. F. H., & Van de Winkel, M. (1985). Interplay of nutrients and hormones in the regulation of glucagon release. *Endocrinology*, 117(3), 817-823.

Pørksen, N. (2002). The in vivo regulation of pulsatile insulin secretion.*Diabetologia*, *45*(1), 3-20.

Rahier, J., Goebbels, R. M., & Henquin, J. C. (1983). Cellular composition of the human diabetic pancreas*. Diabetologia*, 24(5), 366-371.

Ravier, M. A., Güldenagel, M., Charollais, A., Gjinovci, A., Caille, D., Söhl, G., ... & Meda, P. (2005). Loss of connexin36 channels alters β-cell coupling, islet synchronization of glucose-induced Ca2+ and insulin oscillations, and basal insulin release. *Diabetes*, *54*(6), 1798-1807.

Reichlin, S. (1983). Somatostatin. *New England Journal of Medicine*, *309*(24), 1495-1501.

Renström, E., Eliasson, L., & Rorsman, P. (1997). Protein kinase A-dependent and-independent stimulation of exocytosis by cAMP in mouse pancreatic B-cells. *The Journal of physiology*, *502*(1), 105-118.

Ricordi C, Lacy PE, Finke EH, Olack BJ, Scharp, DW. (1998). Automated method for isolation of human pancreatic islets. *Diabetes* 37:413-20

Rocheleau, J. V., Walker, G. M., Head, W. S., McGuinness, O. P., & Piston, D. W. (2004). Microfluidic glucose stimulation reveals limited coordination of intracellular Ca2+ activity oscillations in pancreatic islets. *Proceedings of the National Academy of Sciences of the United States of America*, *101*(35), 12899-12903.

Rocheleau, J. V., Remedi, M. S., Granada, B., Head, W. S., Koster, J. C., Nichols, C. G., & Piston, D. W. (2006). Critical role of gap junction coupled KATP channel activity for regulated insulin secretion. *PLoS biology*, *4*(2), e26.

Rorsman, P., & Renström, E. (2003). Insulin granule dynamics in pancreatic beta cells. *Diabetologia*, *46*(8), 1029-1045.

Rorsman, P. (1997). The pancreatic beta-cell as a fuel sensor: an electrophysiologist's viewpoint. *Diabetologia*, *40*(5), 487-495.

Rouiller, D. G., Cirulli, V., & Halban, P. A. (1991). Uvomorulin mediates calcium-dependent aggregation of islet cells, whereas calcium-independent cell adhesion molecules distinguish between islet cell types. *Developmental biology*, 148(1), 233-242.

Ryan, E. A., Lakey, J. R., Paty, B. W., Imes, S., Korbutt, G. S., Kneteman, N. M., ... & Shapiro, A. J. (2002). Successful islet transplantation continued insulin reserve provides long-term glycemic control. *Diabetes*, *51*(7), 2148-2157.

Samols, E., Marri, G., & Marks, V. (1965). Promotion of insulin secretion by glucagon. *Lancet*, 2(7409), 415.

Santos, R. M., Rosario, L. M., Nadal, A., Garcia-Sancho, J., Soria, B., & Valdeolmillos, M. (1991). Widespread synchronous [Ca2+] i oscillations due to bursting electrical activity in single pancreatic islets. *Pflügers Archiv*, *418*(4), 417-422.

Sakuraba, H., Mizukami, H., Yagihashi, N., Wada, R., Hanyu, C., & Yagihashi, S. (2002). Reduced beta-cell mass and expression of oxidative stress-related DNA damage in the islet of Japanese Type II diabetic patients. *Diabetologia*, 45(1), 85-96.

Seino, S., & Shibasaki, T. (2005). PKA-dependent and PKA-independent pathways for cAMP-regulated exocytosis. *Physiological reviews*, *85*(4), 1303-1342.

Serre-Beinier, V., Bosco, D., Zulianello, L., Charollais, A., Caille, D., Charpantier, E., ... & Meda, P. (2009). Cx36 makes channels coupling human pancreatic β-cells, and correlates with insulin expression. *Human molecular genetics*, *18*(3), 428-439.

Sherman, A., RiNZEL, J. O. H. N., & Keizer, J. (1988). Emergence of organized bursting in clusters of pancreatic beta-cells by channel sharing. *Biophysical journal*, *54*(3), 411-425.

Sheridan, J. D., P. A. Anaya, J. A. Parsons, and R. L. Sorenson. (1988). Increased dye coupling in pancreatic-islets from rats in late-term pregnancy. *Diabetes.* 37:908–911.

Sorenson, R. L., and T. C. Brelje. (1997). Adaptation of islets of Langerhans to pregnancy: b-cell growth, enhanced insulin secretion and the role of lactogenic hormones. *Horm. Metab. Res.* 29:301–307.

Speier, S., Gjinovci, A., Charollais, A., Meda, P., & Rupnik, M. (2007). Cx36-mediated coupling reduces β-cell heterogeneity, confines the stimulating glucose concentration range, and affects insulin release kinetics. *Diabetes*,*56*(4), 1078-1086.

Splawski, I., Timothy, K. W., Sharpe, L. M., Decher, N., Kumar, P., Bloise, R., ... & Keating, M. T. (2004). Ca< sub> V</sub> 1.2 Calcium Channel Dysfunction Causes a Multisystem Disorder Including Arrhythmia and Autism. *Cell*, *119*(1), 19-31.

Sreenan, S., Pick, A. J., Levisetti, M., Baldwin, A. C., Pugh, W., & Polonsky, K. S. (1999). Increased beta-cell proliferation and reduced mass before diabetes onset in the nonobese diabetic mouse. *Diabetes*, 48(5), 989-996.

Stauffer, D., & Aharony, A. (1994). Introduction to percolation theory. CRC press.

Stefan, Y., Orci, L., Malaisse-Lagae, F., Perrelet, A., Patel, Y., & Unger, R. H. (1982). Quantitation of endocrine cell content in the pancreas of nondiabetic and diabetic humans. *Diabetes*, 31(8), 694-700.

Street, C. N., Lakey, J. R., Shapiro, A. J., Imes, S., Rajotte, R. V., Ryan, E. A., ... & Korbutt, G. S. (2004). Islet graft assessment in the Edmonton Protocol implications for predicting long-term clinical outcome. *Diabetes*, 53(12), 3107-3114.

Strogatz, S. H. (2001). Exploring complex networks. *Nature*, 410(6825), 268-276.

Tornheim, K. (1997). Are metabolic oscillations responsible for normal oscillatory insulin secretion?. *Diabetes*, *46*(9), 1375-1380.

Tisch, R., & McDevitt, H. (1996). Insulin-dependent diabetes mellitus: review. *Cell*, *85*, 291-7.

Van Schravendijk, C. F., Kiekens, R., & Pipeleers, D. G. (1992). Pancreatic beta cell heterogeneity in glucose-induced insulin secretion. *Journal of Biological Chemistry*, *267*(30), 21344-21348.

Williams, S. J., Wang, Q., MacGregor, R. R., Siahaan, T. J., Stehno-Bittel, L., & Berkland, C. (2009). Adhesion of pancreatic beta cells to biopolymer films. *Biopolymers,* 91(8), 676-685.

Winther RG (2012) Mathematical modeling in biology: philosophy and pragmatics.*Front. Plant Sci.* **3**:102. doi: 10.3389/fpls.2012.00102

Yang, S. N., & Berggren, P. O. (2005). β-Cell CaV channel regulation in physiology and pathophysiology. *American Journal of Physiology-Endocrinology And Metabolism*, *288*(1), E16-E28.

Yang, S. N., & Berggren, P. O. (2005). CaV2. 3 channel and PKCλ: new players in insulin secretion. *Journal of Clinical Investigation*, *115*(1), 16-20.

Yang, S. N., & Berggren, P. O. (2006). The role of voltage-gated calcium channels in pancreatic β-cell physiology and pathophysiology. *Endocrine reviews*, *27*(6), 621-676.

Zhang, M., Goforth, P., Bertram, R., Sherman, A., & Satin, L. (2003). The Ca< sup> 2+</sup> Dynamics of Isolated Mouse β-Cells and Islets: Implications for Mathematical Models. *Biophysical journal*, *84*(5), 2852-2870.

Zhang M, Houamed K, Kupershmidt S, Roden D, Satin LS (2005) Pharmacological properties and functional role of Kslow current in mouse pancreatic beta-cells: SK channels contribute to Kslow tail current and modulate insulin secretion. *J Gen Physiol 126*, 353–363.

Zhang, Q., Galvanovskis, J., Abdulkader, F., Partridge, C. J., Göpel, S. O., Eliasson, L., & Rorsman, P. (2008). Cell coupling in mouse pancreatic β-cells measured in intact islets of Langerhans. *Philosophical Transactions of the Royal Society A: Mathematical, Physical and Engineering Sciences*, 366(1880), 3503-3523.